AN ABSTRACT OF THE THESIS OF

Garlan Ramadhan for the degree of Master of Science in Civil Engineering presented on December 13, 2013

Title: Seismic Performance of Diagrid Steel Structures Using Single and Double Friction Mass Dampers

Abstract approved:

André R. Barbosa

The steel diagrid structural system is a recent load bearing and lateral resisting structural system for tall building structures that is relatively unexplored in the western United States. One possible reason for the little use of diagrid systems in earthquake prone regions is the lack of guidelines and application examples illustrating the design and analysis of these structures. In this work, a prototype building with 72 stories is used as an example for which the design and analysis of the diagrid system is performed. To mitigate the possible large displacement and base shear demands that these structures may undergo under seismic events, two new design solutions consisting of one or two friction tuned mass damper (TMD) units are explored. In the first solution, a TMD is placed on the top four stories of the building and is tuned to reduce the contribution of the fundamental mode of vibration of the structure. The second solution uses a double TMD system, in which a second TMD unit – tuned to the second period of the structure – is added at mid-height of the building. Using a nonlinear finite element model of the tuned mass damper, the effectiveness of the friction mass damper design is studied. The mass damper system consists of a concrete tank containing sand or water. The tank is placed in between the building reinforce concrete structural core and the exterior steel diagrid system. This mass damper is

connected to the structure using friction pendulum isolators which are chosen due to their ability to undergo large deformations. The models are then subjected to earthquake ground motions from historical shallow crustal and subduction-zone events. Parametric studies are carried out to optimize the mass damper design in improving the seismic performance of the building. Optimization of the seismic performance is assessed in terms of minimization of inter-story drift ratios, base and story forces, as well as floor absolute accelerations. The results show that the single TMD system can reduce significantly the peak base reaction and inter-story drift envelopes. Addition of the second TMD provides further improvements in terms of reducing the peak base reactions, while also producing notable reductions in peak absolute floor accelerations, which are not observed when only one TMD unit is used.

Seismic Performance of Diagrid Steel Structures Using Single and Double Friction Mass Dampers

by

Garlan Ramadhan

A THESIS

submitted to

Oregon State University

in partial fulfillment of
the requirements for the
degree of

Master of Science

Presented December 13, 2013

Commencement June 2014

Master of Science thesis of Garlan Ramadhan presented on December 13, 2013

APPROVED:

Major Professor, representing Civil Engineering

Head of the School of Civil and Construction Engineering

Dean of the Graduate School

I understand that my thesis will become part of the permanent collection of Oregon State University libraries. My signature below authorizes release of my thesis to any reader upon request.

Garlan Ramadhan, Author

ACKNOWLEDGEMENTS

I would like to give a sincere gratitude to my parents, siblings, relatives, and friends for their support. This work is also a present for my parents who are having birthdays in December 3th and 4th.

For his academic input, support, and immense knowledge, I am very grateful to Dr. Andre Barbosa for helping me all the time to complete my master study and research. Without his guidance, this work can never be completed.

TABLE OF CONTENTS

TABLE OF CONTENTS (Continued)

Page

TABLE OF CONTENTS (Continued)

LIST OF FIGURES

LIST OF FIGURES (Continued)

LIST OF FIGURES (Continued)

Figure Page

LIST OF FIGURES (Continued)

LIST OF FIGURES (Continued)

LIST OF TABLES

CHAPTER 1. INTRODUCTION

1.1. BACKGROUND

The first tall buildings were built in United States of America in the late nineteenth century (Ali and Moon 2007). At present times, many tall buildings have been built around the world and The Council of Tall Buildings and Urban Habitat contains information on 10,000+ tall buildings. Several structural systems have also been developed to realize mankind's dream in pursuing new heights. The steel diagrid structural system is one of them. This system consists of diagonal exterior steel members with or without vertical columns. Some prime examples of this kind of structures are shown in Figure 1.1: the Hearst Tower, in New York City; the China Central Television (CCTV) Headquarters in Beijing, China; and the Tornado Tower in Doha, Qatar.

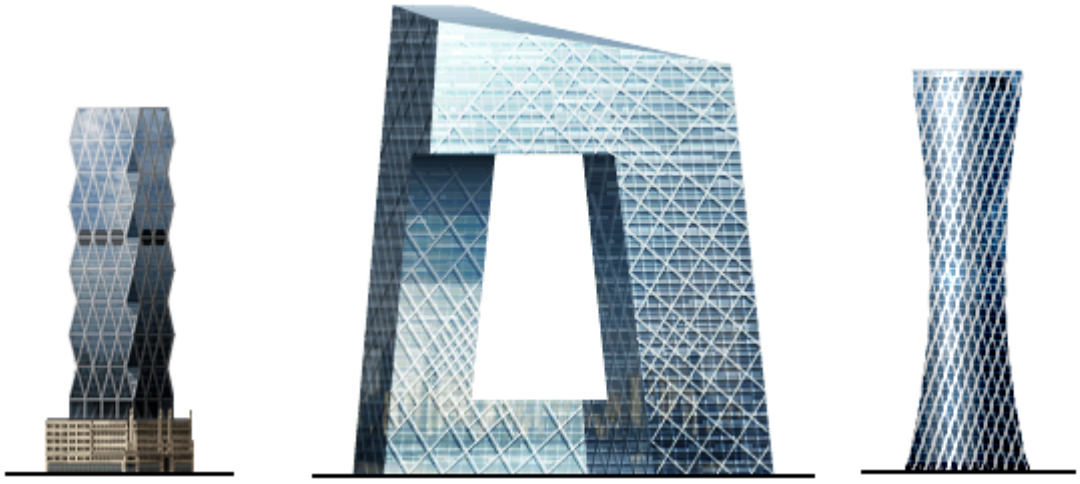

Figure 1.1. Example of diagrid building: (a) 42-Story Hearst Tower in New York, USA; (b) 51-Story CCTV HQ in Beijing, China; (d) 52-Story Tornado Tower in Doha, Qatar (Courtesy of skyscraperpage.com).

The diagrid structural system is known for its redundancy, continuous and uninterrupted load paths. Diagrid structures are considered very efficient (McCain, accessed in 2013), but these efficiencies also come with drawbacks. Most new

structures that designed and built using this system are lighter and more flexible than conventional tall building systems, and thus can suffer large displacement, especially under seismic loading. The diagrid structural system is also relatively new and unexplored in the western United States, and hence engineers lack the guidelines and examples that can be used to promote the design of tall buildings using such a structural system.

In this study an introduction to the design and analysis of diagrid structural systems is exemplified for a prototype 72-story building. For the seismic design, the focus is placed on optimizing the design by mitigating large displacements and shear forces that may appear in these structures. First, a system using a single tuned mass damper (TMD) unit placed at the top of the building is explored. The mass damper is connected to the structure with friction pendulum isolators, which are chosen due to their ability to undergo large deformations. A parametric study is carried out in order to optimize the mass damper design in terms of improving the seismic performance of the building structure. Second, the performance of a double tuned mass damper system is also investigated. In this system, an additional TMD unit is installed at mid-height of the building. In all, this report provides a first example which serves as guidance into design of diagrid structures in regions prone to seismic loading, including single or double tuned mass damper systems. Since the building is designed for a location in downtown Seattle, both shallow crustal earthquake motions as well as subduction zone earthquake motions are used in the analysis. According to past research (Romney 2013), the peak displacement demands resulted from using both types of motions are mostly identical, but the subduction zone motions induce a much larger number of exceedances of reference yielding, indicating that structures excited must be carefully designed to avoid low-cycle fatigue.

1.2. OBJECTIVES

The main objective of this study is to provide guidance for analysis and design of diagrid tall building structures including tuned mass damper systems. A

prototype 72-story building is used as the basic input. The design is optimized by analyzing the improvements in several response parameters, such as story shear, base shear, inter-story drift ratios, floor displacements, and floor absolute accelerations. Furthermore, demand to capacity ratios of the diagrid steel members are evaluated in assessing the seismic performance of systems that include the use of TMD system.

1.3. THESIS OVERVIEW

Figure 1.2 illustrates the flowchart of the work performed in this thesis. First, 72-story prototype building is designed following current US codes and standards even though the current codes are not applicable for direct use for buildings taller than 150ft. This building then serves as a basic structure for incorporating TMD systems. The modeling and all simulations are performed using SAP2000 (Computer and Structures 2011). Moreover, a parametric study is carried out to illustrate the sensitivity of the building's seismic performance to the various parameters that define the behavior of the TMD units. Parameters that are studied are friction coefficient of the isolators, height distribution, and mass of the TMD unit, as well as the inclusion of a second TMD unit.

This thesis consists of 6 chapters. Each chapter presented phases that the author went through to complete this work.

Chapter 2: Literature Review

Chapter 2 highlights the selection of past works and researches that relevant for this thesis. It covers 3 topics: diagrid structural system, tuned mass dampers, and friction pendulum isolator.

Chapter 3: Methodology

Chapter 3 explains the methods the author used for design, modeling, selecting the ground motions, and parametric studies. The modeling process of the TMD and

numerical trials that are done before applying the system to the prototype building are also presented.

Chapter 4: Prototype Building Modeling

Chapter 4 contains detailed explanation of the prototype building design. All parameters required for designing the prototype model are listed.

Chapter 5: Simulation Results and Analysis

Chapter 5 presents the result comparisons and analysis of each simulation. The results of interest are vibration characteristics, base and story reactions, inter-story drifts, floor displacements, and floor absolute accelerations.

Chapter 6: Final Remarks

Chapter 6 summarizes the main conclusions and highlights the novel findings of this works. It also includes discussions on several potential subjects for future works that branches from this thesis.

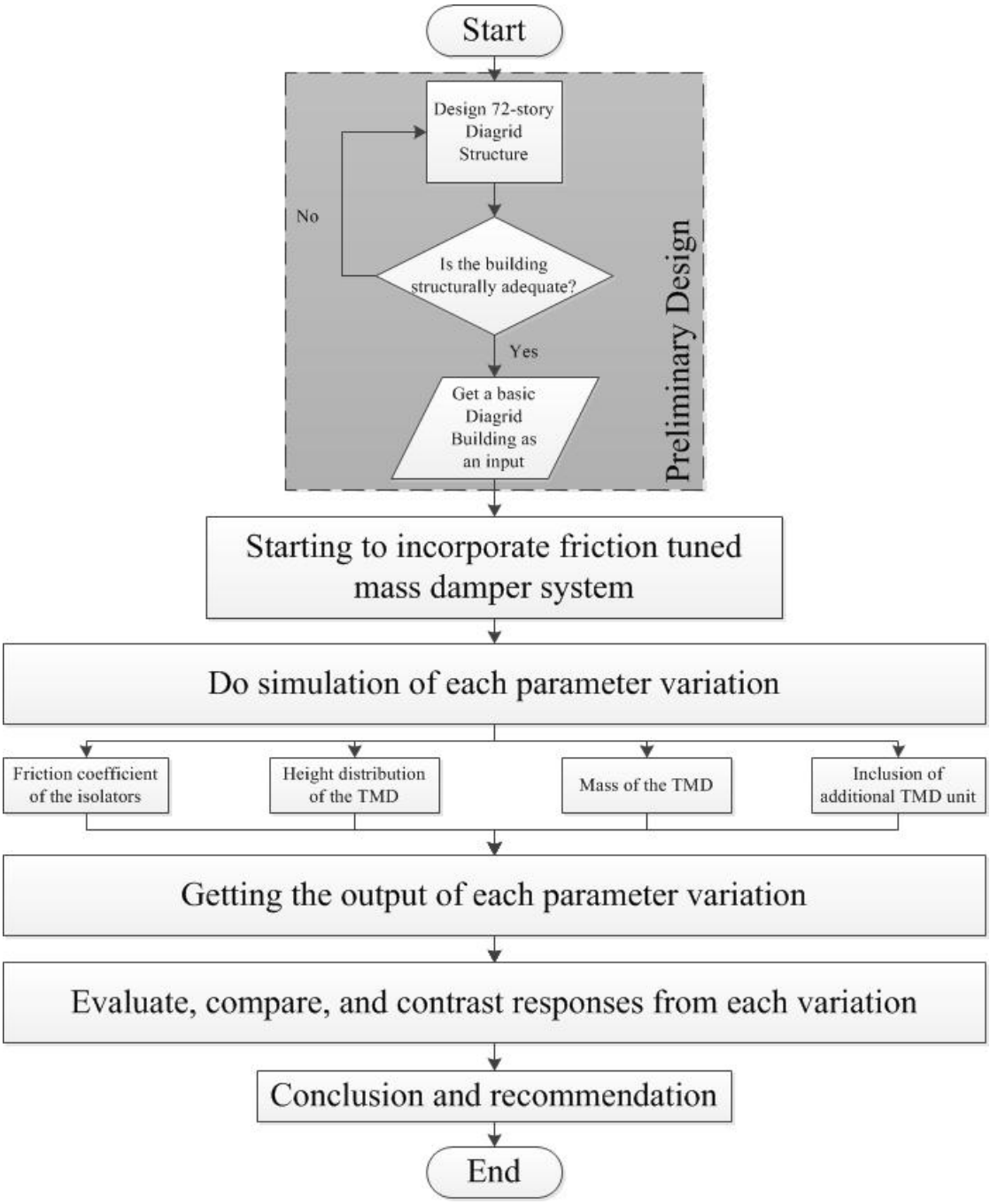

Figure 1.2. Flowchart of the analysis procedure.

CHAPTER 2. LITERATURE REVIEW

2.1. DIAGRID STEEL STRUCTURES AND OPTIONS FOR IMPROVING SEISMIC PERFORMANCE

Diagrid is an abbreviation for “diagonal grid”. The structural system gets its name from the diagonal columns that form triangular trusses. The diagonal trusses are connected by horizontal rings (steel beams), that provide support for the floors and column buckling restrains. The diagonal members carry gravity loads as well as lateral loads, and thus steel is typically used in diagrid structures. The main difference between conventional steel exterior-braced frame trusses (X, K, V, and Chevron type braces) is that in the diagrid structural system almost all vertical columns are typically eliminated.

This system has been shown by other authors to be ideal for use in skyscrapers (McCain, accessed in 2013). To improve the seismic performance of the diagrid system, several alternatives have been proposed to date, which included the use of base isolation and viscous dampers. In the first alternative, Arup (2009) proposed a diagrid structure combined with a base isolation system as a method for reducing the potential for damage as induced by earthquake shaking. In this solution, a 20-story office building was completed in 2006 in Sony City, Japan. The isolation solution was effective since the period of the base isolated building was shifted and the seismic lateral forces applied to the structure were substantially reduced. Base isolation typically adds 5% of the construction cost (Wada and Mori 2013), even after considering the reduction in structural material in the superstructure. The extra cost arises due to the extra floor structure that needs to be constructed in between the building and the foundation in support of the base isolators. Furthermore, design of services and elevator shafts, passing through the isolation requires careful design for allowing for the lateral movement between the foundation and the isolated structure. In a second alternative, Lago et al. (2010) proposed a vertically distributed isolation system. In this solution, the diagrid exterior structure was isolated from the main

seismic mass of the building interior along the height of the structure. The distributed isolation was achieved by attaching viscoelastic dampers between floor diaphragms and horizontal rings of the diagrid structure. Lago et al. showed that this system has the potential to significantly reduce the damage to the architectural façades.

Even though the two systems introduced in the previous paragraph are unique and have several advantages for mitigating seismic demands, they are not suited for very tall building structures. The base isolation system is only effective for relatively stiff structures, since the period of the base isolated structures is typically set in the 2.0 sec to 3.0 sec range (Constantinou and Tadjbakhsh 1985). Tall building structures are typically very flexible and often have fundamental periods close to and above 5.0 sec and therefore the base isolation system is not effective. Following similar discussions, Lago et al. also stated that the vertically distributed isolation system is not effective for tall building structures. Based on purely numerical results, the authors showed that for a 20 story building the dampers had already experienced a stroke on the order of 0.8 m. Any form of extrapolation to the prototype 72-story building, would translate roughly to the need for dampers with approximately 4 m in length, which is beyond the scope of the proposed solutions.

Herein, a third alternative for mitigating seismic demands is proposed for use in tall buildings consisting of a diagrid structural system, which makes use of tuned mass dampers (TMDs). Even though the particular system being proposed is new and the application of this new solution in diagrid systems has never been proposed, the concept of using TMD units have been applied in many skyscrapers built around the world, such as: Taipei 101 in Taipei, Taiwan; One Wall Centre Hotel in Vancouver, Canada; and Shanghai World Financial Center in Shanghai, China. The TMD systems installed in these three buildings are all unique. Taipei 101 featured the heaviest TMD in the world with 660 metric-tons; the One Wall Centre fosters a tuned liquid (water) damping system; and the Shanghai World Financial Center holds a double TMD system. In these three building designs, the TMDs were installed at the top of the buildings and were shown to successfully mitigate the effects of the lateral loading.

The TMD concept in this thesis is somewhat similar to the used in the One Wall Centre Hotel (Glotman Simpson 2001). Further explanation of the concept and its modeling details are provided in section 3.1.2.

2.2. TUNED MASS DAMPERS AND IMPLEMENTATION

Tuned mass dampers (TMDs) have been studied extensively by many researchers (e.g. Chopra 2001, Inaudi and Kelly 1992). TMDs are introduced in structures to improve their performance by providing counteracting (out-of-phase) forces that mitigate the vibration response of the original structure. Earlier studies included implementation of single mass damper units to mitigate wind-induced vibrations of building structures (Wirsching and Campbell 1973). In the literatures (e.g. Sadek et al. 1997, Hadi and Arfiadi 1998), researchers have tuned the mass dampers by adjusting the stiffness and damping of the device or the mass of the TMD unit. In most cases in which TMDs have been used in buildings, these were placed near the top of buildings. The utilizations of multiple TMD units have also been discussed. To the author's knowledge, the pioneering work by Xu and Igusa (1992) proposed the first system with multiple damped oscillators and showed that multiple TMD units can be more effective than a single TMD with the same mass in mitigating vibrations induced motion (displacements). Chen and Wu (2001) showed that multiple dampers are strictly necessary if the objective is to also reduce peak floor absolute accelerations of the building structure to impulsive (seismic) loading. Nonetheless, Lucchini et al. (2013) concluded that the effectiveness of the TMD solutions consisting of two units is reduced if the uncertainty in the characteristics of the earthquake are considered.

In this study, two solutions consisting of a single and double TMD unit is used in the design of a diagrid steel structure. To illustrate its practical application, structural drawings of the diagrid system and the TMD units are provided to visualize how the TMDs can be built within a real structure. In this newly proposed system, the TMD units incorporated in the diagrid steel structures are in the form of concrete

containers, in which sand or water is placed inside. The solution with the water is considered to be an interesting one since this water can also be used for mitigation of fires. Below the containers, friction pendulum isolators are placed as supports that connect the TMD to the main building structure. The volume of sand or water can be adjusted according to optimal mass obtained from modeling and analysis. This concept is somewhat similar to the one used in the One Wall Centre Hotel (Glotman Simpson 2001), where a tuned water damping system was installed at the top of the building to mitigate lateral vibrations.

2.3. FRICTION PENDULUM ISOLATOR PROPERTY AND BEHAVIOR

The friction pendulum isolator (FPS) model in this study has a highly nonlinear behavior. The FPS model consisting of a gap in the axial direction coupled the friction properties for two shear deformations with post-slip stiffness in the shear directions due to the radius of the sliding surfaces, and linear effective-stiffness properties in the torsional deformation. This friction model is based on the one proposed by Wen (1976) and Park et al. (1986).The pendulum local axis of 1, 2, and 3 correspond to the global Z, X, and Y direction, respectively. Illustration of this model is shown in Figure 2.1.

The axial force (P) of the friction isolator model is always nonlinear. Also, in order to generate the nonlinear shear forces, P must take a negative value (compression), with an axial stiffness (k_{u1}) which is always positive. Thus, the force P is given by:

$$F_{\mathrm{u1}} = P = \begin{cases} k_{u1}u_1, & \text{if } u_1 < 0 \\ 0, & \text{otherwise} \end{cases} \tag{2.1}$$

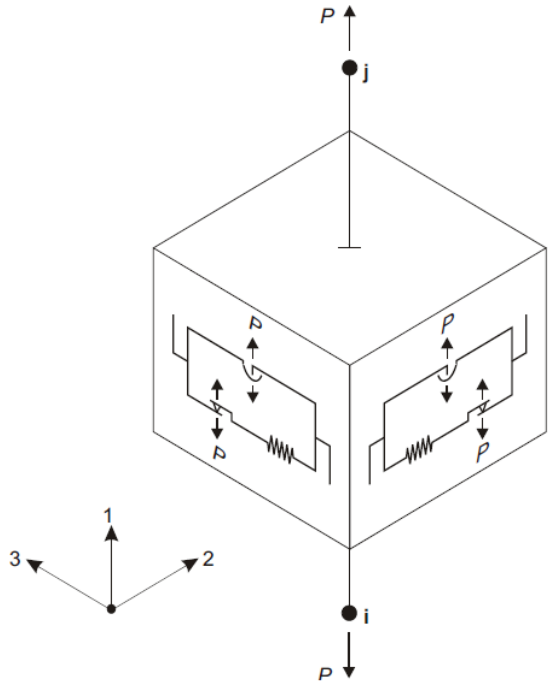

Figure 2.1. Friction-pendulum isolator property (courtesy of CSI 2011).

Shear forces of the friction pendulum isolators are the sum of the frictional shear forces and pendulum shear forces, given by:

$$F_{\mathrm{u2}} = f_{u2f} + f_{u2p} \tag{2.2}$$

$$F_{\mathrm{u3}} = f_{u3f} + f_{u3p} \tag{2.3}$$

The frictional shear forces are given by:

$$f_{\mathrm{u2}f} = -P\mu_2 z_2 \tag{2.4}$$

$$f_{\mathrm{u3}f} = -P\mu_3 z_3 \tag{2.5}$$

and where z_2 and z_3 are internal hysteretic variables, μ_2 and μ_3 are velocity-dependent friction coefficients which are given by:

$$\mu_2 = f_{fast2} - \left(f_{fast2} - f_{slow2}\right)e^{-r\dot{u}} \tag{2.6}$$

$$\mu_3 = f_{fast3} - \left(f_{fast3} - f_{slow3}\right)e^{-r\dot{u}} \tag{2.7}$$

in which f_{slow2} and f_{slow3} are friction coefficients at zero velocity for each respective direction, f_{fast2} and f_{fast3} are friction coefficients at fast velocity, $\dot{u}$ is the resultant of the sliding velocity of $\dot{u}_2$ and $\dot{u}_3$, and r is a constant resulted from:

$$r = \frac{rate_2 \dot{u}_2{}^2 + rate_3 \dot{u}_3{}^2}{\dot{u}^2} \tag{2.8}$$

where $rate_2$ and $rate_3$ are constants which control the characteristics of the friction coefficients with velocity. Additionally, the pendulum shear forces are given by:

$$f_{\mathrm{u2p}} = -P \frac{u_2}{rad_2} \tag{2.9}$$

$$f_{\mathrm{u3p}} = -P \frac{u_3}{rad_3} \tag{2.10}$$

where rad_2 and rad_3 are the radius of sliding surfaces in their respective directions.

Lastly, a linear spring relationship is applied for the torsional deformation of the friction pendulum isolator model. It is given by:

$$F_{r1} = k_{er1} r_1 \tag{2.11}$$

where $k_{er1}$is the effective linear stiffness of torsional direction and r_1 is the torsional deformation. It is assumed that the rotations are negligible.

CHAPTER 3. METHODOLOGY

3.1. DESIGN

3.1.1. PROTOTYPE BUILDING

A 72-story prototype building with uniform floor height of 4 meters was designed following current US codes and standards. The building has a 36 meters × 36 meters floor plan and floors are supported by diagonal columns that cross every four floors. With this configuration, the diagonal columns form isosceles triangles with an angle of 69^{o}. This is the optimal configuration for slender diagrid structures greater than 60 stories according to empirical studies carried out by Moon (2008), since the steel diagonal columns provide the lateral resistance in overturning bending and shear. All beams except horizontal rings in floor diaphragms are designed to carry gravity load only, and thus are pin-connected at both ends. Breakdown of the structural system of the prototype building are described as follows:

- Gravity load resisting system:
  - Concrete floor slab + grid of steel beams
  - Steel diagrid exterior
  - Inner concrete core
- Lateral load resisting system:
  - Dual system consisting of steel diagrid exterior and inner concrete core (with diagrid resisting approximately ±80% of seismic lateral load shown in section 4.3.2).

This building is assumed to be located in Seattle, WA 98104. The assumed latitude and longitude are 47°36'17.43"N and 122°19'51.88"W, respectively.

A two staged design and design verification was performed: (1) in a first stage, the building was designed not considering the effects of the TMDs, as these were not included in the design. The dimensions of the building were estimated using engineering judgment and through an iterative process in which the response spectrum

method was used only for prototype building design (without the TMD). In a second stage, the friction TMD system was incorporated to the basic model obtained from the design performed in the first stage.

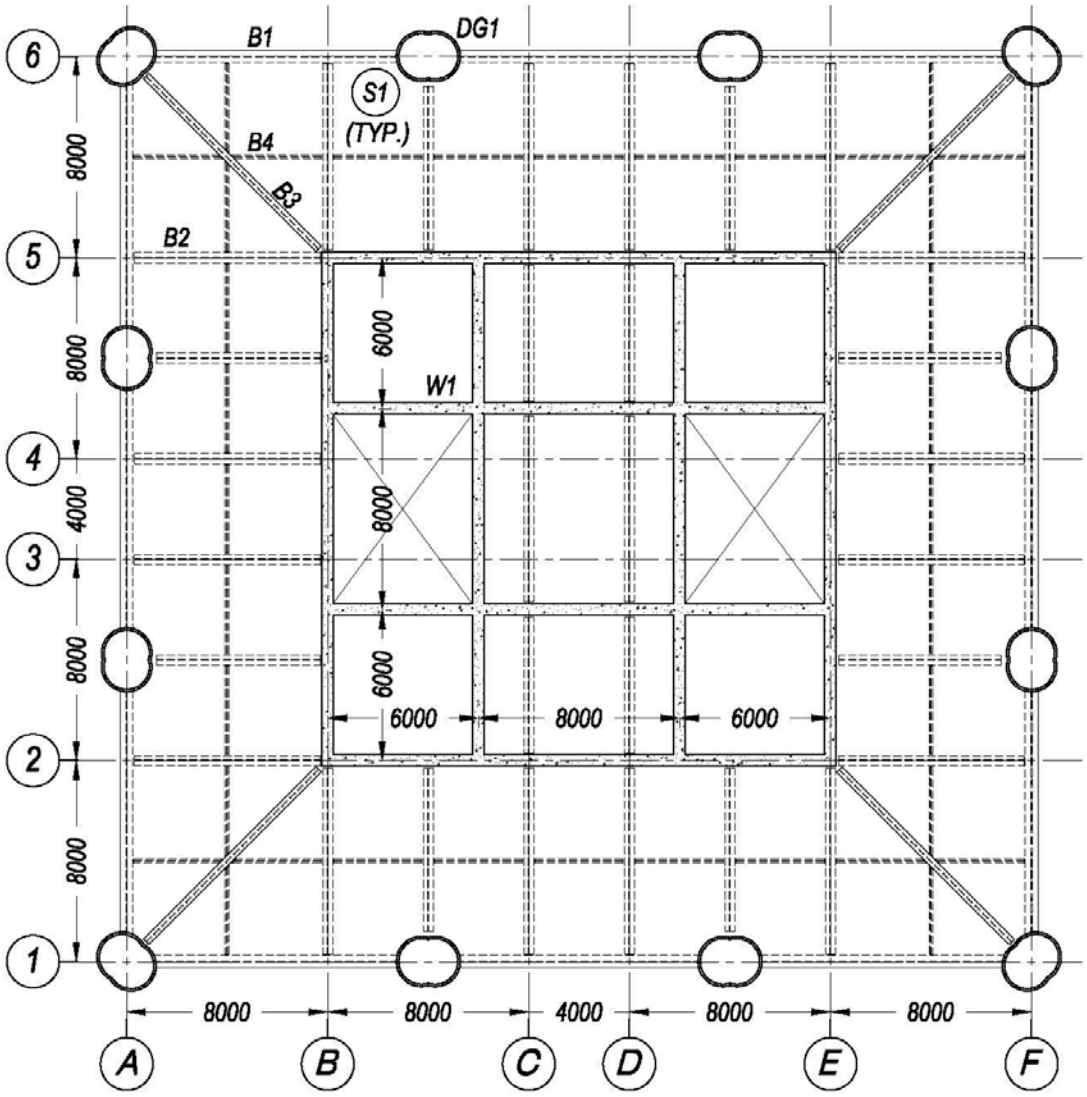

Figure 3.1. Prototype Building Drawing - Plan View (all dimensions in mm).

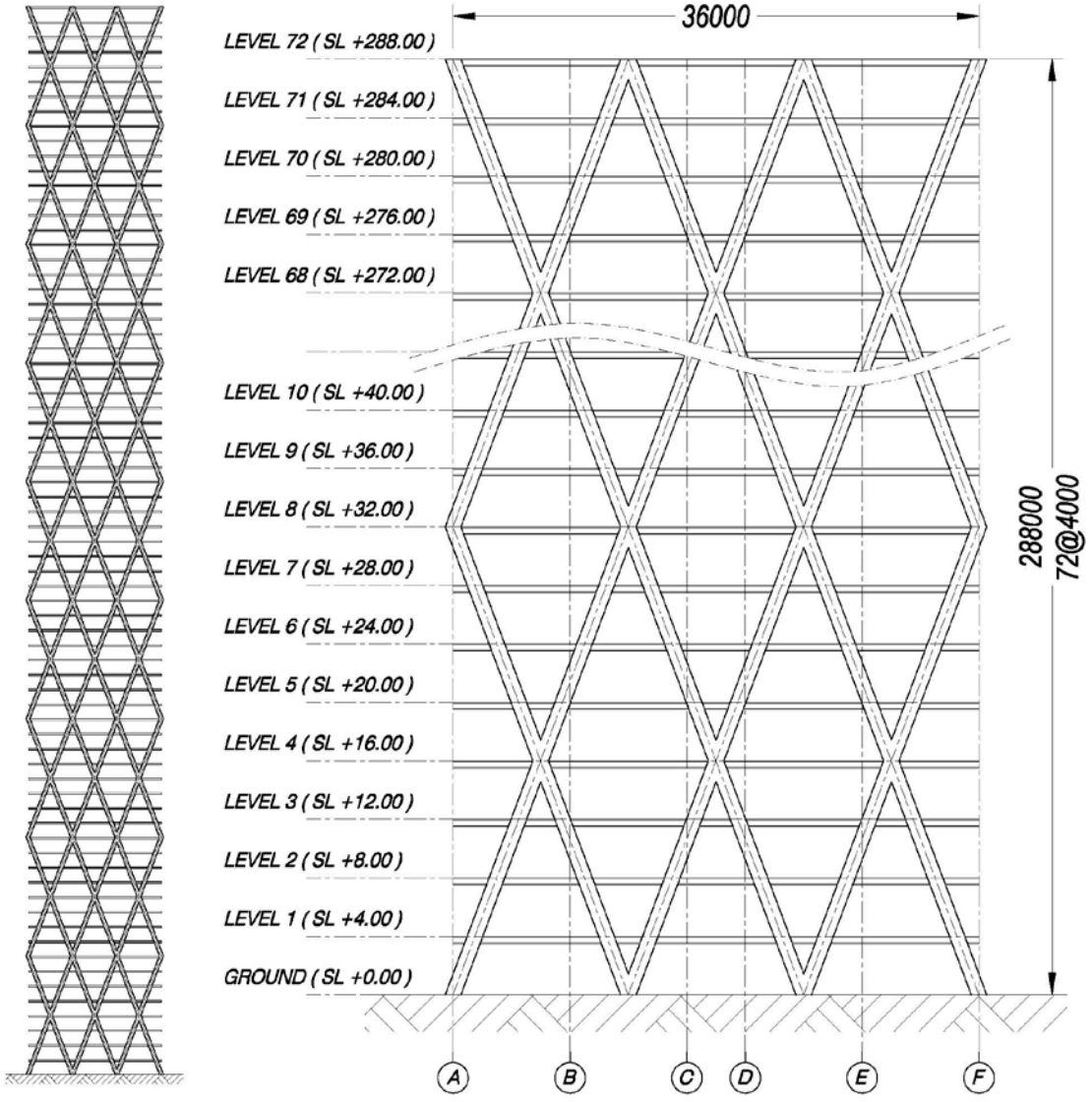

(a) (b)

Figure 3.2. Prototype Building Drawing: (a) Full Height Elevation View, (b) Truncated Elevation View (all dimensions in mm).

3.1.2. REFERENCE BUILDING (WITH TMD)

Mass of the TMD is provided by a concrete container with sand or water inside which is connected to the main structure using friction pendulum isolators. Similar concept can be found in One Wall Centre Hotel in Vancouver, Canada – where it holds a tuned water damping system at the top level of the building. The

volume of sand or water can be adjusted according to optimal mass obtained from modeling and analysis. The reference model has the friction TMD unit placed at story 68 to alleviate the response from the first mode of the structure as shown in Figure 3.5 and Figure 3.6. The top friction TMD unit extends from story 68 to story 72 to provide improved load transfer from the mass damper to the stiffer floors, that is, floors at which the diagonal columns of the diagrid cross. It also serves as a room for the additional required mass that is provided by the sand or water. For the model with two friction TMD units, the first unit is the same as the reference model, while the second is placed at story 32, extending to story 34. The second TMD unit is illustrated in Figure 3.7 and Figure 3.8. Implementing the second mass damper unit aims at reducing the contribution of the second lateral mode of vibration (see Figure 3.16). Due to the usual shape of the seismic design response spectrum (as well as the shape of the response spectra of the ground motions considered) base shear forces due to the second mode (and even third mode) have significant contributions to the floor accelerations and to the total base shear, as confirmed in the results section.

Protective shock absorbers (rubber bearings or an equivalent system) are placed between the outer horizontal rings of the exterior diagrid and the TMD units. These bearings are also placed between the TMD units and the inner reinforced-concrete core. In the reference model, the TMD unit (at story 68) has absorbers – with thickness of 1 meter – placed in stories 69, 70, and 71. Initial gaps of 500 mm are provided, and absorbers are only engaged after the gaps are closed. For the model with double TMD units, the second TMD unit (at story 32) has absorbers – with thickness of 1.5 meters – placed in story 33. The second absorbers do not have gaps. This allows for tuning of the period of the second mass damper to be close to the second mode of the building. Absorbers are also placed above the container to prevent impact due to overturning. Mathematical model of the friction TMD system is shown in Figure 3.4. Lastly, additional rigid truss beam are provided at the floor below the TMD units, to transfer the vertical loads directly to the inner core. The new braces use WF – 300X150X5.5X8 and WF – 250X125X5X8.

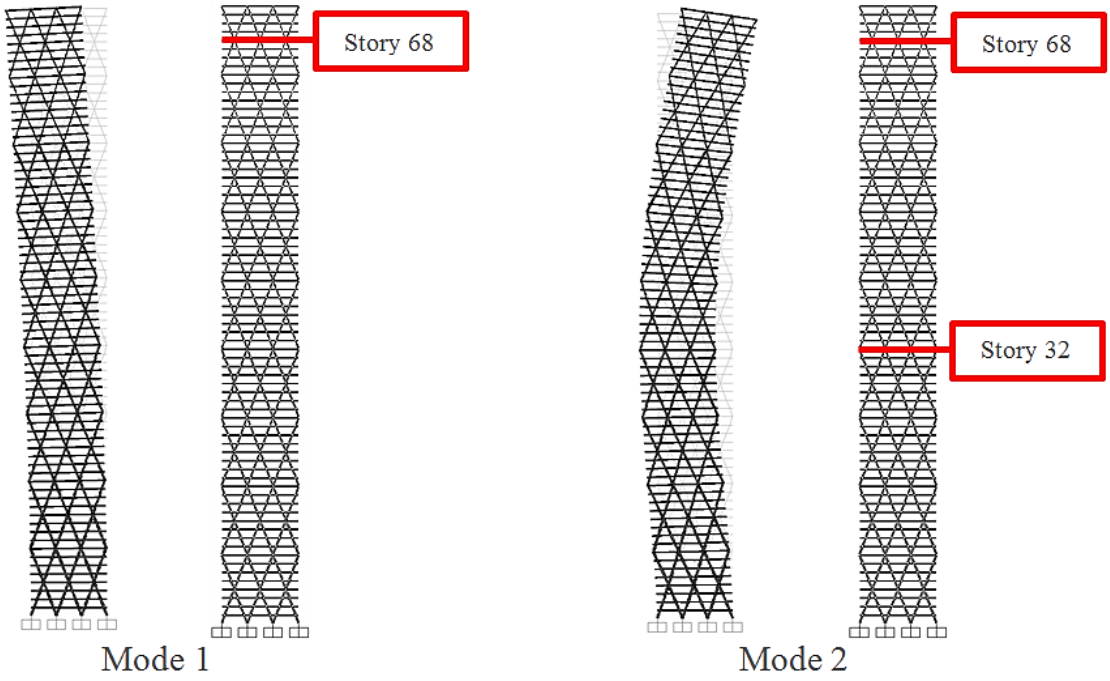

Figure 3.3. Mode shapes of the original structure and mass damper placement: (a) mode 1 and solution with only one TMD unit, and (b) mode 2 and solutions with two TMD units.

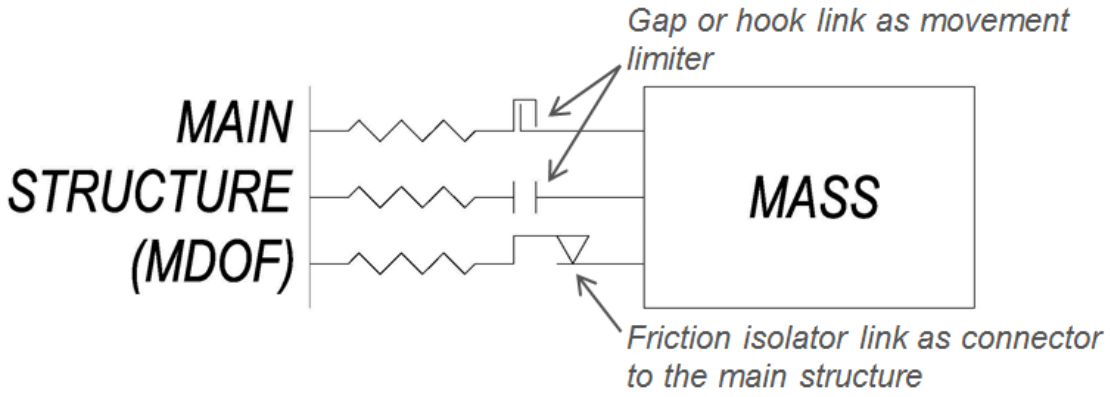

Figure 3.4. The friction mass damper mathematical model.

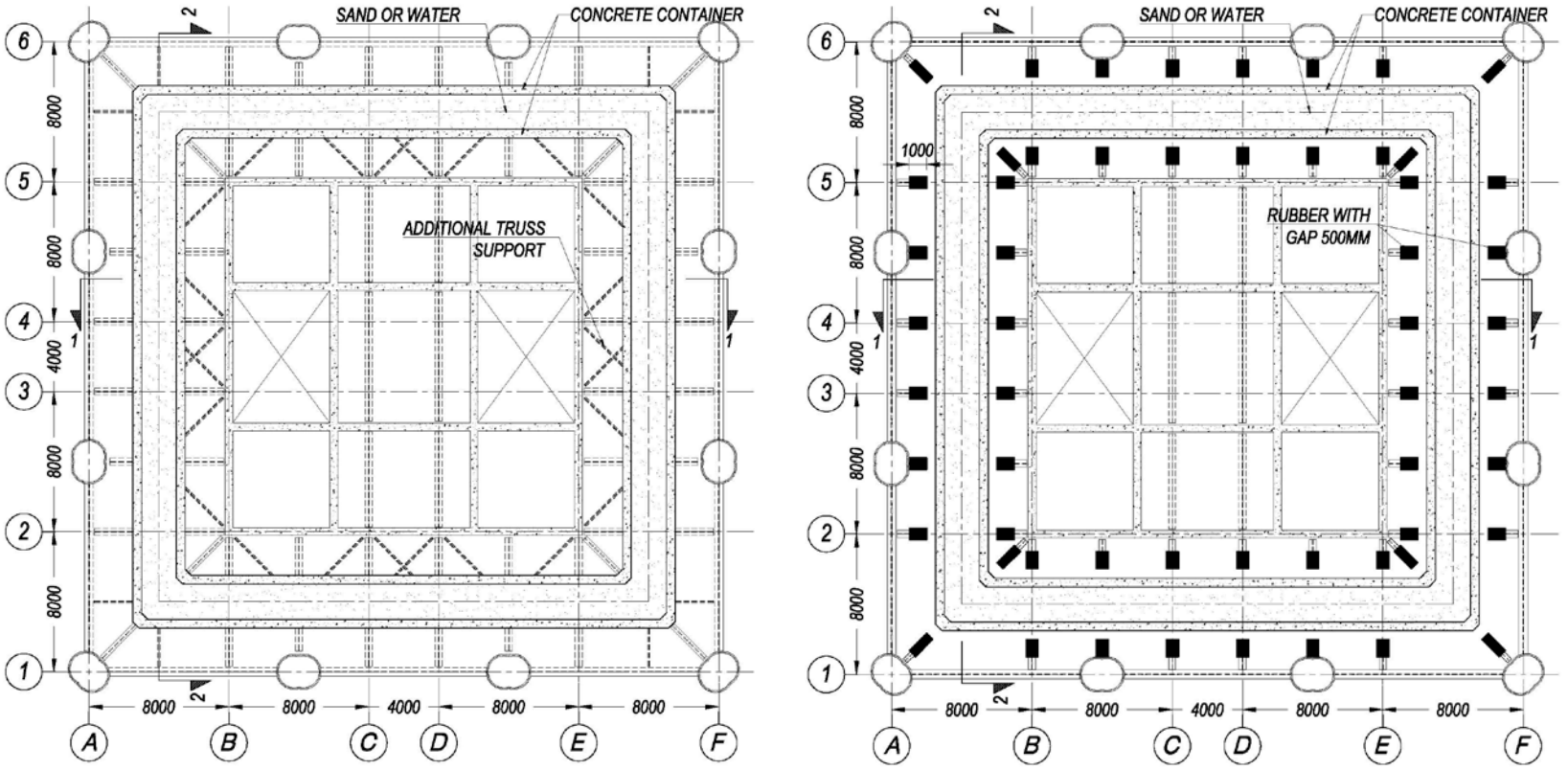

(a) (b)

Figure 3.5. Plan view of the first TMD unit: (a) at story 68, (b) at story 69 to 71. All dimensions in mm.

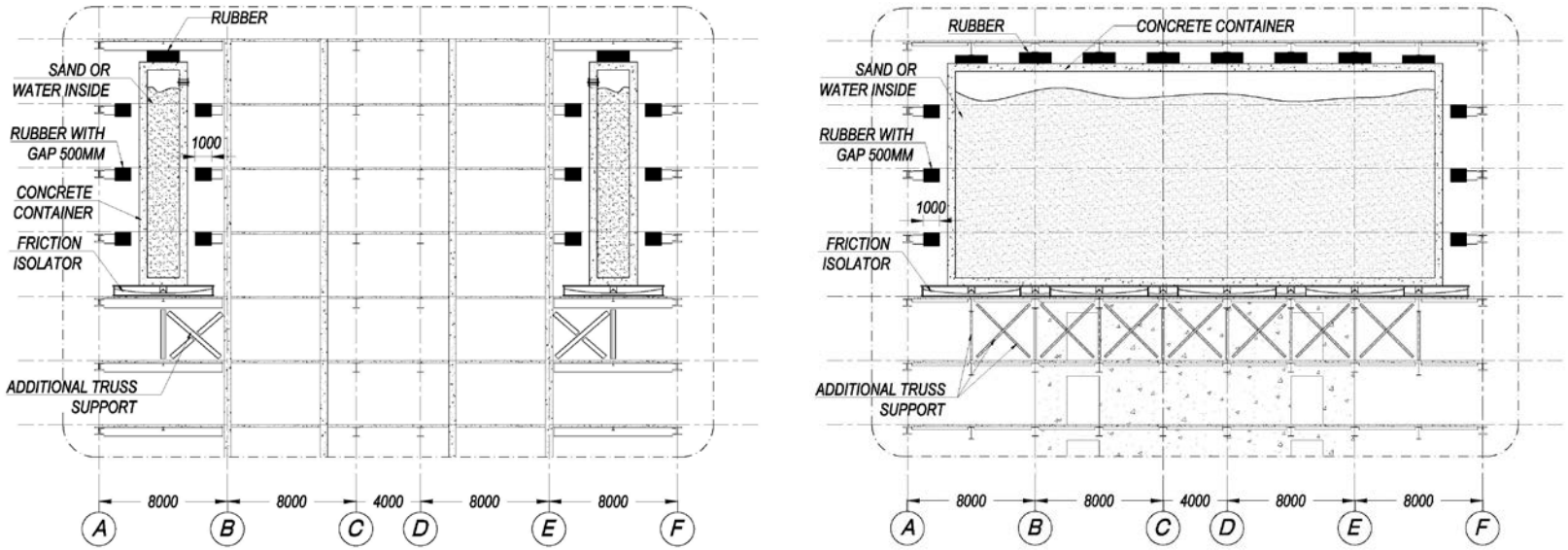

(a) (b)

Figure 3.6. Cross section of the first TMD unit: (a) section 1-1, (b) section 2-2. All dimensions in mm.

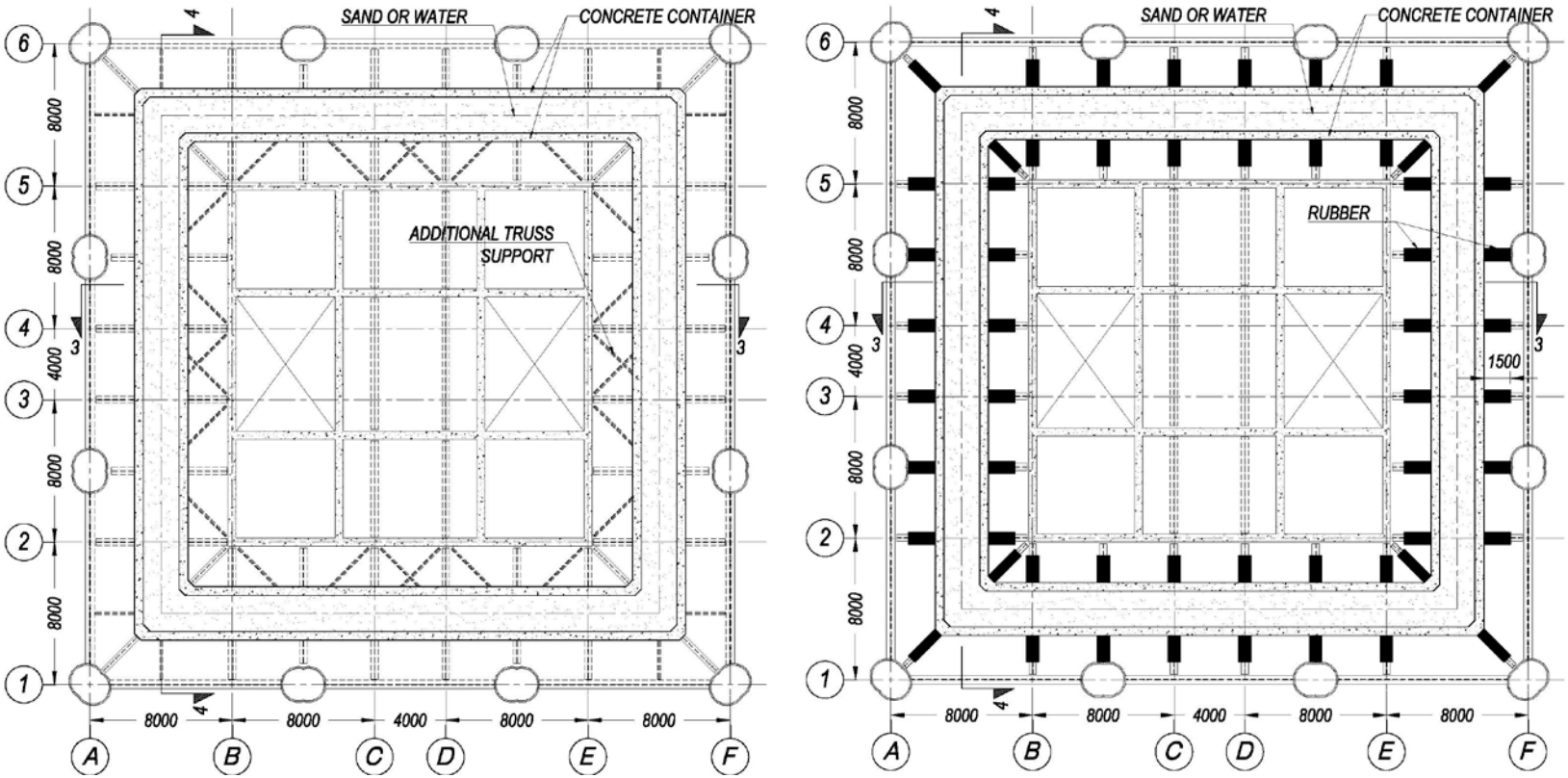

(a) (b)

Figure 3.7. Plan view of the second TMD unit: (a) at story 32, (b) at story 33. All dimensions in mm.

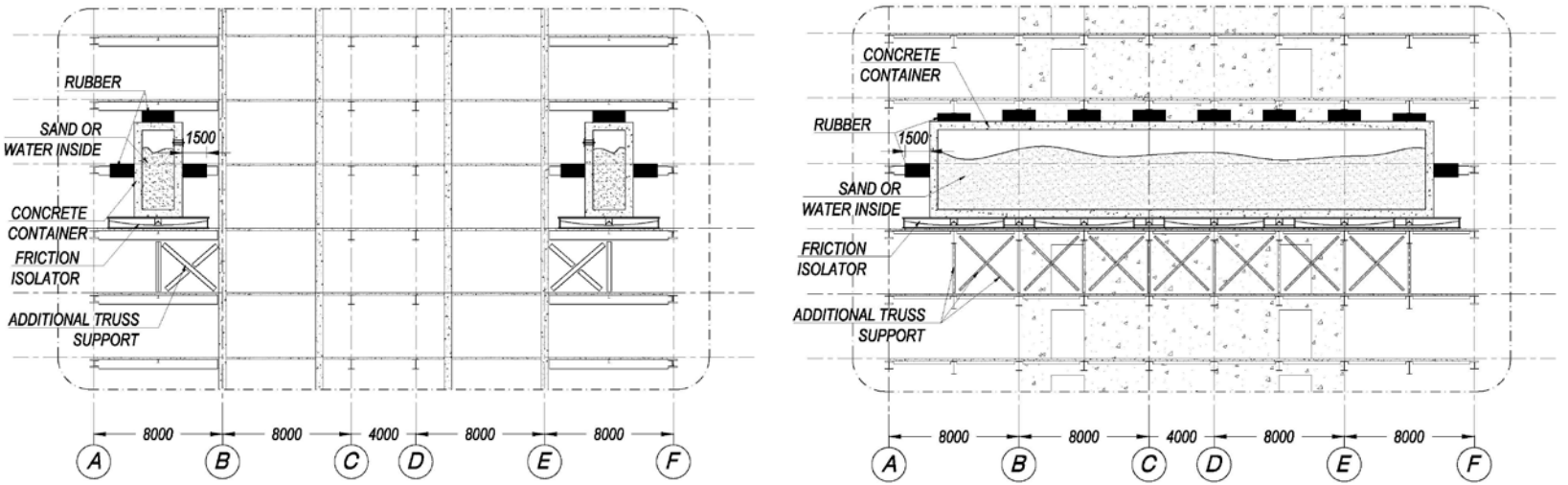

(a) (b)

Figure 3.8. Cross section of the second TMD unit: (a) section 3-3, (b) section 4-4. All dimensions in mm.

3.2. GROUND MOTION SELECTION

The selection and scaling of horizontal component ground motion accelerations time histories are crucial to produce meaningful results and adequate comparisons of the responses of structures subjected to these ground motions. The selection performed herein has the primary objective of producing acceleration histories which are consistent with the seismic hazard at the site.

3.2.1. CRUSTAL EARTHQUAKES

Seven (7) crustal earthquakes, listed in Table 3.1, are chosen and scaled from the 2011 PEER Ground Motion Database. The target spectrum is based on ASCE 7-10 with design earthquake spectral response acceleration parameters, S_{ds} = 0.911g and S_{d1} = 0.529g, and with T_L = 6 sec. The target design response spectrum is shown in Figure 3.9. The Pacific Earthquake Engineering Research Center (PEER) Center makes a ground motion database available and as a web tool linked to it for selection and scaling of acceleration time histories (PEER 2011). In the selection of the earthquake records, some parameters have to be input in the web tool. The range of earthquake magnitudes is set to 6 to 7.25. D5-95, which is the time duration for the intensity to rise from 5% to 95% is set to 0 to 300 seconds. Joyner-Boore distance (R_JB) and the rupture distance (Rrup) is set to 0 to 20.5 km. The range of average shear wave velocity in the top 30 m of soil (Vs30) is set to 190 to 350 m/s. The scale factor is limited to 0.5 to 2.0. Lastly, the weight function is set for periods between 1.0 second to 10 seconds. Figure 3.9 shows the target spectrum as well as geometric mean of the selected response spectra of scaled acceleration time histories. The records selected for the crustal shallow motions are listed in Table 3.1. It is worth noting that these records have the lowest root-mean-squared errors between the target response spectra and the response spectra of all ground motion records, and had the lowest usable frequency with a maximum value of 0.12 Hz (8.33 seconds).

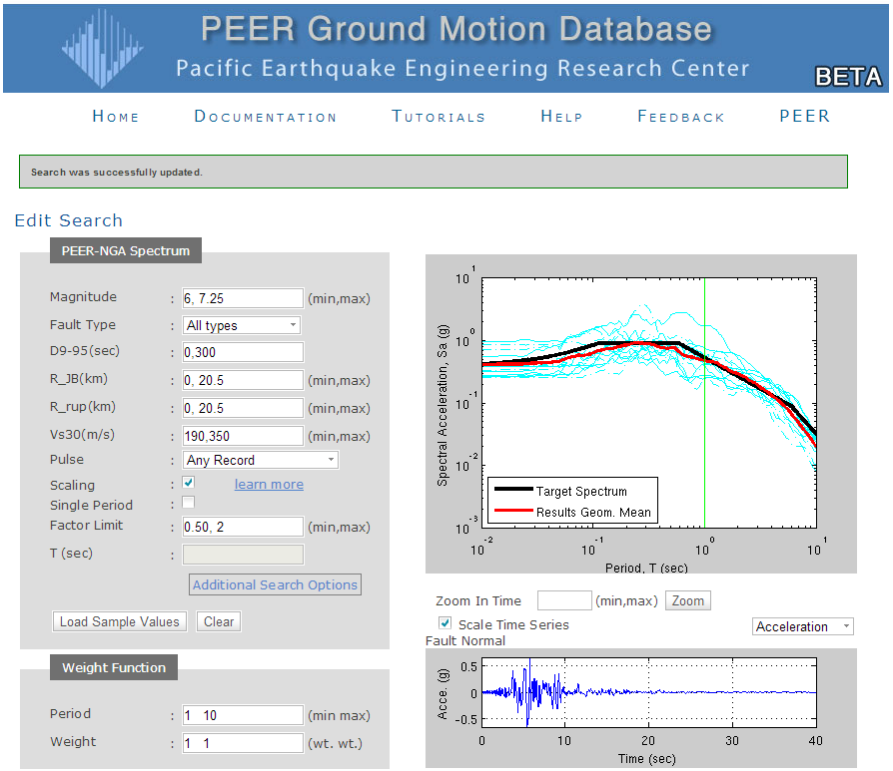

Figure 3.9. Input parameter for selecting and scaling the earthquake time series in PEER ground motion database.

Table 3.1. Properties of selected crustal earthquake records obtained from PEER (2011).

Event	Imperial Valley-06	Imperial Valley-06	Duzce-Turkey	Imperial Valley-06	Northridge-01	Imperial Valley-06	Northridge-01
Year	1979	1979	1999	1979	1994	1979	1994
Station	El Centro Array #8	Brawley Airport	Duzce	El Centro Array #10	Newhall - W Pico Canyon Rd.	Parachute Test Site	Newhall - Fire Sta
NGA#	183	161	1605	173	1045	187	1044
Scale Factor	1.1936	1.9863	0.7426	1.4789	0.9061	2	0.9109
RMSE	0.0148	0.0269	0.0386	0.0457	0.2477	0.2668	0.2705
Pulse (FN/FP)	Yes/No	Yes/No	No/Yes	Yes/Yes	Yes/Yes	No/No	Yes/No
Tp (FN/FP)*	5.4 / --	4 / --	-- / 5.6	4.5 / 2	2.4 / 2.2	-- / --	2.2 / --
Magnitude	6.53	6.53	7.14	6.53	6.69	6.53	6.69
Mechanism	Strike-Slip	Strike-Slip	Strike-Slip	Strike-Slip	Reverse	Strike-Slip	Reverse
Rrup (km)	3.9	10.4	6.6	6.2	5.5	12.7	5.9
Corner frequency	0.12	0.12	0.1	0.12	0.12	0.12	0.12

*TP is pulse period in seconds as defined by Baker (2007).

3.2.2. SUBDUCTION ZONE EARTHQUAKES

Seven (7) subductions earthquakes, shown in Table 3.2, are chosen and scaled from Japanese National Research Institute for Earth Science and Disaster Prevention's database (2013) using the method described in Romney (2013). Those 7 earthquake records are obtained from the “2011 Tohoku Earthquake” of March 11, 2011. It is worth noting that prior to this earthquake event, only very limited data was available for large magnitude earthquake motions, especially for the very large period range of interest of the building structure in analysis. Thus, all motions were selected from a single earthquake event, which may induce some bias. Similarly, it is worth noting that the records for the subduction chosen herein have larger RMSE than the shallow crustal motions and scaling factors were allowed to range from 1/3 to 3. A minimum value for the lowest useable frequency was also set to 0.12 Hz. From the database of Japanese ground motions used, there are a very small number of records that could be used for the analysis in this study due to the very large fundamental period of the tall structures. Often, two different components of the same earthquake need to be filtered using different corner frequencies. Thus, the records shown in Table 3.2 are applied to the two horizontal directions of the building.

Table 3.2. Properties of selected subduction zone earthquake records obtained from National Research Institute for Earth Science and Disaster Prevention's database (2013).

Event	**Tohoku Earthquake**	**Tohoku Earthquake**	**Tohoku Earthquake**	**Tohoku Earthquake**	**Tohoku Earthquake**	**Tohoku Earthquake**	**Tohoku Earthquake**
Date	March 11, 2011	March 11, 2011	March 11, 2011	March 11, 2011	March 11, 2011	March 11, 2011	March 11, 2011
Station	1103111446-AOMH16-EW-Surface	1103111446-FKSH10-EW-Surface	1103111446-FKSH16-NS-Surface	1103111446-FKSH20-EW-Surface	1103111446-IWTH11-NS-Surface	1103111446-IWTH24-NS-Surface	1103111446-TCGH16-NS-Surface
File Name	AOMH16EW2	FKSH10EW2	FKSH16NS2	FKSH20EW2	IWTH11NS2	IWTH24NS2	TCGH16NS2
Scale Factor	3.000	3.000	3.000	1.252	3.000	2.806	1.573
RMSE	0.606	0.520	0.667	0.823	0.778	0.173	0.356
Magnitude	9.000	9.000	9.000	9.000	9.000	9.000	9.000
Corner Frequency*	0.120	0.120	0.120	0.100	0.080	0.090	0.100

*lowest usable frequency.

3.3. MODELING

3.3.1. DIAGRID BUILDING

Structural modeling is a simplification of nature and behavior of a structure into a mathematical model that can be solved and analyzed. SAP2000 uses the finite element method to model all structural elements in the building. The diagrid structure is modeled using linear elastic frame elements with geometric and mechanical properties defined based on section 4.1.2. The inner reinforced concrete core is modeled using linear elastic shell elements. The effective Young's modulus of the linear shell elements is taken as 35% of the nominal concrete modulus E_c. Floor diaphragms consist of a grid of steel beams supporting a concrete slab which are modeled as rigid diaphragms for lateral loading. The effective Young's modulus of the floor slabs are taken as 25% of the nominal concrete modulus in accordance to ACI 318-11 section 10.10.4.1. Additional plan eccentricities in this regular prototype structure were not explicitly considered. The SAP2000 model of the prototype building consists of 8536 frame elements, 60275 joints, and 57624 shell elements. The total number of degrees of freedom in the model is approximately 360,000. Figure 3.10 shows two 3-D views of the building model, while Figure 3.11 shows a typical floor plan.

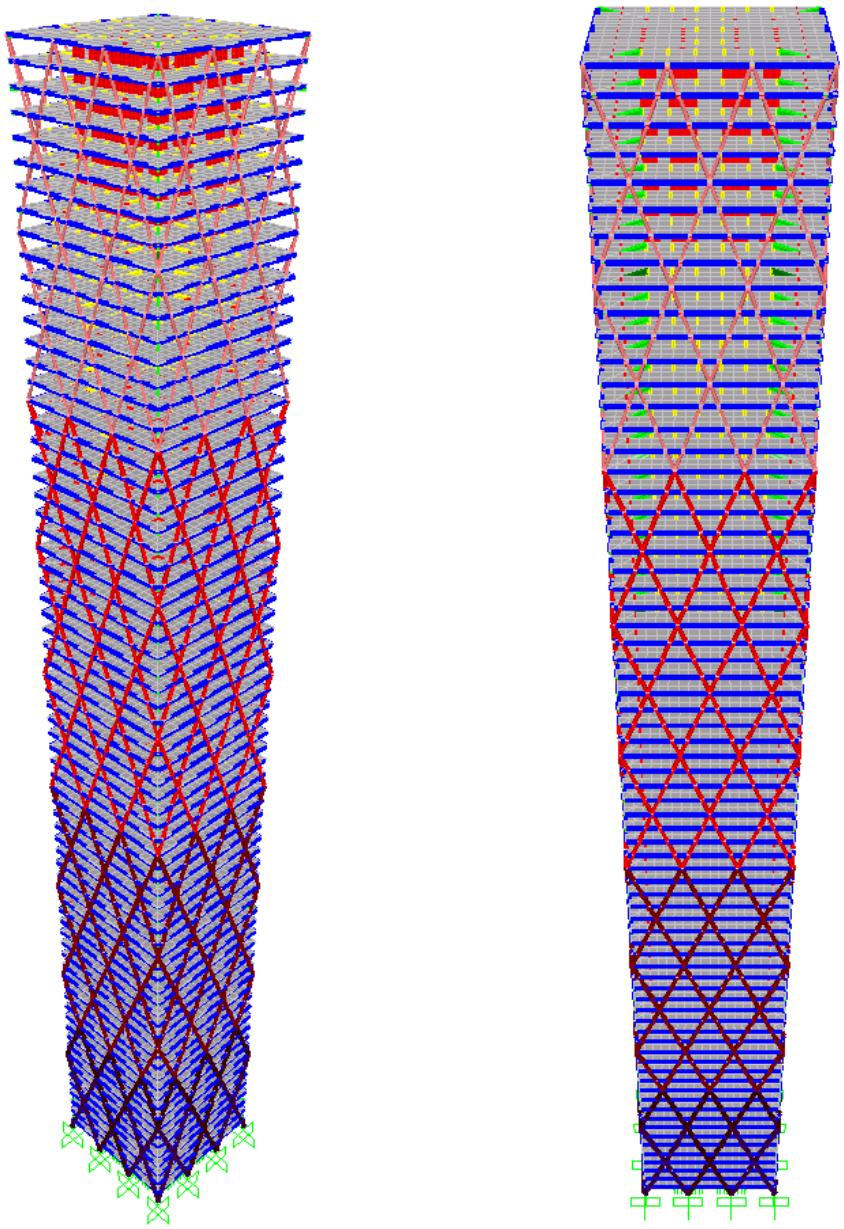

(a) (b)

Figure 3.10. Prototype building model in SAP2000: (a) eagle-eye view; (b) front view.

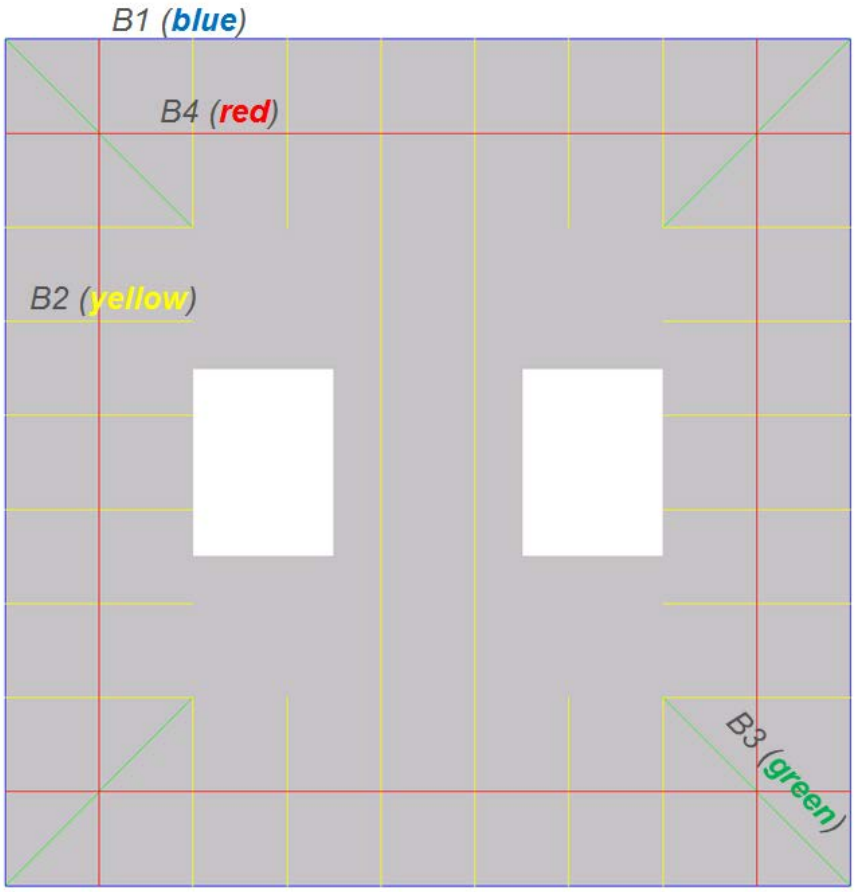

Figure 3.11. Typical floor plan with beam labels shown in SAP2000.

3.3.2. MASS DAMPER

For modeling purposes, the concrete container (with its content) is represented by a single wall, which is placed at mid-distance between the outer diagrid and the inner core. The single wall is modeled by shell elements with thickness and mass defined as to represent the container and its content. It should be noted that sloshing effects of the water surface is neglected as it will not have a considerable effect in seismic loads and performance of the TMD. In the reference model, the ratio between the mass of the TMD unit and the mass of the main structure is approximately 4.7% (the weight of the building is approximately 1.1 giganewton), while, for the model that has two TMD units, the second TMD unit has approximately half the mass of the first.

Above the container, uniaxial linear springs are provided at the connection between the container and slabs to represent the top absorbers. In the first TMD unit of the reference model, two gap links are placed in parallel to each other to model the behavior of absorbers and gaps surrounding the container. The first gap link corresponds to a gap of 500 mm followed by a linear elastic stiffness branch. The second gap link has a gap of 1500 mm, followed by a large stiffness to model the full compression/crushing of the rubber. For the model with double friction TMD units, the behavior of absorbers for the second TMD unit are almost the same as the first, except the first gap links are replaced by uniaxial linear springs. More details are provided in section 3.3.3.

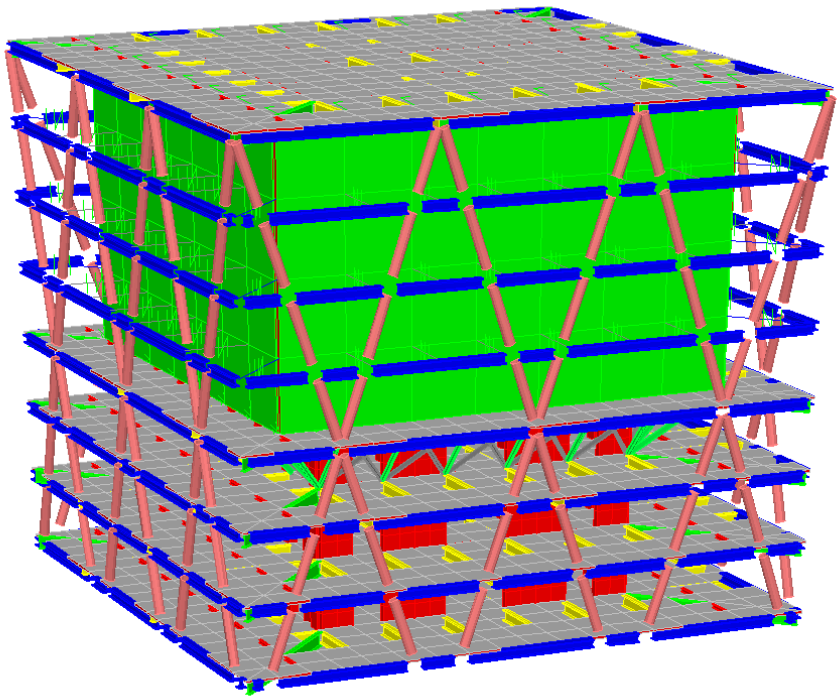

Figure 3.12. Close look at the TMD model (floor level 65 to 72).

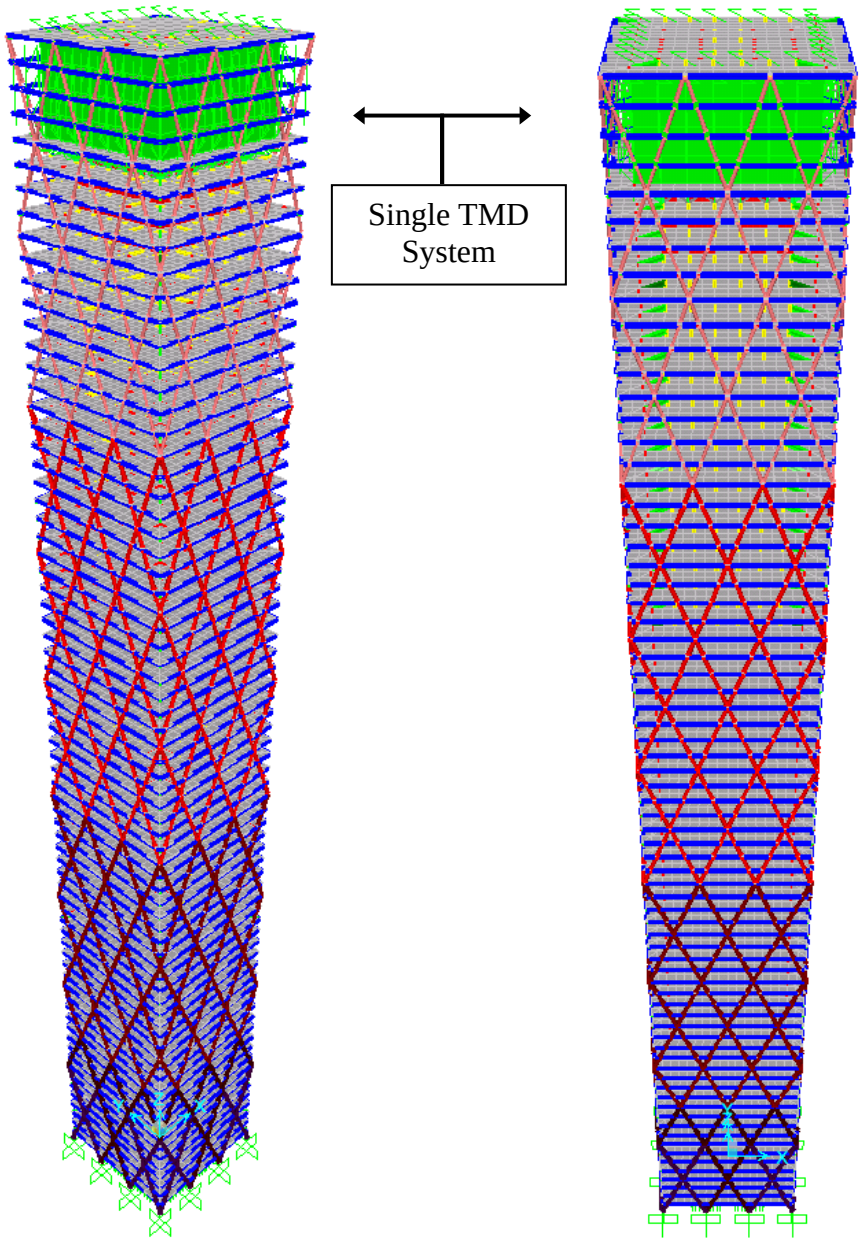

Figure 3.13. Reference building model in SAP2000: (a) eagle-eye view, (b) front view.

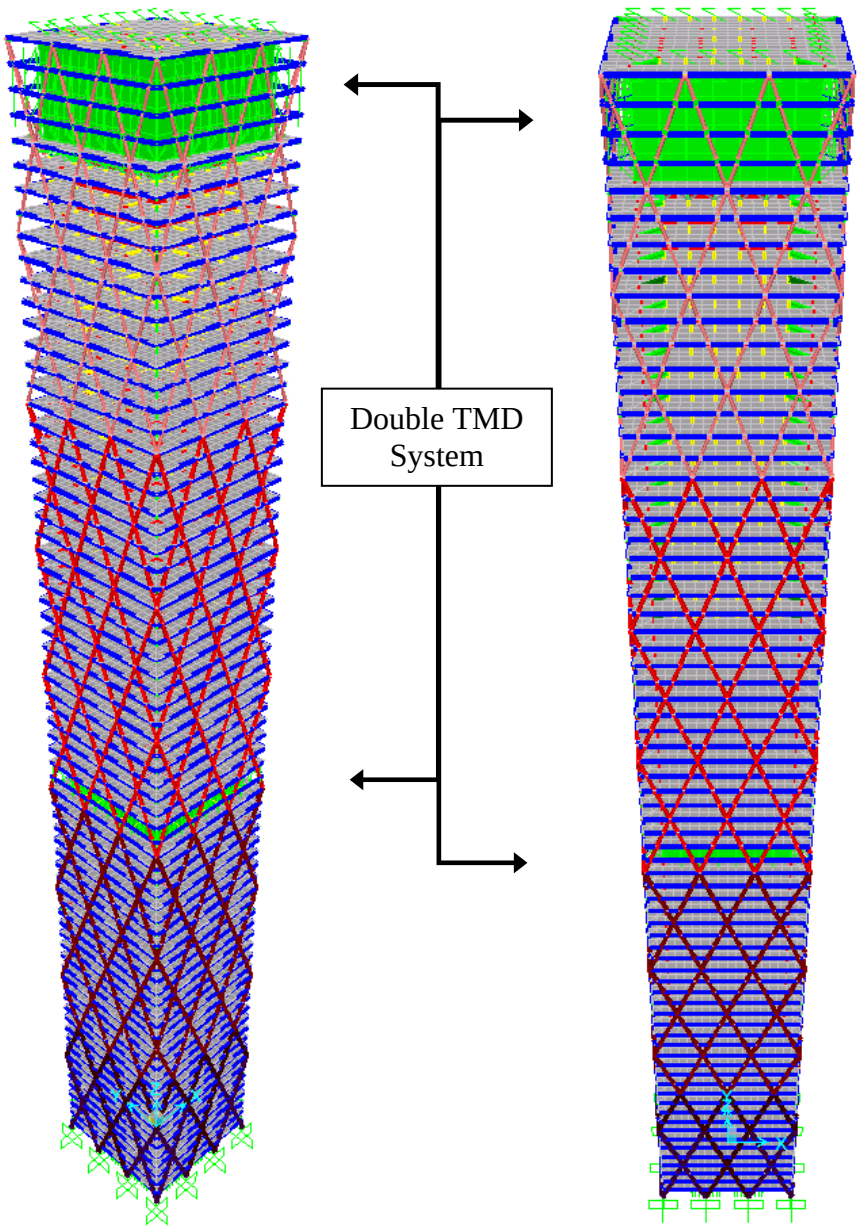

Figure 3.14. Building model with double friction TMD units: (a) eagle-eye view, (b) front view.

3.3.3. LINK PROPERTIES

The material nonlinearity in this model was only explicitly considered in the links provided between the TMD and the main structure. The properties assigned to these links are described in this section.

A. FRICTION PENDULUM ISOLATORS

A total of 392 links were placed in the model for each TMD unit. In the definition of the links for the friction pendulum isolators, the model by Scheller and Constantinou (1999) was chosen as the preferred model. Full details on the behavior of the FPS modeled using this friction isolator are available in SAP2000 analysis reference manual and Scheller and Constantinou (1999). In the model development, the positive local axis 1 is parallel to the positive global Z axis, the positive local 2 axis is parallel to the positive global X axis, and the positive local 3 axis is parallel to the positive global Y axis, k_e is effective stiffness and k is stiffness. Local and global axes can be identified by Figure 2.1 and Figure 3.13, respectively. The properties for all friction isolator links in the reference model are:

- Linear analysis properties:
  - k_e $\{U_1\}$ = 3500 KN/mm
  - k_e $\{U_2, U_3\}$ = 0.2 KN/mm
  - k_e $\{R_1\}$ = 1130000 KN/mm
- Nonlinear analysis properties:
  - k $\{U_1\}$ = 3500 KN/mm
  - k $\{U_2, U_3\}$ = 5.5 KN/mm
  - Friction coefficient, f_{slow} $\{U_2, U_3\}$ = 0.04
  - Friction coefficient, f_{fast} $\{U_2, U_3\}$ = 0.06
  - Rate parameter $\{U_2, U_3\}$ = 0.0429 sec/mm
  - Radius of sliding surface $\{U_2, U_3\}$ = 6000 mm

B. LINEAR SPRINGS

For top absorbers shown in Figure 3.6 and Figure 3.8, the positive local axis 1 is parallel to the negative global Z axis. On the other hand, for the second TMD in the double TMD system, the horizontal absorbers have local axis 1 parallel to their axial directions. The properties for all linear springs are:

- Linear analysis properties:
  - k_e $\{U_1\}$ = 1 KN/mm

C. GAPS

Gap links were provided in parallel with the absorber links. For the gap links, the positive local axis 1 is parallel to their axial directions. Gap1 is the gap type assigned to the horizontal shock absorbers surrounding the TMD, while the Gap2 links are correspond to the beam members which the absorbers attach to. The stiffness of the Gap2 links is defined using simple axial stiffness equation:

$$k = {EA}/{L} \tag{4.1}$$

with E = 199,948 MPa, A = 30,500 mm^2, and L is the length of the beam. Thus, the stiffness of Gap2 is proportional to the length of the beam members. The properties assigned to the gaps are:

- Nonlinear analysis properties:
  - Gap1, k $\{U_1\}$ = 1 kN/mm
  - Gap2, k $\{U_1\}$ = 2440 kN/mm
  - Gap1, opening = 500 mm
  - Gap2, opening = 1500 mm

In the corners of the buildings, the absorbers and gaps had to be defined in a diagonal. For the diagonal gap links, length of the beams and gaps are multiplied by $\sqrt{2}$. Thus, the properties for diagonal gap links are:

- Gap1, k $\{U_1\}$ = 1 kN/mm
- Gap2, k $\{U_1\}$ = 1725 kN/mm
- Gap1, opening = 707.1 mm
- Gap2, opening = 2121.3 mm

The combination of Gap1 and Gap2 links allows for the definition of the axial force – axial displacement behavior shown in Figure 3.5.

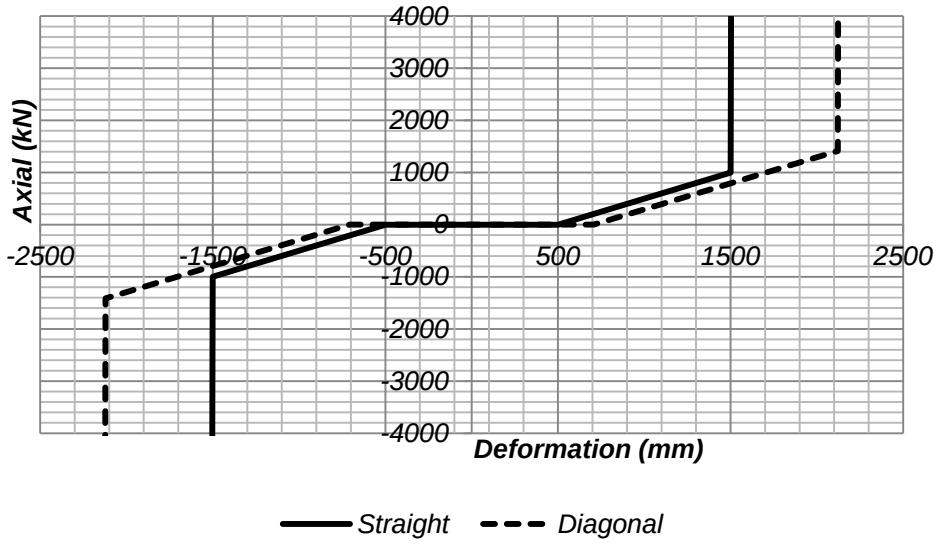

Figure 3.15. Force-deformation relationship of horizontal shock absorbers.

3.4. NUMERICAL TRIALS

Tuning the TMD unit is not an easy task as there are many parameters that need to be adjusted. Because of that, the author at this thesis did some numerical trials for determining which parameters should be addressed in the parametric study. Each possible parameter was tested and evaluated to see how perturbations of these parameters affect the results. This step is really important knowing that there are already many parameters used in friction pendulum isolators only, as varying all the values are not feasible.

3.4.1. STRUCTURAL DAMPING

For applying structural damping of 2% to each mode of vibrations, the author tried two methods, that is: mass and stiffness proportional (Rayleigh) damping and constant damping. Overall, both methods provide for sufficient damping, which means that the time-history response due to the seismic loads is damped. However, two different results are attained: the Rayleigh damping method resulted in much bigger responses than constant damping method.

Initially, Rayleigh damping method was selected. The main reason for this selection was to provide larger damping to the higher modes to avoid spurious high frequencies that can create numerical instabilities and convergence issues. The author thus specified the first reference period as $1.5 \times$ the first mode of vibrations of the building and 0.1 sec as the second period of reference. Comparison of the results obtained using Rayleigh damping and those obtained using the constant damping method set at 2% shows approximately 30% larger base shears compared to the constant damping method. The constant damping method is the one chosen in all analyses results shown herein. Furthermore, the choice of constant damping also provides for more reasonable outputs for designing the steel diagrid members.

3.4.2. LINK PARAMETERS

There are three kinds of links that are used for this research, that is, friction pendulum isolators, linear springs, and gap links. However, only friction coefficient of the friction pendulum isolators is addressed in the parametric study discussed later. The top linear springs and gap links are not changed throughout the numerical models, and preliminary study was performed to validate the assumption used for these links.

The linear springs at the top of the TMD unit is installed to prevent the impact due to overturning. Thus, changing the axial stiffness of those springs will not give considerable effect to the building’s seismic performance. The same can be said for the gap links which represents the horizontal shock absorbers that surrounding the TMD. The 1 meter thick shock absorbers (rubber) are used to absorb the movement of

the TMD, thus preventing it from hitting the exterior diagrid and inner concrete core. Increasing the gap to allow larger TMD movements might provide significant change to the results, but the author chose not to do so due to space limitations of the real-world prototype structure.

In the friction isolator link, there are 2 parameters that have the largest effect on the responses, which are: friction coefficients and radius of sliding surface. However, only the friction coefficients are included in parametric studies. The author did some numerical testing of the radius of sliding in order to find the optimal values. The building base shears were used to tune the radius of the FPS. It turned out that an infinite sliding radius (flat surface) yielded the smallest base shears. The downside was it produced significant residual displacements of the TMD units at the end of the earthquake analyses, which means the TMD was not returned to its initial undeformed position, which would require the use of at least an actuation device to force the TMD to go back to its initial position. Because the author want to keep the mass damper as a passive system, the flat surface option was not chosen. On the other hand, there are no notable differences in peak base shears when using sliding radius of 6 to 10 meters. However, increasing the sliding radius will also increase the damping effect during the free vibration phase. In the end, sliding radius of 6 m is chosen since it provides acceptable damping and since it can be manufactured by most of friction pendulum isolator vendors.

3.4.3. LOCATION AND MASS OF THE TMD EFFECTS

Locations of the TMDs were decided based on the mode shapes of the prototype building. For example, mode 1 (see Figure 3.16) has the largest displacement at the top of the building, and therefore the TMD unit was placed at the top of the building. The top placement of the TMD also affects the contribution of mode 2, slightly. Utilization of a double TMD system aims at reducing the contribution of mode 2. This provides significant differences in the measured response as compared to reference structure and worthy to be shown in this report.

In addition, solution for location of the second TMD was also explored to reduce the contribution of mode 3 to the response. From the shape of mode 3 shown in Figure 3.16, TMD units were placed in 1/3 (story 24) and 2/3 (story 48) of the building height which – from visual observation – show the largest lateral displacements. The two TMD units then were tuned to the third mode by making their fundamental periods close to the third fundamental period of the main structure. This solution provided notable improvements in base shears generated from some earthquake acceleration time series. However, overall it was not deemed effective on the majority of the tested acceleration time histories. Hence, the author decided to not include this solution in the subsequent parametric study. Utilization of 3 TMD units to reduce the contributions of the three major mode shapes of the main structure is, theoretically, also a possible option, but knowing the increased cost and an increase in number of floors that would need to be sacrificed in this study, the author decided to not include solutions with more than two TMD units.

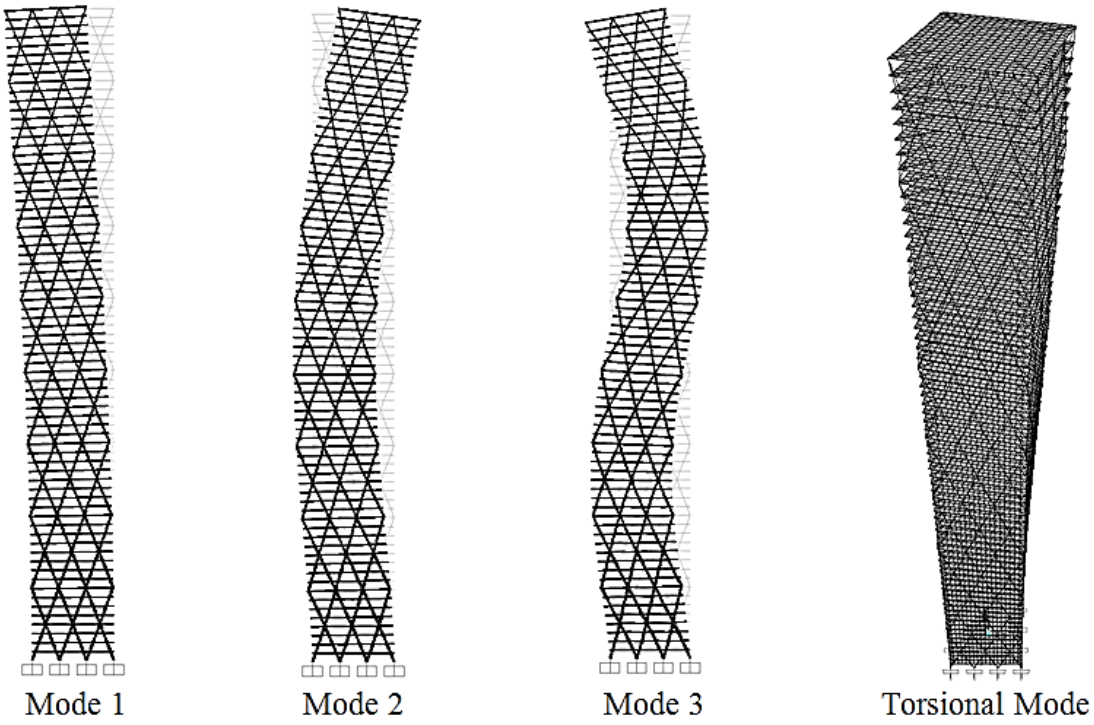

Figure 3.16. Main mode shapes of the prototype building structure.

Last thing to note, due to the lowest usable frequencies used for the earthquake acceleration time series in the analysis, the mass of TMD could only be increased by 20% because the first natural frequency of the reference structure is already close to the lowest usable frequencies. Thus, in the subsequent parametric study, the mass perturbation from the reference model is ±20%.

3.5. PARAMETRIC STUDY

There are 4 variables addressed in this research: friction coefficients of the TMD unit, height distribution of the TMD, mass of the TMD, and number of TMD units. In each model, 7 shallow crustal motions and 7 subduction zone motions are applied to the models. Each of the crustal motions has three components of accelerations time series and they are assigned randomly, that is the fault normal (FN) acceleration record in the X-direction, fault parallel (FP) record in the Y-direction, and vertical in the Z-direction. However, the subduction motions only have one component motions which are applied to both horizontal directions. The properties of each of earthquake record are listed at section 3.2. The perturbations from reference models are shown in Figure 3.17. In all, the number of nonlinear time history performed for this parametric study is 98 analyses.

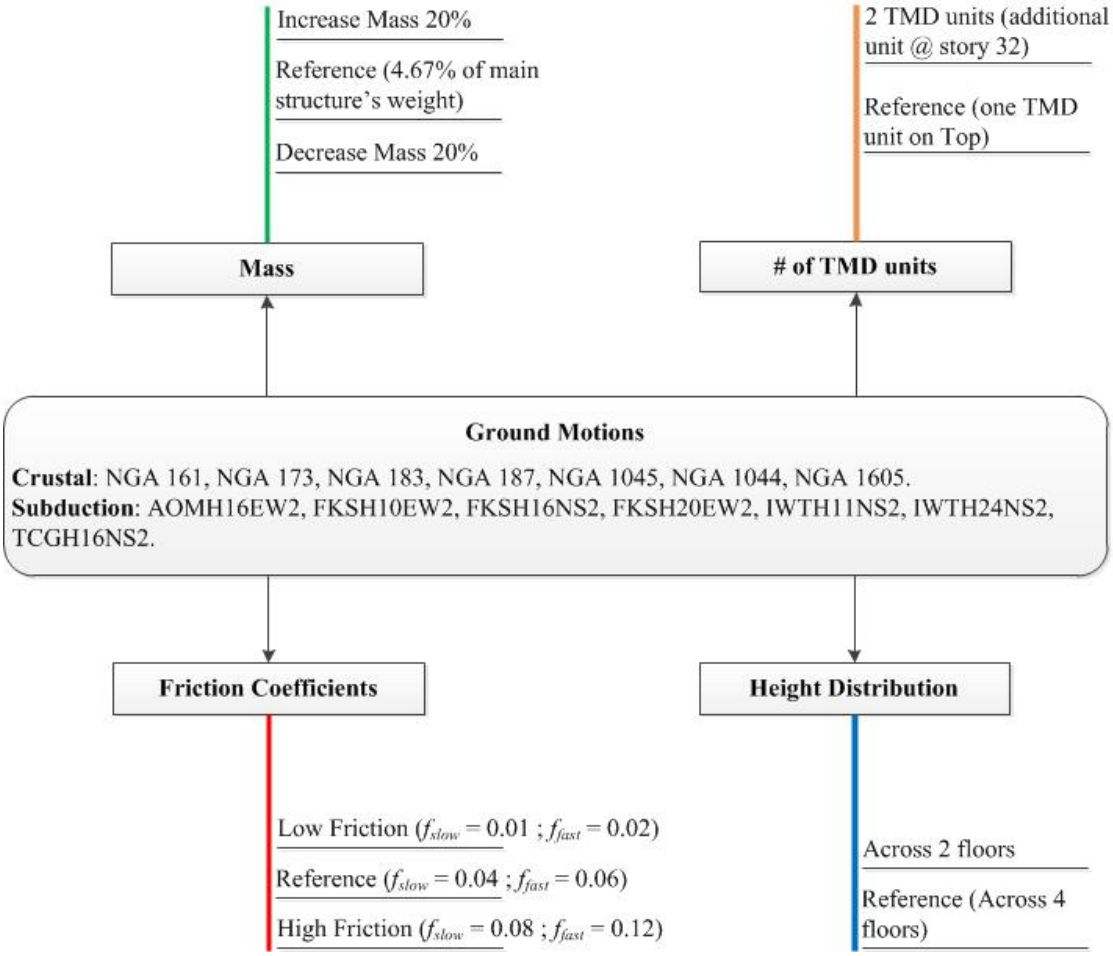

Figure 3.17 Schematic view of variables address in this research.

CHAPTER 4. PROTOTYPE BUILDING DESIGN

4.1. STRUCTURAL DESIGN CRITERION

4.1.1. STANDARD AND CODES

The following standards and codes are used in this works:

- Minimum Design Loads for Buildings and Other Structures, ASCE/SEI 7-10 by American Society of Civil Engineers, 2010.
- Specification for Structural Steel Buildings, ANSI/AISC 360-05 by ANSI, 2005.
- Building Code Requirements for Structural Concrete, ACI 318-11 by A. C. I. Committee (2011)

4.1.2. MATERIAL CRITERIA

Nominal values that are used for this building are:

- Concrete slab : 4000 psi ($f'c$ = 27.6 MPa)
- Concrete wall : 5000 psi ($f'c$ = 34.5 MPa)
- Reinforcing steel : A615Gr60 (fy = 413 MPa)
- Structural steel : A992Fy50 (fy = 345 MPa)

4.2. STRUCTURAL LOADING

All loading are done in accordance to ASCE 7-10 (American Society of Civil Engineers 2010).

4.2.1. DEAD LOADS AND SUPERIMPOSED DEAD LOADS

Dead Loads (DL) of structural members and additional dead loads consist of:

- Reinforced concrete : 23.6 kN/m^3
- Steel : 77.0 kN/m^3

- Partition walls : 0.96 kN/m^2
- Ceiling : 0.1 kN/m^2
- Flooring : 1.58 kN/m^2
- Waterproofing membrane : 0.07 kN/m^2

4.2.2. LIVE LOADS

Live loads (LL) are applied to each floor, they consist of:

- Typical floor (office load) : 2.4 kN/m^2
- Roof load : 0.96 kN/m^2
- Elevator machine : 1.33 kN

4.2.3. SNOW LOADS

Snow loads are assigned to the building roof, assuming ordinary flat roof snow load (ASCE 7-10 equation 7.3-1):

$$p_f = 0.7 C_e C_t I_s p_g = 0.738 \text{ kN/m}^2 \quad (3.1)$$

where:

- C_e (exposure factor) = 1.0 (terrain category C and partially exposed).
- C_t (thermal factor) = 1.0.
- I_s (Importance factor) = 1.1 (risk category III).
- p_g (ground snow load) assume 20 lb/ft^2 = 0.958 kN/m^2.

4.2.4. EARTHQUAKE LOAD

Soil type D is assumed. By using java web tool application provided by U.S. Geological Survey (2013), the following design response spectrum is generated:

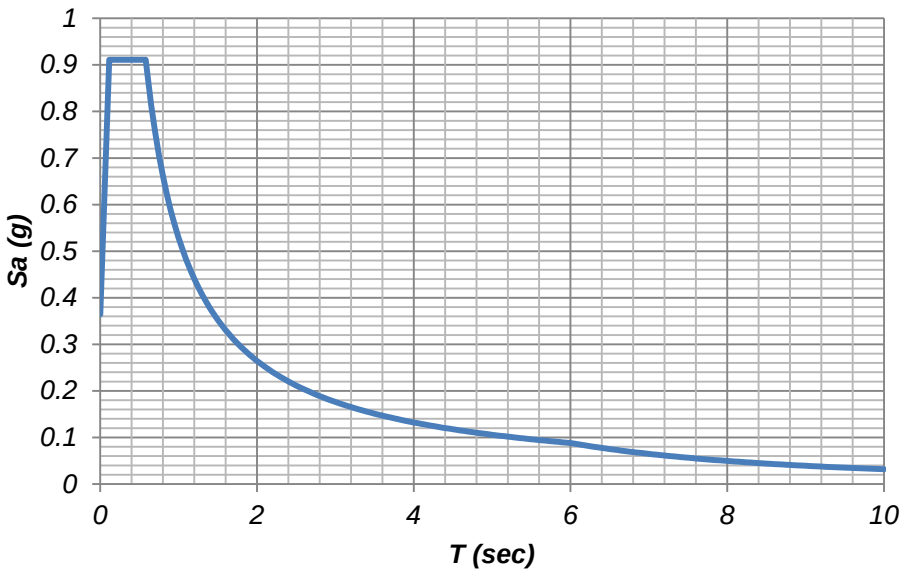

Figure 4.1. Design response spectrum.

where the controlling parameters that define the response spectrum are:

- S_{ds} = 0.911 g
- S_{d1} = 0.529 g
- T_L = 6 second

It is worth noting that the preliminary design is done using the response spectrum method only for prototype building design. The design verifications for all other building designs (with a single TMD and double TMD) were carried through nonlinear time history analysis.

4.2.5. WIND LOAD

The wind loads are applied to the diaphragm of each floor. SAP2000 uses the directional procedure that can be applied to most building types. These following parameters are used for computing the design wind load:

- Windward coefficient (Cp) = 0.8
- Leeward coefficient (Cp) = 0.5

- Wind speed = 110 mph
- Exposure Type = 1.0
- Gust Factor = 0.85
- Directionality Factor (K_d) = 0.85

It is worth nothing that for very tall buildings wind tunnel testing should be performed to verify these wind load coefficients.

4.2.6. LOAD COMBINATIONS

Load combinations that are used in the prototype building design are based on ASCE 7-10 section 2.3.2:

- 1.4 (DL+SDL)
- 1.2 (DL+SDL) + 1.6 LL + 0.5 (L_r or S)
- 1.2 (DL+SDL) + 1.6 (L_r or S) + (LL or 0.5 W)
- 1.2 (DL+SDL) + 1.0 W + LL + 0.5 (L_r or S)
- (1.2 + E_V) (DL + SDL) + 1.0 E + LL + 0.2 S
- 0.9 (DL + SDL) + 1.0 W
- (0.9 – E_V) (DL + SDL) + 1.0 E

With E_V (vertical seismic load effect) is ±0.1, and where:

DL	= Dead Load	*S*	= Snow load
SDL	= Super imposed dead load	*W*	= Wind load
LL	= Live load	*E*	= Earthquake load
Lr	= Roof live load		

4.3. STRUCTURAL ANALYSIS

The following are preliminary analyses to identify the behavior of the prototype diagrid building and determine if the building is adequate as a basic input of this study.

4.3.1. NATURAL PERIOD AND MODE SHAPES OF THE STRUCTURE

To fulfill the requirements of 90% mass participation ratios, 24 modes are used for the basic diagrid model while 48 modes are used for the diagrid model with TMD units. The latter has more modes due to additional modes generated by TMD. Figure 3.16 shows the four modes of interest that characterize the building behavior under earthquake events. Those modes are holding the biggest percentage of mass participation factors on each major direction except UZ (vertical direction). Table 4.1 shows the first seven vibration periods of the building with their respective modal participation factors that represent the four main mode shapes of the building. The total mass participation ratios for each directions of the prototype building model accounting for the 24 modes are:

- U_X = 95.87% > 90%
- U_Y = 96.03% > 90%
- U_Z = 86.68%
- R_X = 99.96% > 90%
- R_Y = 99.95% > 90%
- R_Z = 94.29% > 90%

Table 4.1. Fundamental period of the building and mass participation ratios

#	Period (sec)	Modal Participating Mass Ratios						Notes
		UX	UY	UZ	RX	RY	RZ	
1	6.546	0.00%	**59.91%**	0.00%	**96.80%**	0.00%	0.00%	Mode 1
2	6.487	**60.04%**	0.00%	0.00%	0.00%	**96.86%**	0.00%	
3	1.549	0.00%	**20.69%**	0.00%	**2.77%**	0.00%	0.00%	Mode 2
4	1.546	**20.79%**	0.00%	0.00%	0.00%	**2.73%**	0.00%	
5	1.531	0.00%	0.00%	0.00%	0.00%	0.00%	**73.36%**	Torsion
6	0.740	**6.91%**	0.00%	0.00%	0.00%	**0.29%**	0.00%	Mode 3
7	0.732	0.00%	**7.04%**	0.00%	**0.30%**	0.00%	0.00%	

4.3.2. BASE AND STORY SHEAR

Base shears that are attained from the seismic loads provided by ASCE 7-10 design response spectrum are V_x = 142,437 kN and V_y = 143,175 kN. The results from each horizontal direction are not identical due to the difference in shear wall opening at related directions as well as slight differences in the floor openings in either direction. The diagrid absorbs base shear V_x of 116229 kN and V_y of 28408.88 kN which are approximately 80% of the total. Story shear in X and Y directions can be seen in Figure 4.2.

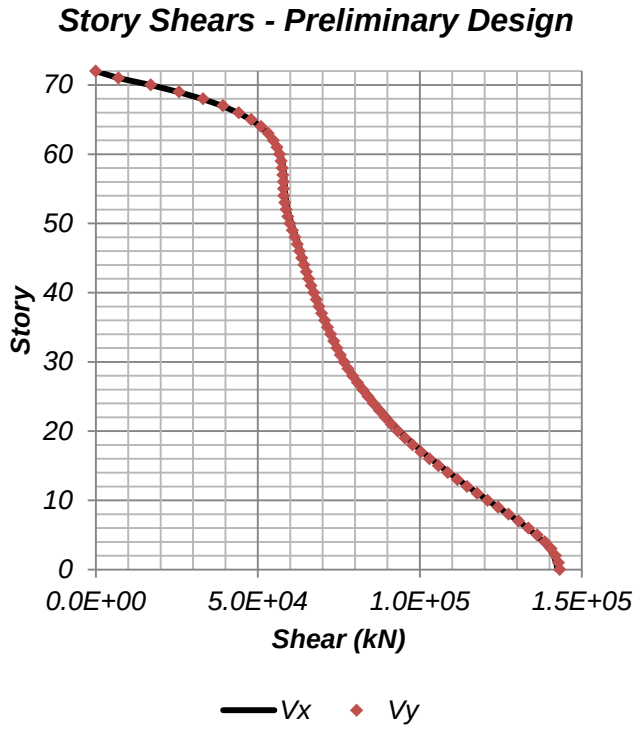

Figure 4.2. Story Shears – Preliminary Design.

4.4. STRUCTURAL DESIGN

This section shows the dimensions and sizes of each structural component as a result of preliminary design. Reinforcements for inner concrete core and floor slabs are not designed in this study, even though values of axial load in walls is relatively

low, which allows for quick preliminary design that allows for confidence in the dimensions used. R- factors are not – existent for this structural type. However, accounting for the properties of steel and with future testing to verify the assumptions performed herein the following parameters that are used for the steel design preferences as assigned in SAP2000:

- R = 8
- Phi (bending) = 0.9
- Phi (compression) = 0.9
- Phi (tension-yielding) = 0.9
- Phi (tension-fracture) = 0.75
- Phi (shear) = 0.9
- Phi (torsion) = 0.9

4.4.1. STEEL PROFILE DIMENSION

The structural steel members are divided into groups that can be seen in Figure 3.1. Wide flange (WF) and H-sections are used in beams, whereas the diagonal columns of diagrid are using custom-made circular hollow sections (CHS). The dimensions obtained from this design are:

- B1
  Typical dimension : H – 500X500X30X60
- B2
  Typical dimension : WF – 600x400x12x30
  Story 32, 40, 48, 51, 56, 64
  : WF – 600x400x12x30 and H-600X600X20X40
- B3
  Typical dimension : WF – 800X300X14X22
  Story 32, 48, 64 : WF – 800X300X14X26
  Story 56 : WF – 900X350X14X25

- B4

  Typical Dimension : WF – 200X150X6X9

- DG1

  Story 1 – 8 : CHS – 1200X120 and CHS – 1200X100

  Story 8 – 12 : CHS – 1200X100

  Story 12 – 32 : CHS – 1000X100

  Story 32 – 56 : CHS – 850X75

  Story 56 – 72 : CHS – 600X50

4.4.2. STRUCTURAL CONCRETE COMPONENT SIZES

All floor slabs have an effective thickness of 130 mm. It is assumed that a concrete slab on steel deck is used. The inner concrete core has thickness of 450 mm from bottom to top of the building.

CHAPTER 5. SIMULATIONS AND ANALYSIS RESULTS

5.1. ANALYSIS METHODOLOGY

5.1.1. ANALYSIS PARAMETERS

The nonlinear finite element analysis of the models is divided by three stages. In the first stage a linear static analysis of gravity loads and wind loads (for design verification only) are applied to the building. The second stage involves performing an eigen analysis to compute natural frequency, mode shapes, and mass participation ratios of the building models. The third and final stage includes the nonlinear time-history analysis for computing the response of the building to the applied earthquake acceleration ground motions time-histories. Duration of analysis of 60 seconds and integration time step of 0.005 second is used for computing the building's responses to shallow crustal motions. On the other hand, the building's responses to subduction earthquake records are computed with analysis duration of 350 seconds and integration time step of 0.01 second. These time steps used herein provide sufficient accuracy in the displacement responses for the structure with the large fundamental periods.

5.1.2. PROCESSING RESPONSE PARAMETERS

Response parameters that are monitored in this analysis are:

- Vibration characteristics (modal parameters)
- Base reactions
- Story reactions
- Floor displacements
- Inter-story drifts
- Floor absolute accelerations
- Link reactions
- Demand to capacity ratios of diagrid steel members

In the following sub-sections, the methods and equations for each response parameter used in this study is presented. The definitions and equations presented follow descriptions in Barbosa (2011), but are shown here for completeness.

A. VIBRATION CHARACTERISTICS

These correspond to the natural period of the building, building mode shapes, and mass participation of each mode. These parameters provide information on the behavior of the building in dynamic analysis, thus can be used to estimate the outcome of the building's seismic performance under lateral loads.

B. BASE REACTIONS

For base reactions, the total structural response envelopes are monitored.

- Base shear envelopes

  These are defined as the peak of the base shear values relative to each horizontal direction, explained by the following equation:

$$V_{B_{x,y}} = \max\left|V_{x,y}(t)\right| \tag{5.1}$$

- Overturning bending moment envelopes

  These are defined as the peak of the absolute overturning bending moment values relative to each horizontal direction:

$$M_{B_{x,y}} = \max\left|M_{x,y}(t)\right| \tag{5.2}$$

C. STORY AND FLOOR RESPONSES

For story and floor responses, both envelope responses are monitored and also geometric means of the envelope responses due to shallow crustal and subduction zone motions are also calculated. Story reactions of the whole structure are also included in this evaluation.

- Story shear envelopes

  These are defined as the peak of the positive and negative story shear values at each horizontal direction. For each ground motion, the story shear envelopes are given by:

$$\boldsymbol{V}^{+}_{x,y} = \left\{V_{1}{}^{+}_{x,y}, V_{2}{}^{+}_{x,y}, V_{3}{}^{+}_{x,y}, \cdots, V_{n}{}^{+}_{x,y}\right\}^{T}, n = \text{\# story levels} \quad (5.3)$$

$$\boldsymbol{V}^{-}_{x,y} = \left\{V_{1}{}^{-}_{x,y}, V_{2}{}^{-}_{x,y}, V_{3}{}^{-}_{x,y}, \cdots, V_{n}{}^{-}_{x,y}\right\}^{T}, n = \text{\# story levels} \quad (5.4)$$

  where:

$$V^{+}_{i_{x,y}} = \max\left\{V_{i_{x,y}}(t)\right\}, i = \{1, \cdots, n\} \quad (5.5)$$

$$V^{-}_{i_{x,y}} = \min\left\{V_{i_{x,y}}(t)\right\}, i = \{1, \cdots, n\} \quad (5.6)$$

- Geometric means of story shears

  These are the geometric means of peak story shears due to each ground motion for both horizontal directions, given by:

$$\boldsymbol{V}_{GM} = \left\{V_{1_{GM}}, V_{2_{GM}}, V_{3_{GM}}, \cdots, V_{n_{GM}}\right\}, n = \text{\# of story levels} \quad (5.7)$$

  $V_{i_{GM}}$ is the geometric means of story shears in both horizontal directions, according to:

$$V_{i_{GM}} = \sqrt{V_{i_{GMx}} \cdot V_{i_{GMy}}}, i = \{1, \cdots, n\} \quad (5.8)$$

  where $V_{i_{GMx}}$ and $V_{i_{GMy}}$ are the geometric means of the absolute maximum story shears due to each ground motion, given by:

$$V_{i_{GMx}} = \sqrt[K]{V_{i_{EQ1x}} V_{i_{EQ2x}} V_{i_{EQ3x}} \cdots V_{i_{EQKx}}}, K = \text{Earthquake record} \quad (5.9)$$

$$V_{i_{GMy}} = \sqrt[K]{V_{i_{EQ1y}} V_{i_{EQ2y}} V_{i_{EQ3y}} \cdots V_{i_{EQKy}}}, K = \text{Earthquake record} \quad (5.10)$$

It should be noted that geometric means are computed instead arithmetic means since responses have been shown (by other authors) to follow log-normal distributions and the geometric means computed here corresponds to the median (central value) of the responses.

- Story moment envelopes

  These are the peak of the positive and negative story moment values at each horizontal direction:

$$\boldsymbol{M}^{+}_{x,y} = \left\{M_{1}{}^{+}_{x,y}, M_{2}{}^{+}_{x,y}, M_{3}{}^{+}_{x,y}, \cdots, M_{n}{}^{+}_{x,y}\right\}^{T}, n = \text{\# story levels} \quad (5.11)$$

$$\boldsymbol{M}^{-}_{x,y} = \left\{M_{1}{}^{-}_{x,y}, M_{2}{}^{-}_{x,y}, M_{3}{}^{-}_{x,y}, \cdots, M_{n}{}^{-}_{x,y}\right\}^{T}, n = \text{\# story levels} \quad (5.12)$$

  where:

$$M_{i}{}^{+}_{x,y} = \max\left\{M_{i_{x,y}}(t)\right\}, i = \{1, \cdots, n\} \quad (5.13)$$

$$M_{i}{}^{-}_{x,y} = \min\left\{M_{i_{x,y}}(t)\right\}, i = \{1, \cdots, n\} \quad (5.14)$$

- Geometric means of story moments

  These are the geometric means of peak story moment due to each ground motion for both horizontal directions, given by:

$$\boldsymbol{M}_{GM} = \left\{M_{1_{GM}}, M_{2_{GM}}, M_{3_{GM}}, \cdots, M_{n_{GM}}\right\}, n = \text{\# story levels} \quad (5.15)$$

  $M_{i_{GM}}$ is the geometric means of story moments in both horizontal directions, according to:

$$M_{i_{GM}} = \sqrt{M_{i_{GMx}} \cdot M_{i_{GMy}}}, i = \{1, \cdots, n\} \quad (5.16)$$

  where $M_{i_{GMx}}$ and $M_{i_{GMy}}$ are the geometric means of the absolute maximum story moments due to each ground motion, given by:

$$M_{i_{GMx}} = \sqrt[K]{M_{i_{EQ1x}} M_{i_{EQ2x}} M_{i_{EQ3x}} \cdots M_{i_{EQKx}}},\ K = \text{Earthquake record} \quad (5.17)$$

$$M_{i_{GMy}} = \sqrt[K]{M_{i_{EQ1y}} M_{i_{EQ2y}} M_{i_{EQ3y}} \cdots M_{i_{EQKy}}},\ K = \text{Earthquake record} \quad (5.18)$$

D. FLOOR DISPLACEMENTS

Envelope responses and the geometric means of envelope responses are evaluated. The floor displacements are measured from the centroid of the building plan.

- Floor displacement envelopes

  The peak of positive and negative displacements of each floor levels, are given by:

  $$\Delta^{+}_{x,y} = \left\{\Delta_1{}^{+}_{x,y}, \Delta_2{}^{+}_{x,y}, \Delta_3{}^{+}_{x,y}, \cdots, \Delta_n{}^{+}_{x,y}\right\}^T,\ n = \#\text{ floor level} \quad (5.19)$$

  $$\Delta^{-}_{x,y} = \left\{\Delta_1{}^{-}_{x,y}, \Delta_2{}^{-}_{x,y}, \Delta_3{}^{-}_{x,y}, \cdots, \Delta_n{}^{-}_{x,y}\right\}^T,\ n = \#\text{ floor level} \quad (5.20)$$

  where:

  $$\Delta_i{}^{+}_{x,y} = \max\left\{\Delta_{i_{x,y}}(t)\right\},\ i = \{1, \cdots, n\} \quad (5.21)$$

  $$\Delta_i{}^{-}_{x,y} = \min\left\{\Delta_{i_{x,y}}(t)\right\},\ i = \{1, \cdots, n\} \quad (5.22)$$

- Geometric means of floor displacements

  These are the geometric means of peak floor displacements due to each ground motion for both horizontal directions, given by:

  $$\Delta_{GM} = \left\{\Delta_{1_{GM}}, \Delta_{2_{GM}}, \Delta_{3_{GM}}, \cdots, \Delta_{n_{GM}}\right\},\ n = \text{floor level} \quad (5.23)$$

  $\Delta_{I_{GM}}$ is the geometric means of floor displacements in both horizontal directions, according to:

$$\Delta_{i_{GM}} = \sqrt{\Delta_{i_{GMx}} \cdot \Delta_{i_{GMy}}}\,,\ i = \{1, \cdots, n\} \tag{5.24}$$

where $\Delta_{n_{GMx}}$ and $\Delta_{n_{GMy}}$ are the geometric means of the absolute maximum floor displacements due to each ground motion, given by:

$$\Delta_{i_{GMx}} = \sqrt[K]{\Delta_{i_{EQ1x}} \Delta_{i_{EQ2x}} \Delta_{i_{EQ3x}} \cdots \Delta_{i_{EQKx}}},\ K = \text{Earthquake record} \tag{5.25}$$

$$\Delta_{i_{GMy}} = \sqrt[K]{\Delta_{i_{EQ1y}} \Delta_{i_{EQ2y}} \Delta_{i_{EQ3y}} \cdots \Delta_{i_{EQiy}}},\ K = \text{Earthquake record} \tag{5.26}$$

E. INTER-STORY DRIFTS (IDR)

Response history, envelopes responses, and geometric means of the envelope responses are evaluated. IDR for each floor are calculated by:

$$\theta_{i_{x,y}}(t) = \frac{\Delta_{i_{x,y}}(t) - \Delta_{i-1_{x,y}}(t)}{h_i - h_{i-1}},\ n = \text{floor level } i = \{1, \cdots, n\} \tag{5.27}$$

where h_n is the height of floor n from the base.

- IDR envelopes

  The peak of positive and negative of IDR of each floor levels are defined by the following equations:

$$\theta^{+}_{x,y} = \left\{\theta_{1}^{+}_{x,y}, \theta_{2}^{+}_{x,y}, \theta_{3}^{+}_{x,y}, \cdots, \theta_{n}^{+}_{x,y}\right\}^{T},\ n = \#\text{ floor level} \tag{5.28}$$

$$\theta^{-}_{x,y} = \left\{\theta_{1}^{-}_{x,y}, \theta_{2}^{-}_{x,y}, \theta_{3}^{-}_{x,y}, \cdots, \theta_{n}^{-}_{x,y}\right\}^{T},\ n = \#\text{ floor level} \tag{5.29}$$

  where:

$$\theta_{i}^{+}_{x,y} = \max\left\{\theta_{i_{x,y}}(t)\right\} \tag{5.30}$$

$$\theta_{i}^{-}_{x,y} = \min\left\{\theta_{i_{x,y}}(t)\right\} \tag{5.31}$$

- Geometric means of IDRs

  These are the geometric means of peak IDRs due to each ground motion for both horizontal directions, given by:

$$\boldsymbol{\theta}_{GM} = \{\theta_{1_{GM}}, \theta_{2_{GM}}, \theta_{3_{GM}}, \cdots, \theta_{n_{GM}}\},\ n = \#\text{ floor levels} \tag{5.32}$$

  $\theta_{n_{GM}}$ is the geometric means of IDRs in both horizontal directions, according to:

$$\theta_{i_{GM}} = \sqrt{\theta_{i_{GMx}} \cdot \theta_{i_{GMy}}},\ i = \{1, \cdots, n\} \tag{5.33}$$

  where $\theta_{i_{GMx}}$ and $\theta_{i_{GMy}}$ are the geometric means of the absolute maximum IDRs due to each ground motion, given by:

$$\theta_{i_{GMx}} = \sqrt[K]{\theta_{i_{EQ1x}}\theta_{i_{EQ2x}}\theta_{i_{EQ3x}} \cdots \theta_{i_{EQKx}}},\ K = \text{Earthquake record} \tag{5.34}$$

$$\theta_{i_{GMy}} = \sqrt[K]{\theta_{i_{EQ1y}}\theta_{i_{EQ2y}}\theta_{i_{EQ3y}} \cdots \theta_{i_{EQKy}}},\ K = \text{Earthquake record} \tag{5.35}$$

F. FLOOR ABSOLUTE ACCELERATIONS

For this parameter, envelope responses are monitored and geometric means of the envelope responses due to shallow crustal and subduction zone motions are also calculated. Floor absolute accelerations are measured from the point at the middle of the building plan.

- Floor absolute acceleration envelopes

  These are the peak of positive and negative of the absolute accelerations of each floor levels and are given by:

$$\ddot{U}^{+}_{x,y} = \left\{\ddot{U}_{1}^{+}{}_{x,y}, \ddot{U}_{2}^{+}{}_{x,y}, \ddot{U}_{3}^{+}{}_{x,y}, \cdots, \ddot{U}_{n}^{+}{}_{x,y}\right\},\ n = \#\text{ story levels} \tag{5.36}$$

$$\ddot{U}^{-}_{x,y} = \left\{\ddot{U}_{1}^{-}{}_{x,y}, \ddot{U}_{2}^{-}{}_{x,y}, \ddot{U}_{3}^{-}{}_{x,y}, \cdots, \ddot{U}_{n}^{-}{}_{x,y}\right\},\ n = \#\text{ story levels} \tag{5.37}$$

where:

$$\ddot{U}_{i_{x,y}}^{+} = \max\left\{\ddot{U}_{n_{x,y}}(t)\right\}, i = \{1, \cdots, n\} \quad (5.38)$$

$$\ddot{U}_{i_{x,y}}^{-} = \min\left\{\ddot{U}_{n_{x,y}}(t)\right\}, i = \{1, \cdots, n\} \quad (5.39)$$

- Geometric means of floor absolute accelerations

  These are the geometric means of peak floor absolute accelerations due to each ground motion for both horizontal directions, given by:

$$\ddot{U}_{GM} = \left\{\ddot{U}_{1_{GM}}, \ddot{U}_{2_{GM}}, \ddot{U}_{3_{GM}}, \cdots, \ddot{U}_{n_{GM}}\right\}, n = \text{\# floor levels} \quad (5.40)$$

  $\ddot{U}_{i_{GM}}$ is the geometric means of floor absolute accelerations in both horizontal directions, according to:

$$\ddot{U}_{i_{GM}} = \sqrt{\ddot{U}_{i_{GMx}} \cdot \ddot{U}_{i_{GMy}}}, i = \{1, \cdots, n\} \quad (5.41)$$

  where $\ddot{U}_{i_{GMx}}$ and $\ddot{U}_{i_{GMy}}$ are the geometric means of the absolute maximum floor absolute accelerations due to each ground motion, given by:

$$\ddot{U}_{i_{GMx}} = \sqrt[K]{\ddot{U}_{i_{EQ1x}} \ddot{U}_{i_{EQ2x}} \ddot{U}_{i_{EQ3x}} \cdots \ddot{U}_{i_{EQKx}}}, K = \text{Earthquake records} \quad (5.42)$$

$$\ddot{U}_{i_{GMy}} = \sqrt[K]{\ddot{U}_{i_{EQ1y}} \ddot{U}_{i_{EQ2y}} \ddot{U}_{i_{EQ3y}} \cdots \ddot{U}_{i_{EQKy}}}, K = \text{Earthquake records} \quad (5.43)$$

G. LINK REACTIONS

Response history of the links is monitored for this parameter. This particular parameter includes gap link axial forces and its deformations, as well as shear forces in the friction isolator and its deformations.

H. DEMAND TO CAPACITY RATIOS OF DIAGRID STEEL MEMBERS

For this particular parameter, the outputs are presented by screenshots of steel design of diagrid and shown for design verification of the reference model.

5.2. DESIGN VERIFICATION OF THE REFERENCE MODEL

There are two design aspects that are verified for the reference structure containing one TMD unit, which are (i) demand over capacity (D/C) ratios of the steel diagrid exterior members, and (ii) peak displacements of the TMD unit. Moreover, the force-deformation behavior of the friction isolator pendulums are also evaluated and compared to the experimental model by Scheller and Constantinou (1999).

For the member design check, the 7 shallow crustal motions are averaged and incorporated in the design combinations following ASCE 7-10. The design check was performed based on AISC 360-05. A peak D/C ratio of 0.90 was obtained over all diagrid members as shown in Figure 5.1. The TMD has limited movement. For this design, the displacement limit is approximately 1.5m, that is when the shock absorber is crushed and the mass damper would tend to pound on the exterior diagrid and/or inner concrete core. From the reference design the absorbers are proven to safely limit the TMD movement as shown in Figure 5.2. Lastly, from the force-deformation plots shown in Figure 5.3, the behavior of the friction isolator links show adequate response following discussions provided by Scheller and Constantinou (1999). Although the direct comparison is not shown herein, overlay of the experimental results with the ones obtained herein show that the friction pendulum isolators have been correctly simulated.

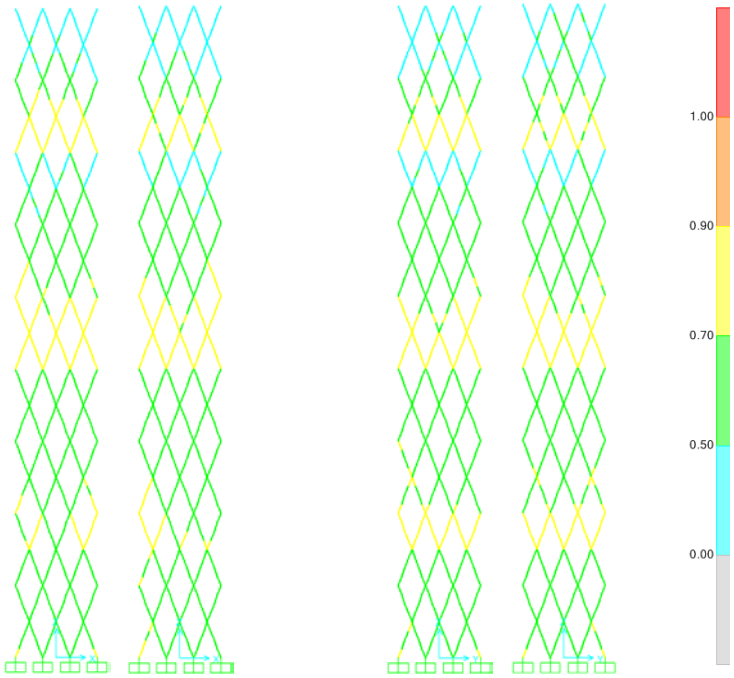

(a) (b)

Figure 5.1. Demand / capacity ratio of steel diagrid exterior member: (a) at x-direction, (b) at y-direction.

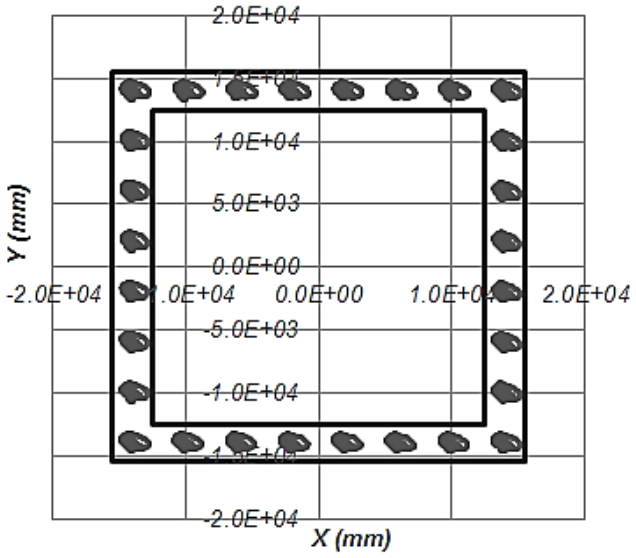

Figure 5.2. Peak TMD movement due to the shallow crustal earthquake that produces the largest TMD motion. Solid straight line is displacement limit of the TMD unit.

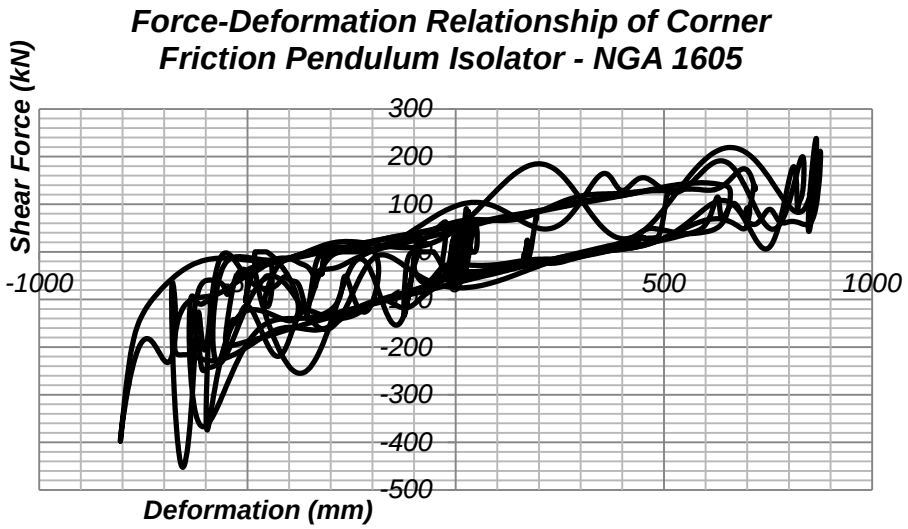

Figure 5.3. Force-deformation relationship of corner (link label 1) friction pendulum isolator due to earthquake record of NGA 1605.

5.3. ANALYSIS RESULTS

5.3.1. COMPARISON WITH REFERENCE MODEL

The improvements in terms of seismic response from the prototype building model to the reference model with one TMD unit can first be examined from the comparison of modal parameters and mass participation factors shown in Table 5.1. By placing the TMD at the top of the building, the mass participation ratios of the first mode shape in the X- and Y-direction are decreased by 29.3% and 28.5%, respectively. From this preliminary observation, it is reasonable to expect a 30% reduction in the base shear for earthquake ground motions that excite mainly the first mode of the building. Minimal seismic performance improvements are expected for any records that mainly excite the building at the higher modes.

Table 5.1. Natural period and mass participation ratios of the main structure: (a) without TMD and (b) reference model (with one TMD unit)

(a) Without TMD

Mode	Period-X	Period-Y	UX	UY	RX	RY
1	6.487	6.546	0.600	0.600	0.970	0.970
2	1.546	1.549	0.210	0.210	0.028	0.027
3	0.740	0.732	0.069	0.070	0.003	0.003

(b) Reference model (with TMD)

Mode	Period-X	Period-Y	UX	UY	RX	RY
1	7.718	7.765	0.424	0.429	0.760	0.753
2	1.506	1.509	0.196	0.195	0.023	0.023
3	0.729	0.723	0.065	0.066	0.003	0.002

Figure 5.5a shows that the utilization of a TMD system provides improvements in the peak base shear response to all shallow crustal motions, averaging (over both directions) 17.6% in reduction. Significant improvements can be seen for a few earthquake motions, with reductions of approximately 30% in base shears and base overturning moments. These improvements are related to the fact that these ground motion records excite mainly the first mode, which is the mode to which the TMD is tuned to. On the other hand, poor improvements can be seen at the base shear for NGA 1045 FN (X-dir), NGA 1044 FN (X-dir), and NGA 1605 FP (Y-dir), since those earthquakes have large contributions to the building response from higher modes. Base overturning moments receive better improvements of approximately 22.4% (averaging over both horizontal directions) due to the fact that the TMD system effectively reduces the first mode contribution and corresponding shear forces distribution at the upper part of the building, as shown in Figure 5.6. The reduction in story shear is especially notable at story 68 (where the TMD is located) in which a 25% story shear reduction for both type of the earthquakes is observable. On Average (over all floors), the reference model generates 14.1% less story shear and 13.3% less story overturning moment when compared to the basic diagrid building.

Observing the result of subduction earthquakes, the average (over both directions) improvement of peak base shears is 12.2%. This percentage is lower than the one obtained for the shallow crustal because the setting of the TMD system is not suitable for one of the earthquake tested, that is the FKSH20EW2. However, significant improvements can still be seen at some of the earthquakes, with the maximum reductions of 40% in base shears and overturning moments. Following the same trend, the TMD system is very effective in reducing the base overturning moment as it provide average improvements of 24.8%. Also, by observing the geometric means of the story response, the reference model with TMD has, on average (over all floors) 17.44% smaller story shears and 20.7% less story overturning moments when compared to the one without. This is an interesting result and it is worth noting that the TMD system works better in reducing the story reactions due to subduction-zone earthquakes than the crustal ones.

Figure 5.7 shows the geometric mean of peak inter-story drift, peak floor displacements, and peak absolute floor acceleration responses. It is worth noting that even though the building model (steel diagrid and reinforced concrete core) is linear, the displacements obtained from these analyses are expected to be identical to the ones that would be obtained using a nonlinear building model because the period of the building is relatively large and the “equal displacement” rule applies (Chopra 2001). The reference structure (with TMD) reduces the floor displacements (on average over all floors) by 19.8% for crustal earthquakes and 22.5% for subduction earthquakes. It also provides inter-story drift improvements of 17.5% for crustal earthquakes and 21.8% for subduction earthquakes. However, this TMD system is not as effective to reduce the floor accelerations as it only provides average reductions of 8.1% for crustal earthquakes and less than 1% for subduction earthquakes. This is because floor accelerations are usually controlled by higher modes which are not affected by this TMD system. Also, it is worth noting that the reference model has 10 times the floor acceleration around the TMD level due to FKSH20EW2 ground motion. Showing how

much the higher modes influenced the floor accelerations due to this particular earthquake.

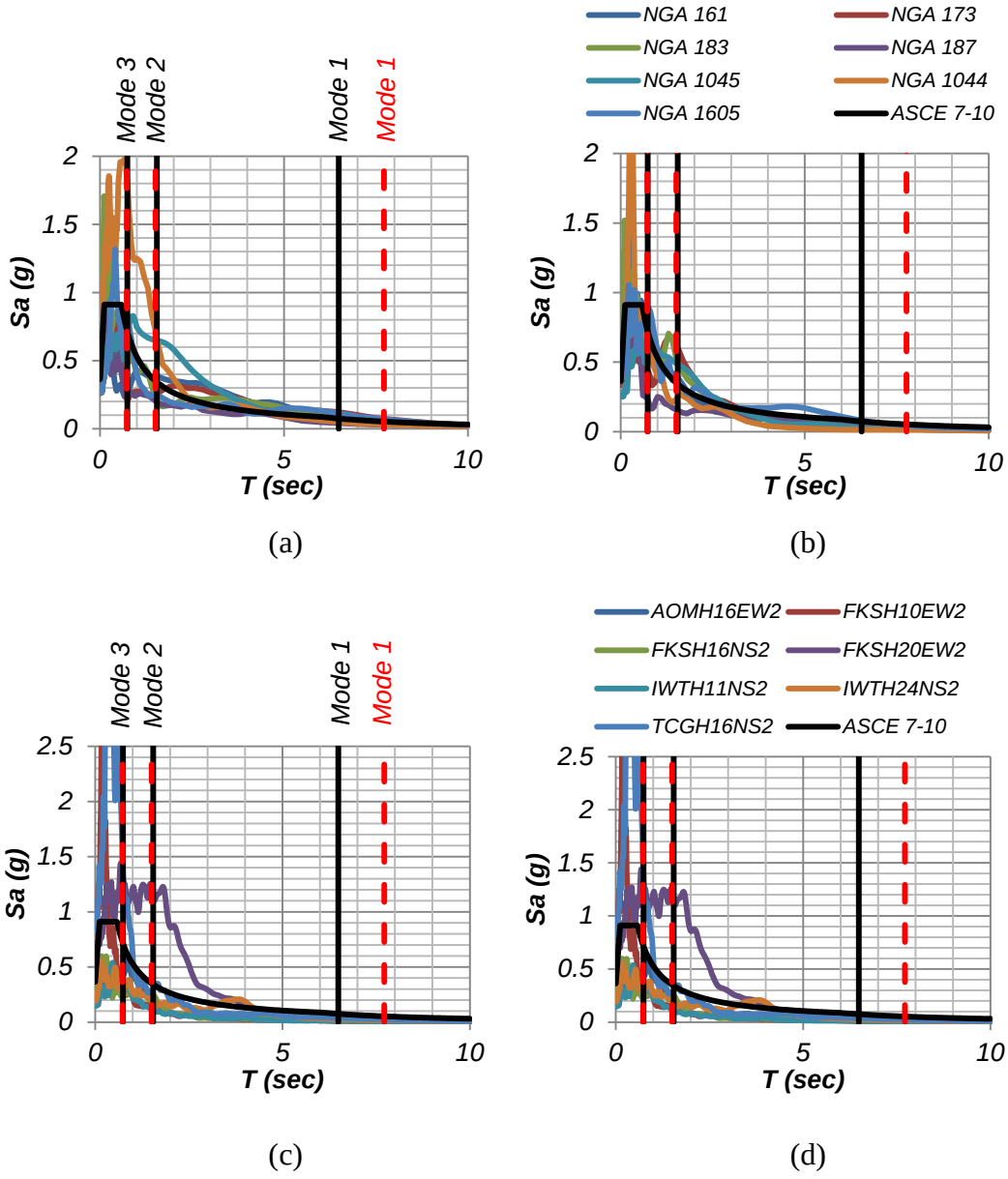

Figure 5.4. Response spectrum of each tested ground motions: (a) crustal – fault normal applied in X-dir, (b) crustal – fault parallel applied in Y-dir, (c) subduction – applied in X-dir, (d) subduction – applied in Y-dir; straight line legend: (i) without TMD [–], (ii) reference model (with TMD) [- - -].

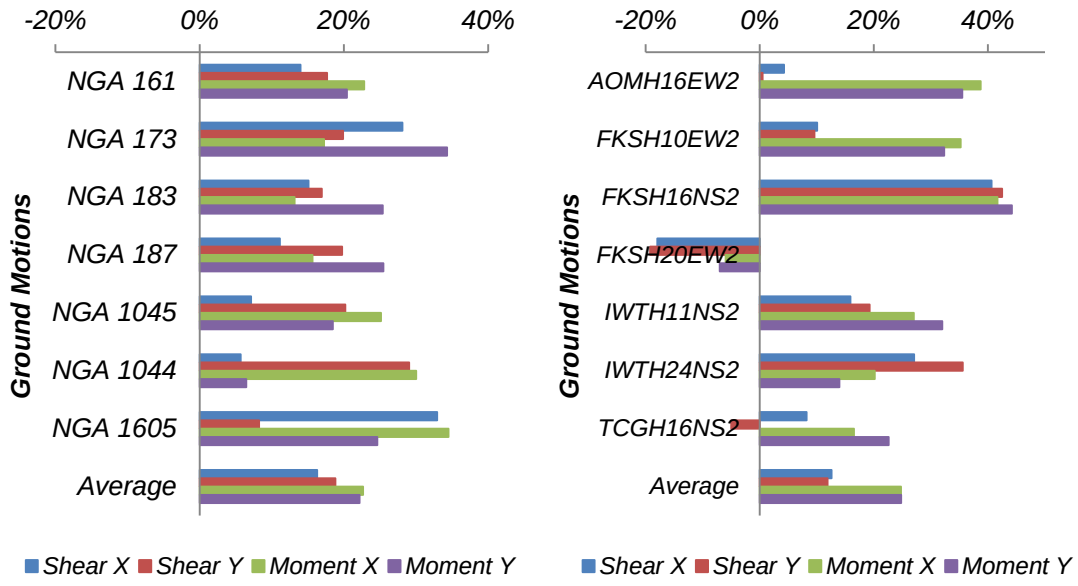

(a) (b)

Figure 5.5. Improvements peak base reactions from basic diagrid building: (a) shallow crustal earthquakes, (b) subduction zone earthquakes.

The TMD's ability to provide more damping to the structure is explored next, through the observation of the number of cycles that the IDR exceeds a reference IDR yield of 0.5%. Figure 5.8, Figure 5.9, Figure 5.10, and Figure 5.11 present the absolute inter-story drift ratio of floor 64, which is the location where the largest geometric means of IDR occurs. It can be seen from these figures that additional damping is provided by the TMD system, as the number of cycles that exceed the yield IDR is reduced. It is also worth noting that the number of inelastic cycles is significantly higher in the responses due to subduction zone motions. Thus, this TMD system can also be used to avoid the low-cycle fatigue that can occur due to subduction zone motions.

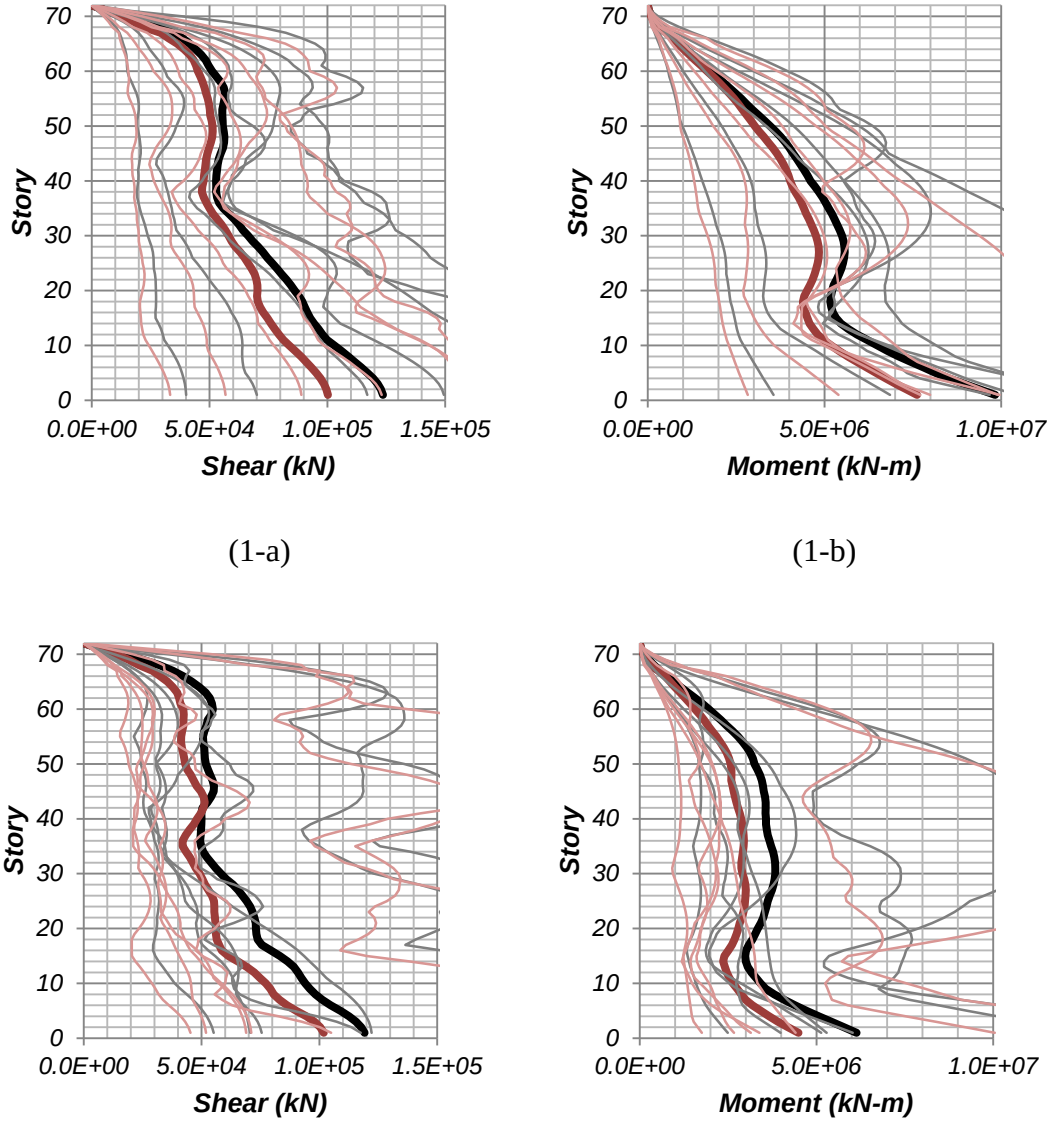

(1-a) (1-b)

(2-a) (2-b)

Figure 5.6. Geometric means of story reactions due to (1) crustal earthquakes and (2) subduction earthquakes: (a) story shears, (b) story moments; thin lines are the story reactions of each model (according to color) due to individual earthquake; legend: (i) **black line** is without TMD; (ii) **red line** is with TMD**.**

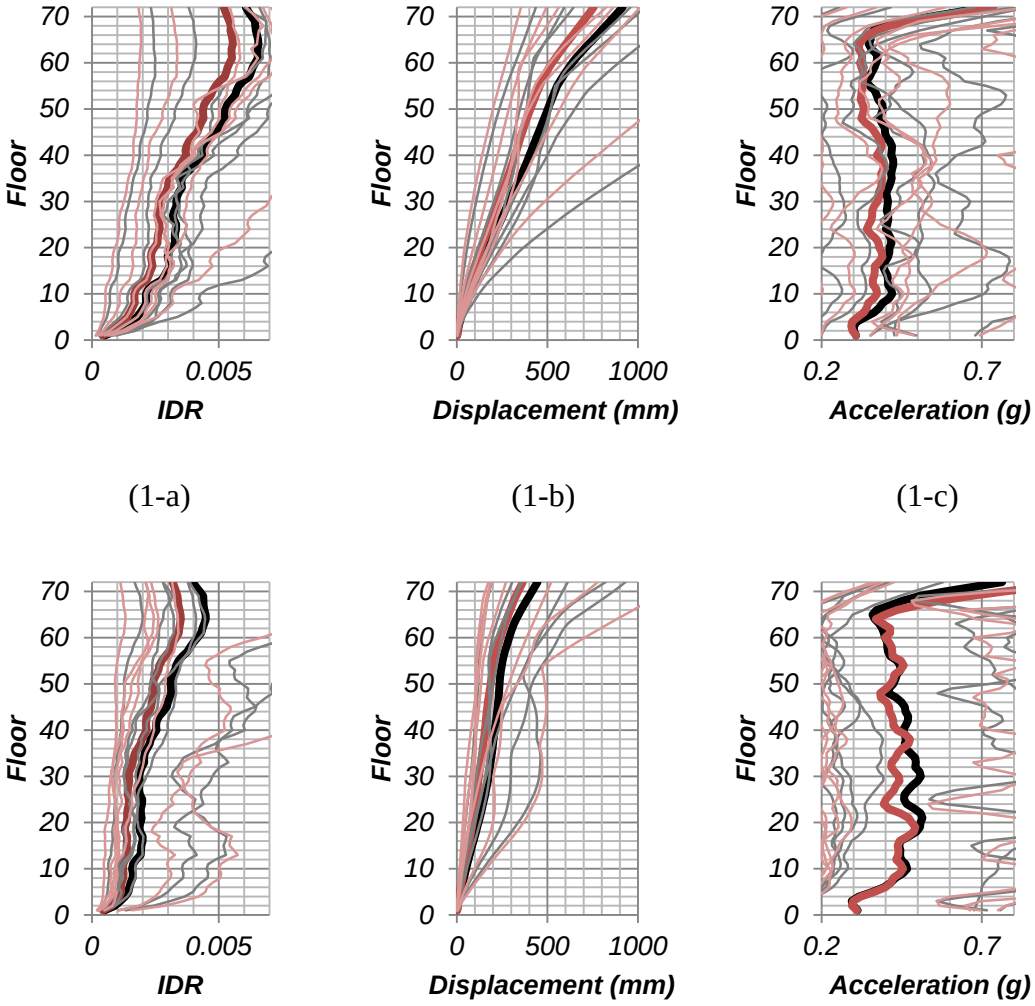

(1-a) (1-b) (1-c)

(2-a) (2-b) (2-c)

Figure 5.7. Geometric means of envelope responses due to (1) crustal earthquakes and (2) subduction earthquakes for: (a) inter-story drift (IDR), (b) floor displacement, (c) absolute floor acceleration; thin lines are the responses of each model (grouped by colors) due to individual earthquake; legend: (i) **black line** is without TMD; (ii) **red line** is with TMD**.**

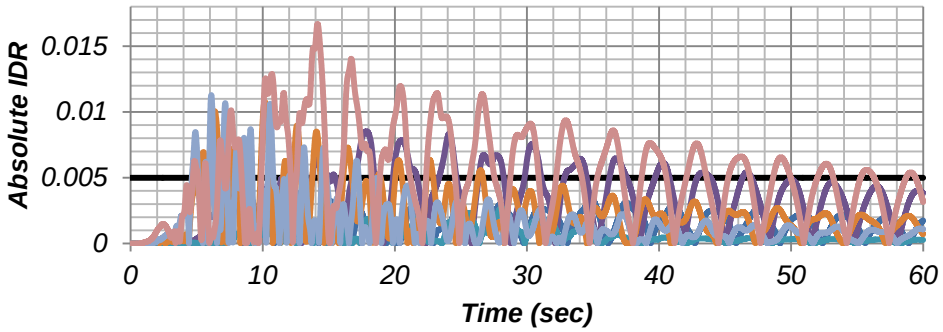

(a)

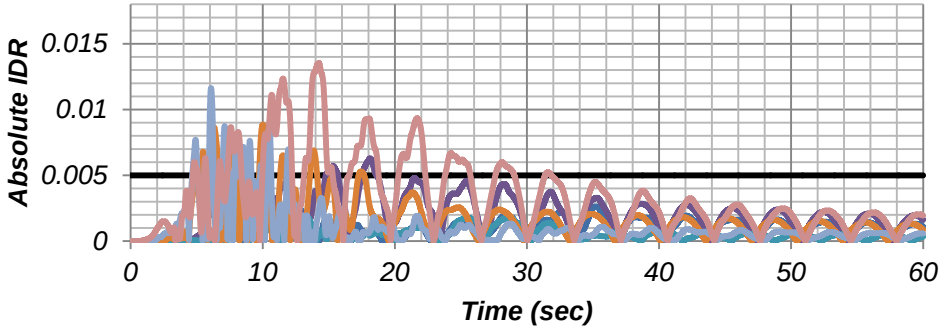

(b)

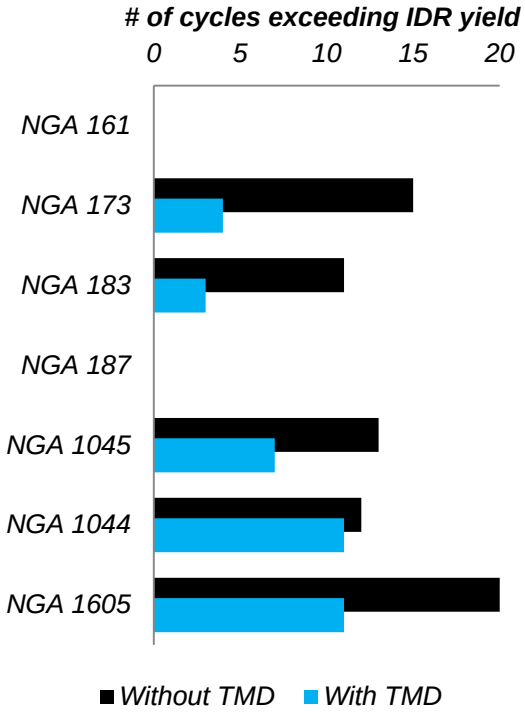

(c)

Figure 5.8. Inter-story drift ratio of floor 64 in X-dir due to shallow crustal earthquakes: (a) without TMD, (b) with TMD, (c) number of cycles that IDR exceeds IDR yield of 0.5%.

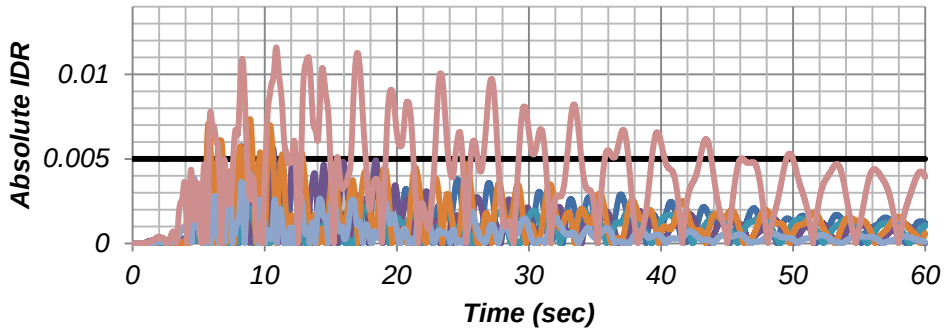

(a)

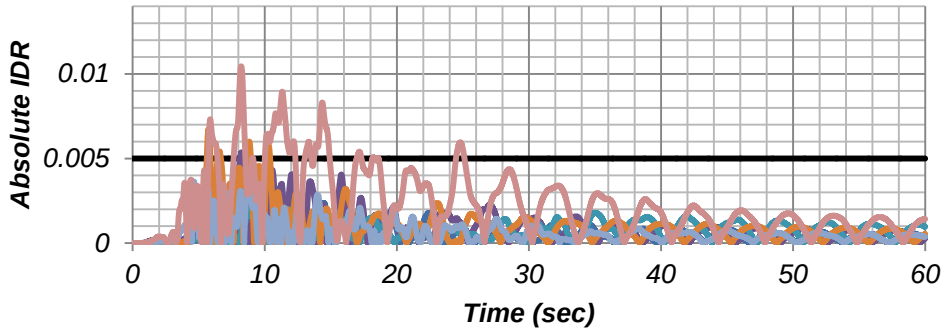

(b)

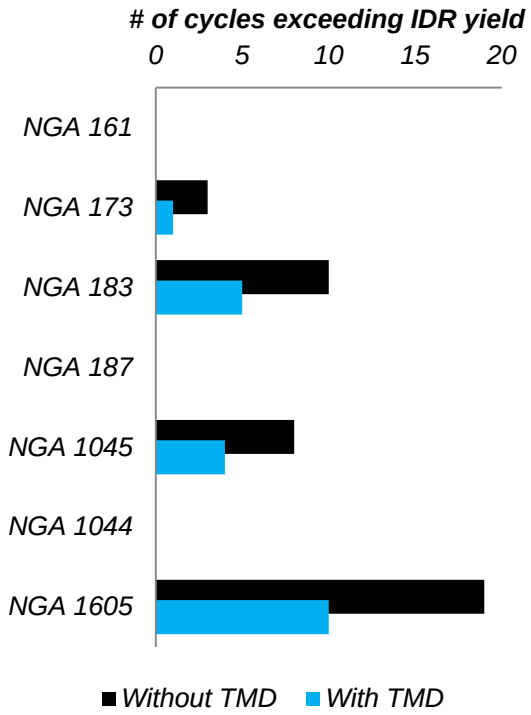

(c)

Figure 5.9. Inter-story drift ratio of floor 64 in Y-dir due to shallow crustal earthquakes: (a) without TMD, (b) with TMD, (c) number of cycles that IDR exceeds IDR yield of 0.5%.

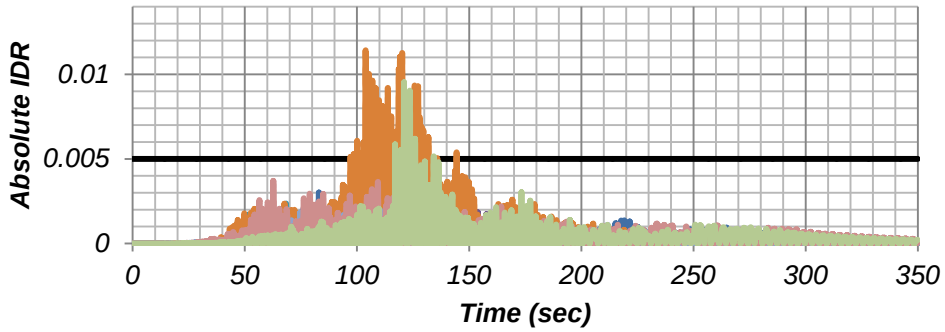

(a)

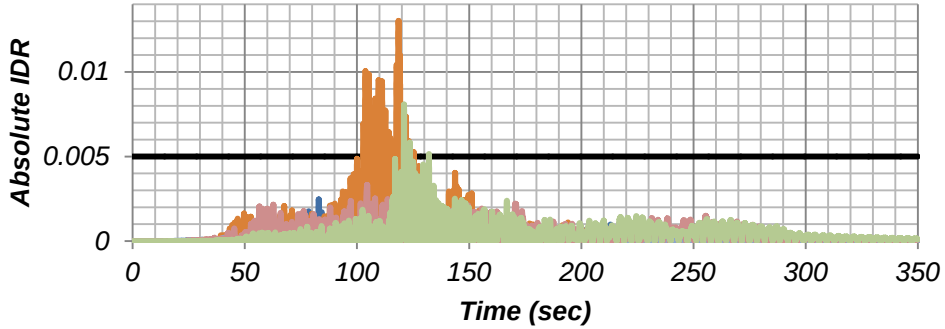

(b)

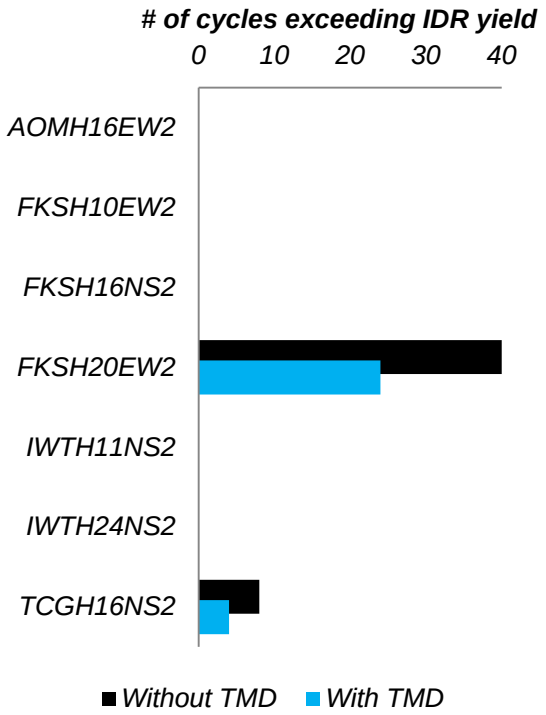

(c)

Figure 5.10. Inter-story drift ratio of floor 64 in X-dir due to subduction zone earthquakes: (a) without TMD, (b) with TMD, (c) number of cycles that IDR exceeds IDR yield of 0.5%.

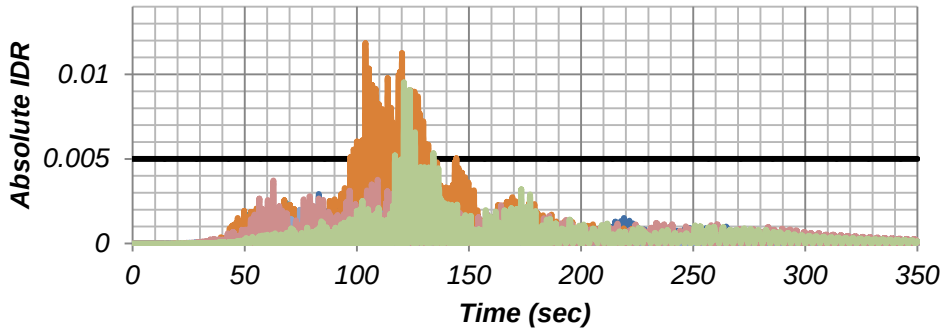

(a)

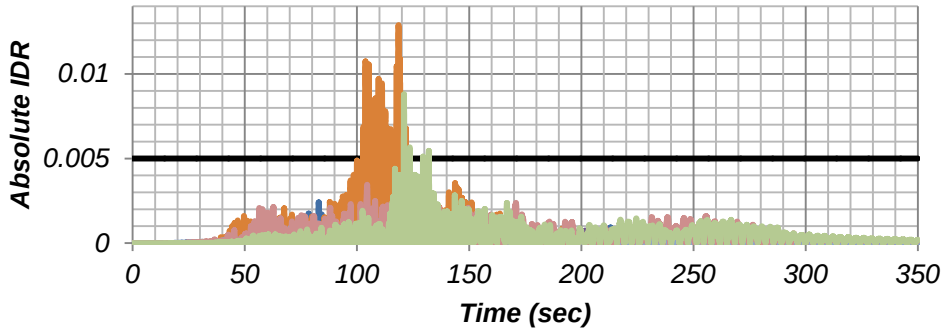

(b)

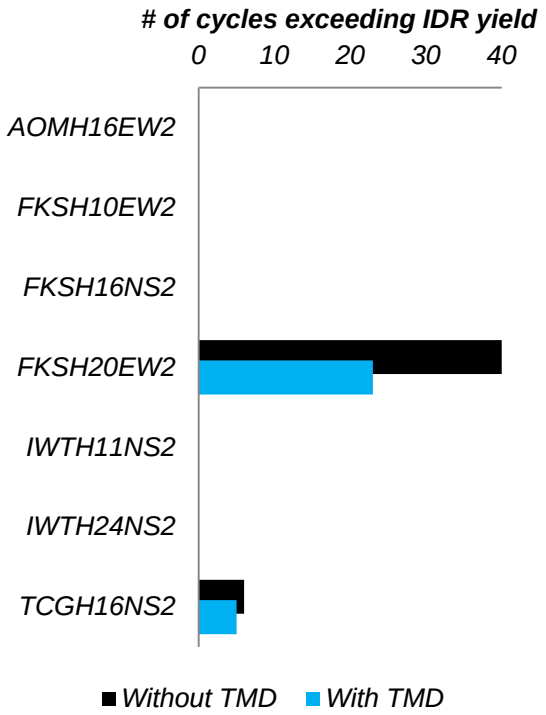

(c)

Figure 5.11. Inter-story drift ratio of floor 64 in Y-dir due to subduction zone earthquakes: (a) without TMD, (b) with TMD, (c) number of cycles that IDR exceeds IDR yield of 0.5%.

5.3.2. PARAMETRIC STUDY ON REFERENCE MODEL

A. FRICTION COEFFICIENT VARIATION

The parameters used in the reference structure with the TMD unit are f_{slow} = 0.04 and f_{fast} = 0.06. To study the effect of changing the friction coefficients of the friction isolators two new levels of friction coefficients are introduced: low friction (f_{slow} = 0.01, f_{fast} = 0.02); and high friction (f_{slow} = 0.08, f_{fast} = 0.12). By observing the base shears (Figure 5.13), it can be seen that the structure benefits when increased friction is specified. This conclusion had also been reached elsewhere (Morgan and Mahin 2008). In shallow crustal motions, improvements can be seen at almost all tested ground motions. Significant reductions in base shear can be seen in NGA 161 FP (Y-dir) and NGA 173 FP (Y-dir) in which additional reductions of approximately 13% from reference model. However, increasing the friction does not significantly affect the overall improvements in peak base shear due to subduction zone earthquakes. It also does not provide notable changes in base overturning moment for both types of the earthquakes. Nevertheless, maximum additional reduction of 14% in base shear is still observed in subduction zone motion's response. The friction coefficient of f_{fast} = 0.12 can be produced by the friction of two lubricated hard steel materials (Ramsdale 2013). On the other hand, lowering the friction coefficients results in smaller friction forces than those required to counteract the seismic forces and therefore, the results in the observed response are worse.

It is worth noting that the envelopes of inter-story drift, floor displacement, and peak absolute floor acceleration due to shallow crustal motions are not sensitive to changes in friction coefficient. Increasing friction introduces negligible changes in those floor responses. Also, by reducing the friction, the observed floor responses due to crustal shallow motions only increase by approximately 3%. However, for subduction-zone motions, the floor displacements are still not sensitive to changes in the friction coefficient, but the inter-story drift ratios and absolute floor acceleration

are quite sensitive. High friction provides significant absolute floor acceleration reductions of 10.5% while low friction increases the inter-story drift by 7.9%.

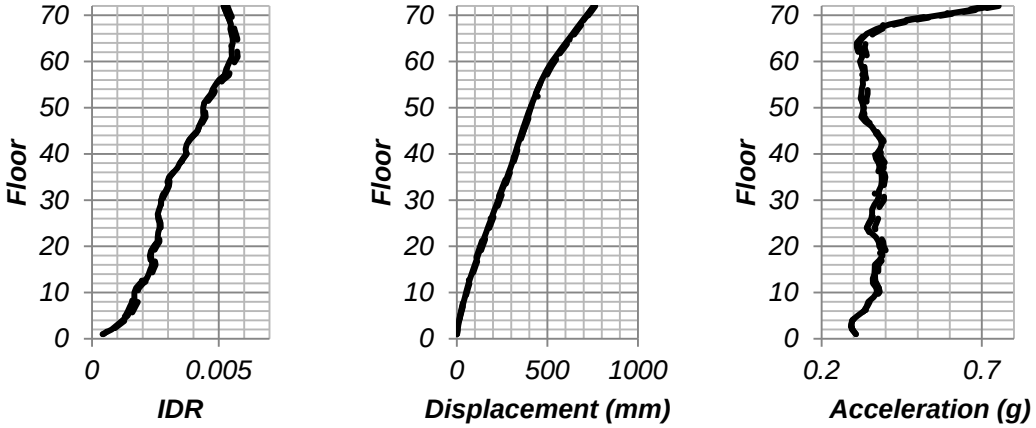

(1-a) (1-b) (1-c)

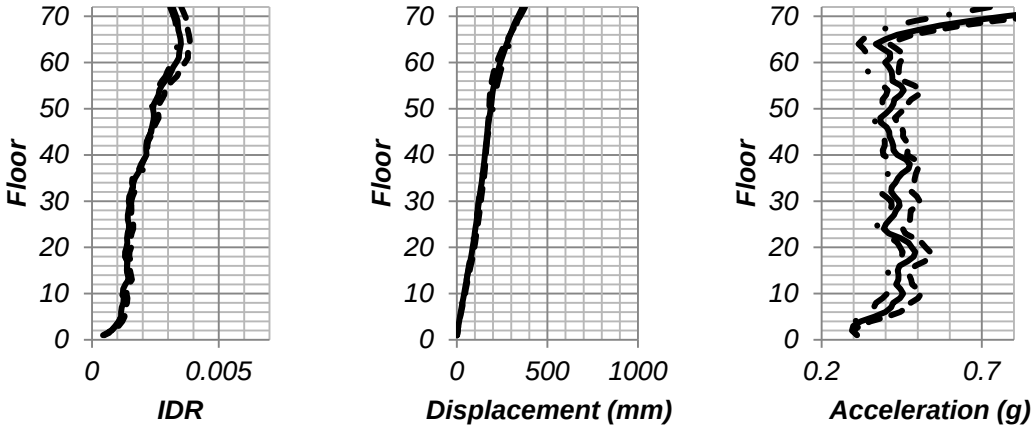

(2-a) (2-b) (2-c)

Figure 5.12 Floor responses due to variations in friction coefficient: (1) shallow crustal motions and (2) subduction zone motions; (a) inter-story drift, (b) floor displacement, (c) floor absolute acceleration; legend: (i) low friction [- - -], (ii) reference [–], (iii) high friction [— · —].

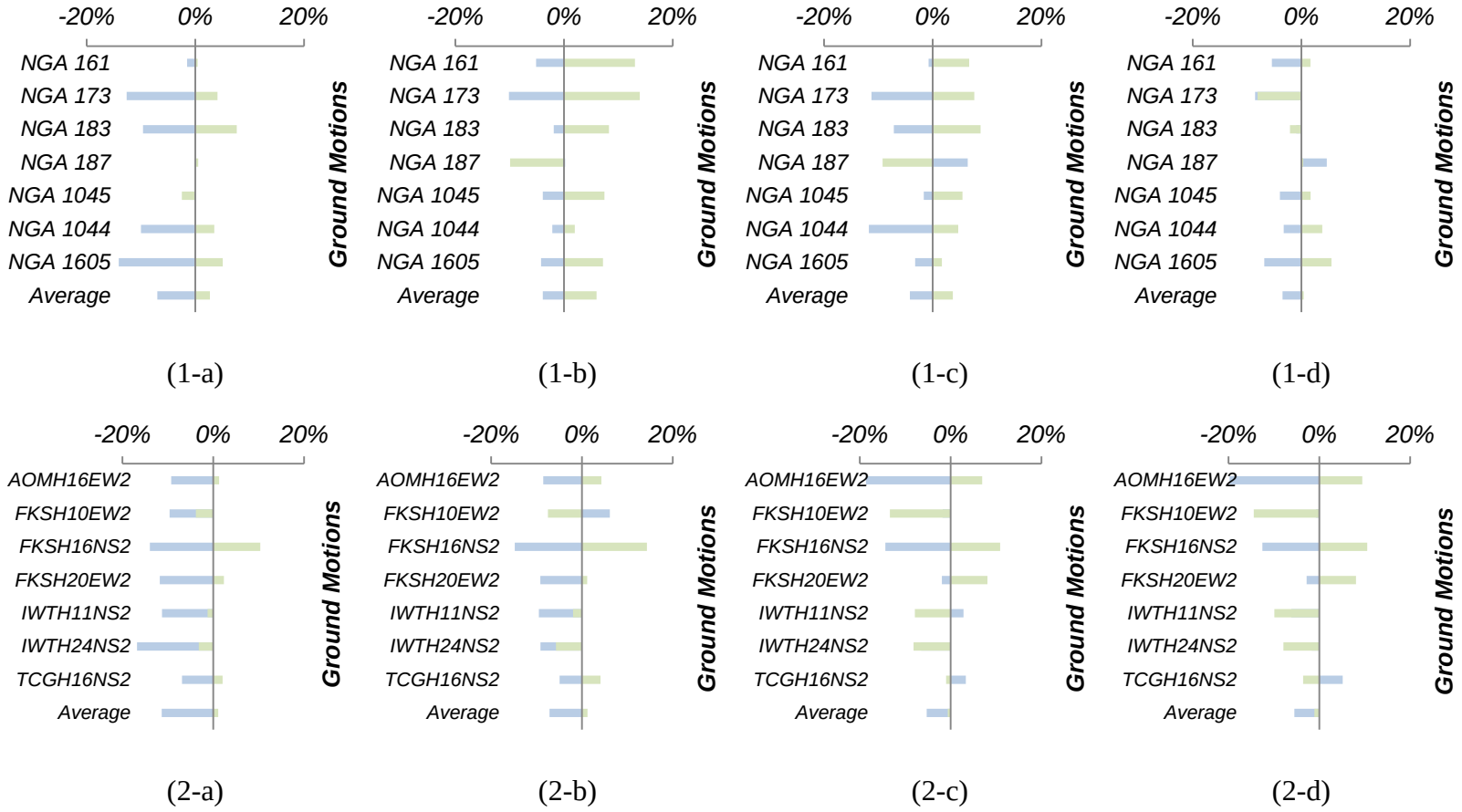

Figure 5.13. Tornado plots for peak base reactions due to variations of the friction coefficient about the reference model: (1) crustal shallow motions and (2) subduction zone motions; (a) base shear X, (b) base shear Y, (c) base overturning moment X, (c) base overturning moment Y; legend: (i) **blue bar** is low friction, (ii) **green bar** is high friction.

B. HEIGHT DISTRIBUTION AND MASS VARIATION

As stated in the methodology section, the configuration for the TMD system needs the mass damper to be extended for four floors for optimal load transfer to the exterior diagrid structure. Nonetheless, concentration of the same mass over half the height, results in an increase in base shear forces (average of both directions) of approximately 3.8% for shallow crustal motions and a decrease of 1.6% in subduction zone motions compared to the reference model. The average results due to subduction-zone ground motions are somewhat irregular. One of the reasons has to do with the fact that the ground motion FKSH20EW2 has a very irregular response spectrum with exceptionally large spectral accelerations at periods around 1.0 sec. The inclusion of the TMD unit makes the response of that particular earthquake to be larger, thus any form of parameter changes that benefit to typical earthquakes will not be as effective here. The averages of base overturning moments produce negligible changes in both types of motions. Even though this slight improvement is noted, it is worth saying that the 4.67% of tall building weight would have to be condensed in 2 stories only which may not be practical. No significant changes are observed in displacement and acceleration floor responses due to crustal earthquakes compared to the reference model that has the TMD ($\leq$3% differences). In subduction zone earthquake's responses, the floor drift and displacement also show insignificant changes, but the absolute floor acceleration decrease by 6.0% from the reference due to the reduction of FKSH20EW2's responses.

Finally, by maintaining the height and friction parameters fixed to the values of the reference model, the mass was varied by two levels (+20% and -20%). By reducing the mass by 20%, the overall base reactions improvements for X and Y directions due to shallow crustal motions decrease by 3 and 5%, respectively, compared to the reference model. On the other hand, the average base reaction changes due to subduction zone motions are still irregular. Nonetheless, decreasing the mass of the TMD is still decreasing the overall base reactions improvements compared

to the reference model. Additionally, increasing the mass by 20% corresponds to overall base reaction improvements of only 3% from the reference for shallow crustal motions and 4% for subduction zone motions. The changes in mass are also not affecting the displacement and acceleration floor response for shallow crustal motions. The observed floor responses only fluctuated by approximately 3.3%. However, the changes are reasonably significant in subduction earthquakes. While floor displacements do not differ much, increasing the mass by 20% increase the overall floor absolute accelerations improvement by 7.6% while decreasing the mass will do the contrary.

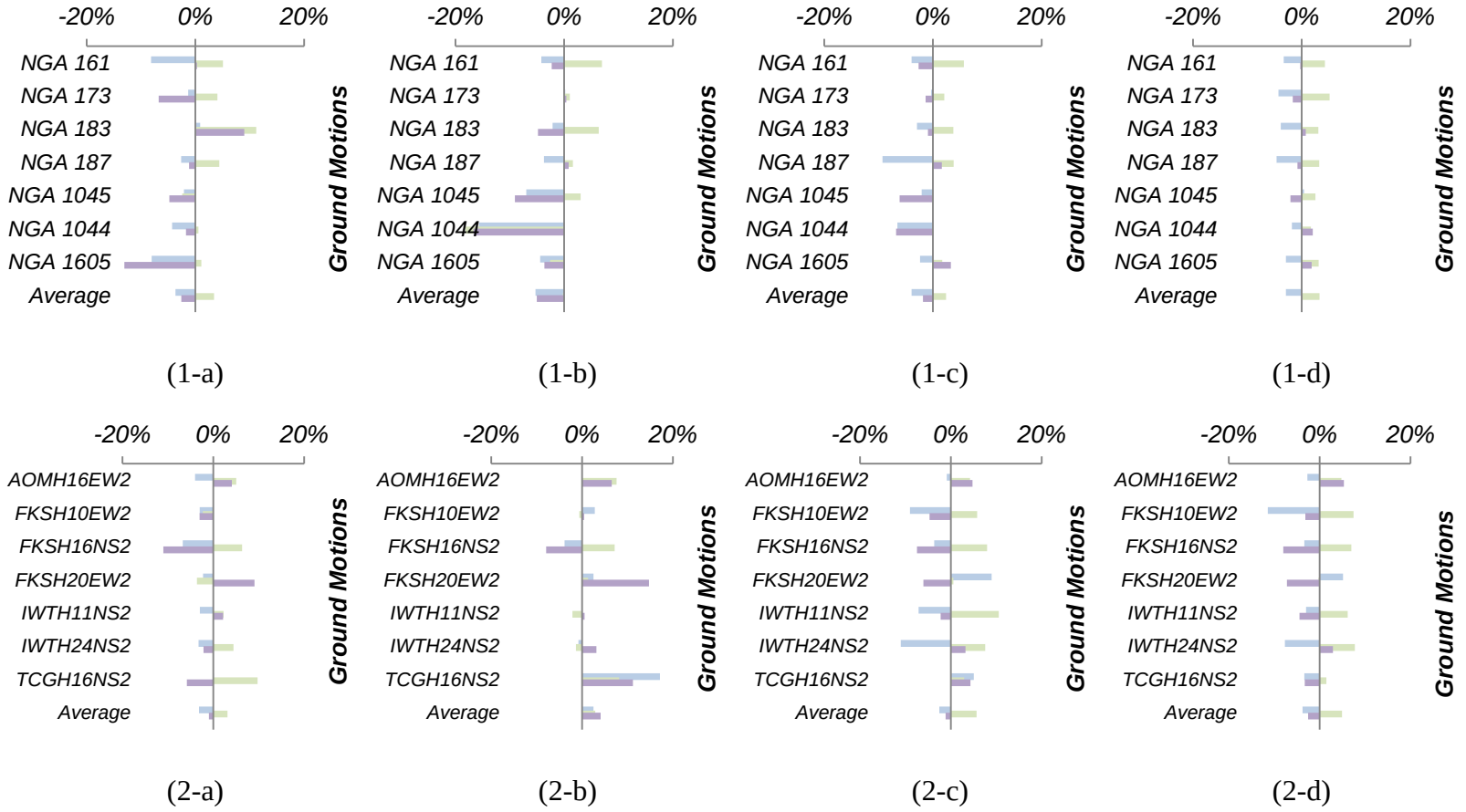

Figure 5.14. Tornado plots for peak base reactions due to variation in height and mass of TMD about the reference model: (1) shallow crustal motions and (2) subduction zone motions; (a) base shear X, (b) base shear Y, (c) base overturning moment X, (c) base overturning moment Y; legend: (i) **blue bar** is decrease mass, (ii) **green bar** is increase mass, (iii) **purple bar** is reduce height.

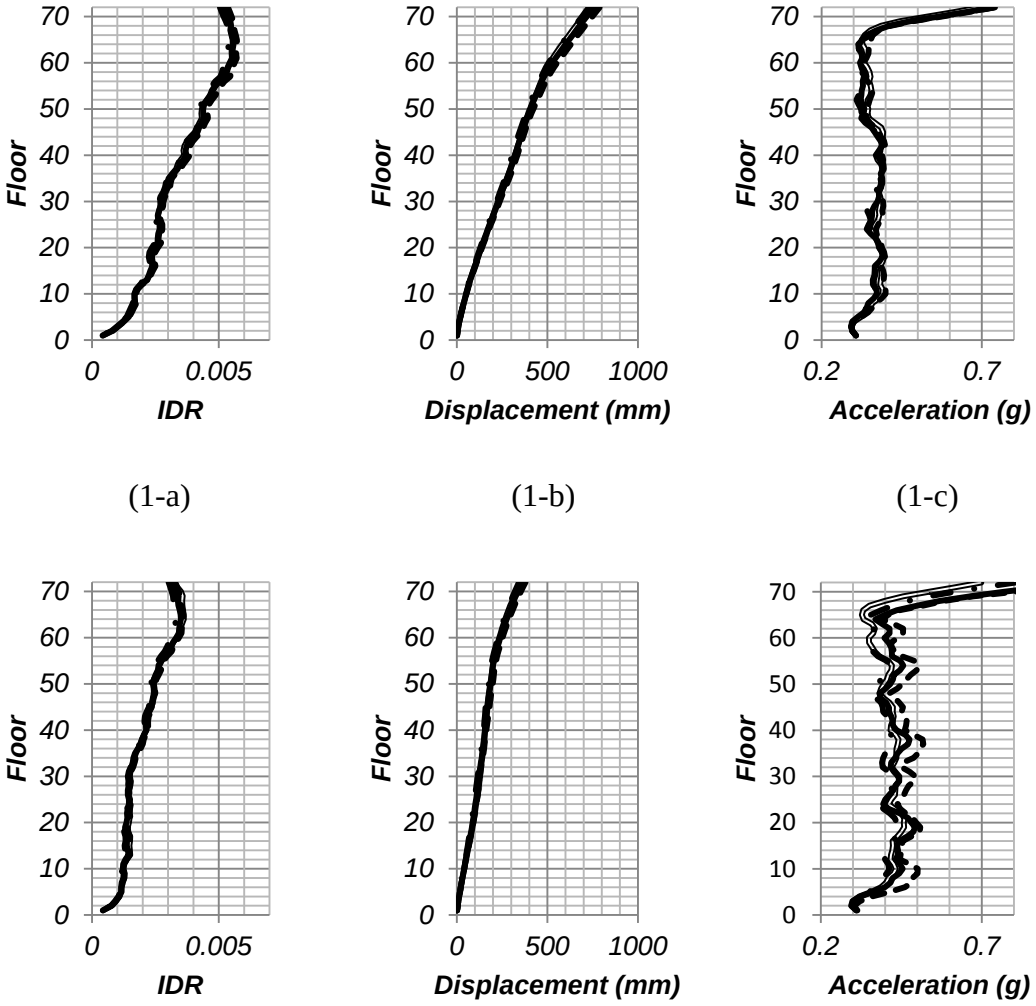

Figure 5.15 Floor response due to variation in height and mass: (1) shallow crustal motions and (2) subduction zone motions; (a) inter-story drift, (b) floor displacement, (c) floor absolute acceleration; legend: (i) decrease mass [- - -], (ii) reference [–], (iii) increase mass [– · –]; reduce height [=].

5.3.3. COMPARISON WITH DOUBLE TMD SYSTEM

The modal parameters and mass participation factors are still useful to estimate the expected improvements in terms of seismic response of the model with the double TMD system. Table 5.2 lists the three main periods of vibration of the structure in the X- and Y-direction. Figure 5.16 shows the mode shapes and mass participation ratios of each mass damper in the double TMD system in comparison the single TMD system (reference model). It can be seen that for the model with the additional TMD in story 32, the mass participation of the first mode increases slightly, while a decrease of the mass participation ratio for the second mode is observed. It is clear, that the inclusion of the second TMD unit influences mainly the participation of the second mode, and thus this TMD unit is said to be tuned for the second mode only.

Table 5.2. Fundamental periods and mass participation ratios of the main structure with double TMD system.

Mode	Period-X	Period-Y	UX	UY	RX	RY
1	7.727	7.775	0.427	0.431	0.761	0.754
2	1.433	1.435	0.142	0.140	0.017	0.017
3	0.728	0.722	0.065	0.066	0.003	0.002

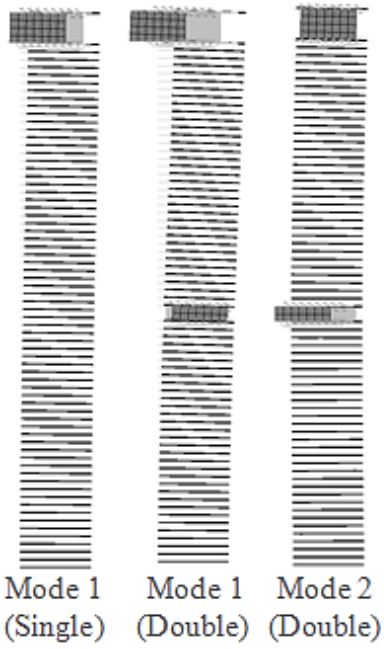

Single TMD

Mode	Period-X	Period-Y	UX	UY	RX	RY
1	4.982	4.996	0.197	0.191	0.213	0.221

Double TMD

Mode	Period-X	Period-Y	UX	UY	RX	RY
1	4.994	5.008	0.198	0.192	0.212	0.219
2	1.843	1.844	0.054	0.054	0.006	0.006

Figure 5.16. Mode shapes and mass participation ratios of each mass damper in the two models.

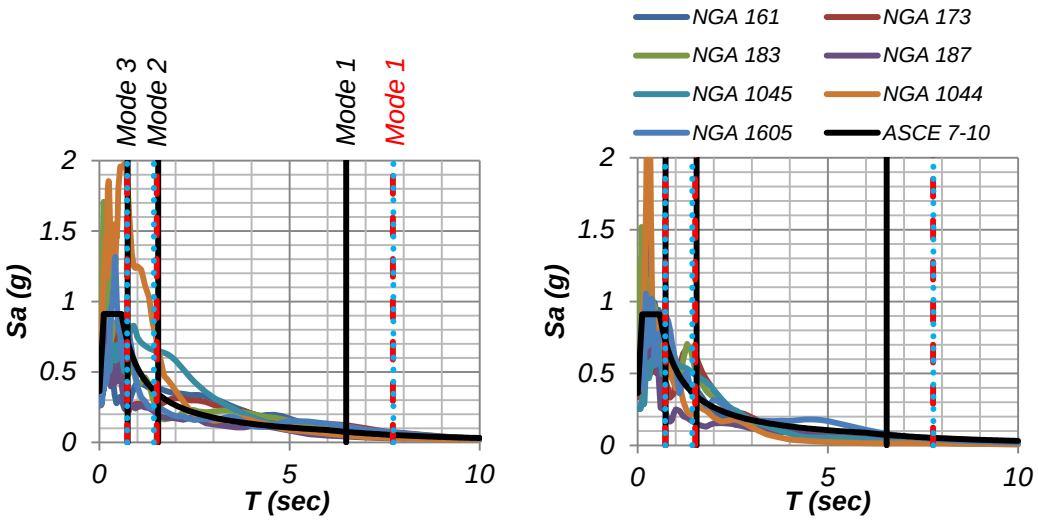

(a) (b)

Figure 5.17. Response spectrum of each crustal ground motion: (a) crustal – fault normal applied in X-dir, (b) crustal – fault parallel applied in Y-dir; straight line legend: (i) without TMD [–], (ii) reference model (with single TMD unit) [- - -], (iii) with double TMD units [⋯].

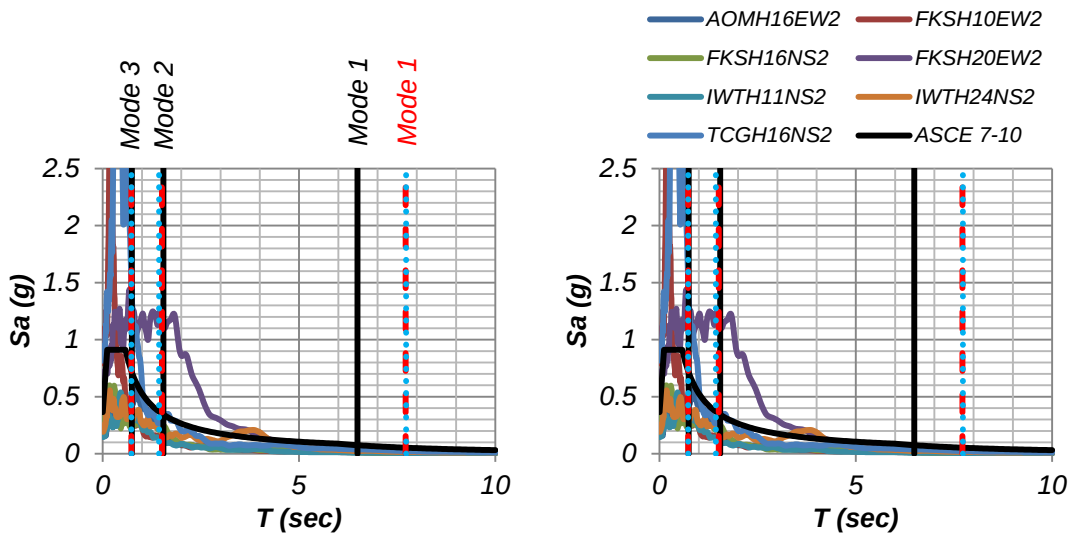

(a) (b)

Figure 5.18. Response spectrum of each subduction-zone ground motion: (a) subduction – applied in X-dir, (b) subduction – applied in Y-dir; straight line legend: (i) without TMD [–], (ii) reference model (with single TMD unit) [- - -], (iii) with double TMD units [···].

Figure 5.19 shows that the utilization of double TMD system results in improvements in the peak base reaction responses for almost all tested ground motions. For the shallow crustal motions, the double TMD system gives additional improvements of 5.7% to peak base shear responses (averaging in both directions) over the reference model and also resulting in a reduction of 23.3% of total peak base shear reduction. Significant improvements are observed for NGA 161 FP, NGA 173 FP, and NGA 183 FP with approximately 15% of additional improvements in peak base shear over the reference model. Peak base overturning moments are also improve by 4.6% in average. In the response generated by subduction zone motions, a similar trend is observed. The double TMD system reduce the overall peak base shear responses by 6.0% with maximum reduction of approximately 20%, also overall peak base overturning moment is reduced by 8.7%. However, for one particular earthquake, that is FKSH20EW2, although the double TMD system reduces the peak base shear

responses by 11.6% over the reference model, it still resulted in 7% higher peak base shear compared to the prototype building that has no TMD installed.

Looking at story shear and moment responses shown in Figure 5.20, the double TMD units provide additional story shear improvements of 4% and story moment of 3% to the geometric mean responses due to shallow crustal motions. In the subduction zone motions, the double TMD system provide even better improvements of approximately 6.5% for both story reactions.

Figure 5.21 shows the geometric mean of peak story-drifts, peak floor displacements, and peak absolute floor acceleration responses. All responses show that the double TMD system has the smallest responses. In responses due to shallow crustal motions, the floor drifts and displacements improve by 4.3% from the reference model, while the floor absolute accelerations provide improvements of 5.1%. For the subduction zone motions, the double TMD system reduces the inter-story drift and displacement responses of reference model by 9.5%. Furthermore, floor absolute accelerations are also decrease by 13.1%, which is a notable improvement from the reference model.

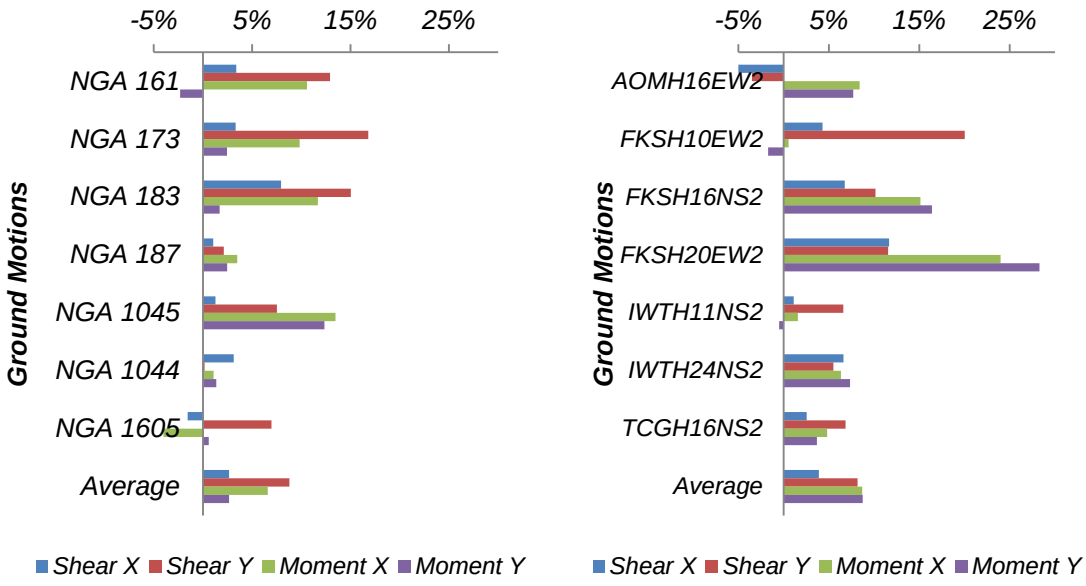

(a) (b)

Figure 5.19. Improvements in peak base reactions of double TMD system from reference model (single TMD system) due to: (a) shallow crustal motions, (b) subduction zone motions.

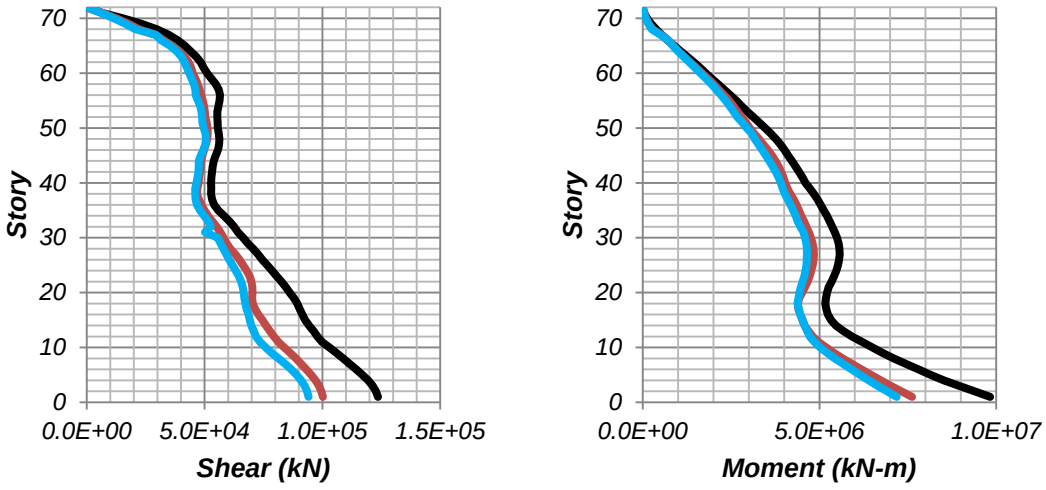

(1-a) (1-b)

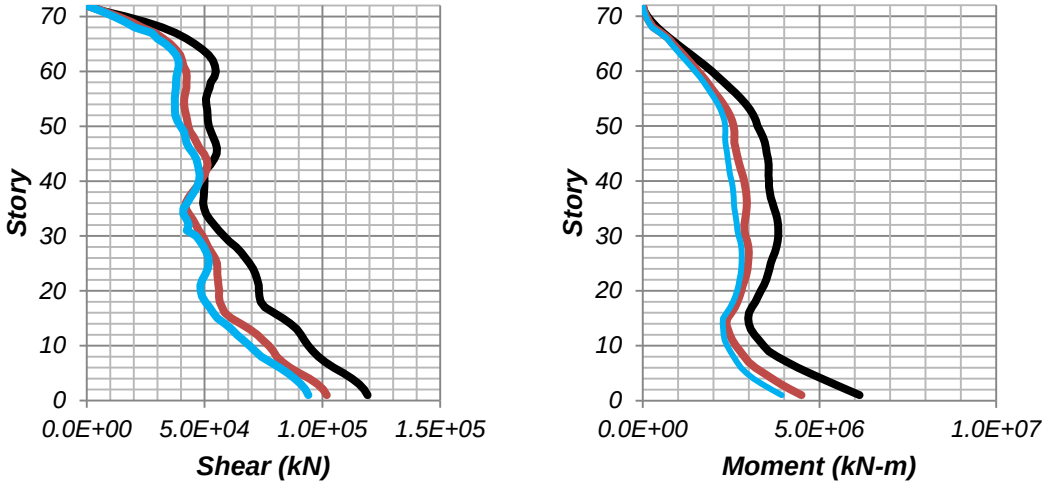

(2-a) (2-b)

Figure 5.20. Geometric means of story reactions due to (1) crustal earthquakes and (2) subduction earthquakes: (a) story shears, (b) story moments; legend: (i) **black line** is model without TMD; (ii) **red line** is model with single TMD system (reference model); (iii) **blue line** is model with double TMD system**.**

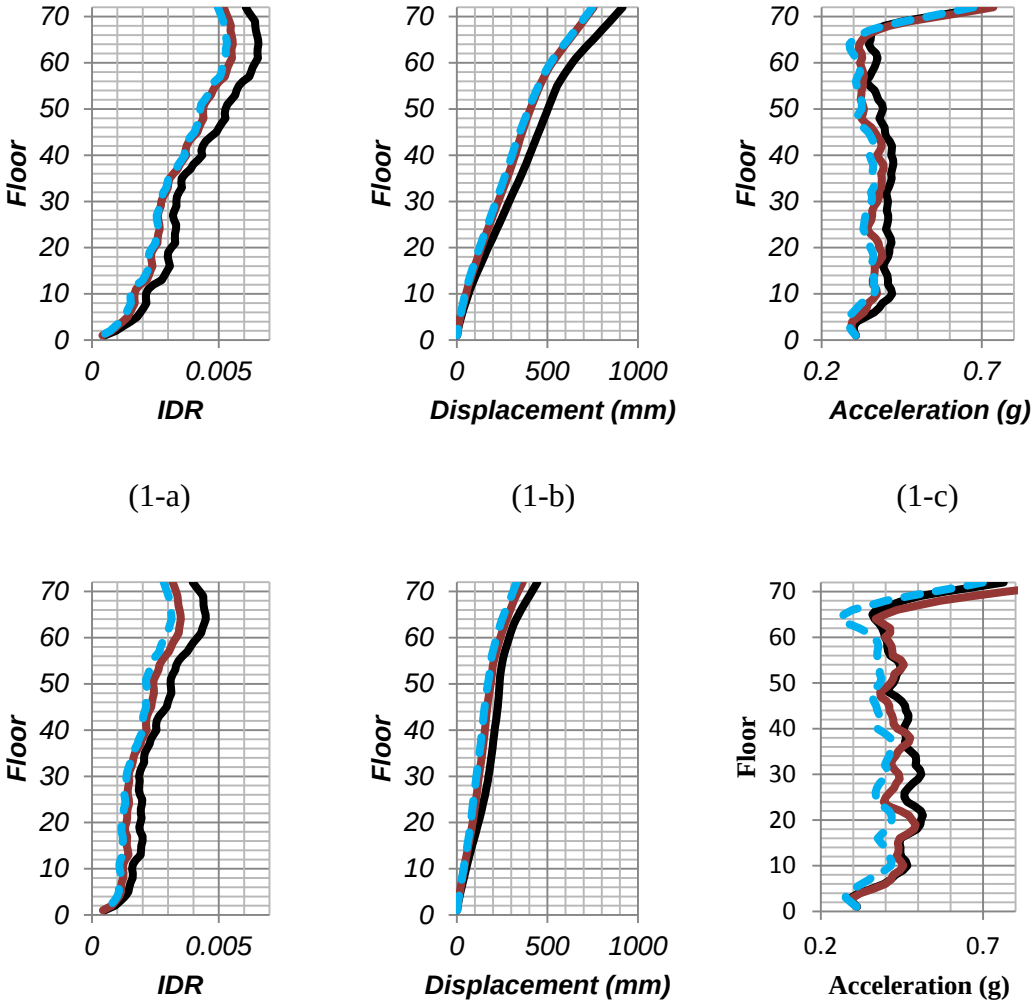

(1-a) (1-b) (1-c)

(2-a) (2-b) (2-c)

Figure 5.21. Geometric means of envelope responses due to (1) crustal earthquakes and (2) subduction earthquakes for: (a) inter-story drift (IDR), (b) floor displacement, (c) absolute floor acceleration; legend: (i) **black line** is model without TMD; (ii) **red line** is model with single TMD system (reference model)**;** (iii) **blue dashed line** is model with double TMD system.

CHAPTER 6. FINAL REMARKS

6.1. CONCLUSIONS

This thesis presents the design approach and an analysis methodology of a 72-story diagrid steel structure, in which two solutions for mitigating earthquake-induced vibrations are tested, considering the use of one or two friction tuned mass dampers (TMDs) units. A prototype diagrid building that has been designed according to the U.S. code is used as the basic input. The friction TMD units – that consist of a reinforced concrete container with sand or water inside – are then connected to the prototype building using friction pendulum isolators. Shock absorbers are placed between the TMDs and exterior diagrid and also between the TMDs and inner reinforced-concrete building core to limit their movement. For assessing the improvements in seismic performance for each solution, seven crustal and seven subduction zone motions are applied to the structural models. The nonlinear finite element models of the structure consist of linear elastic steel frame elements (diagrid and floor beams), linear shell elements for the reinforced-concrete core and slab on deck (based on effective stiffness of cracked concrete members), linear shell elements for the TMD units, linear spring elements, and nonlinear gap and friction isolator links.

First a single TMD was placed at the top 4-stories of the building. The TMD unit was tuned to the first mode of the main structure. By using one TMD unit at the top of the building (reference model), significant mitigation of displacement, shear, and moment demands are obtained in comparison to the demands obtained for the building without TMD. Reduction of the peak base shear and overturning moment of approximately 30% can be achieved; overall (average for 7 ground motions, 2 directions, and over all floors) reductions of 19.8 % in displacement and 17.5% in inter-story drift are observed. It is also worth noting that the single TMD system can significantly provide more damping to the diagrid structure, which is shown by reducing the number of cycles that the IDR exceeds the reference IDR yield of 0.5%

by as much as 70%. The reference model also produce 14.1% less story shear and 13.3% less story overturning moment as compared to the basic diagrid building. The overall seismic performances of the reference model (with one TMD unit) due to subduction zone motions are also increased. Although the single TMD system is not effective on some of the subduction motions tested, the improvements in terms of base shear and overturning moment are similar. Thus, peak improvements base shear and overturning moment of 40% are observed. The improvements of 17.44% for story shears, 20.7% of story moments, 22% of inter-story drift ratios and displacements are also observed.

In this study, it was identified that the single TMD system is not suited for earthquakes that have a large contribution from higher modes to the response of the building, which has to do with the fact that the single TMD unit can only be tuned to one mode. Thus, it is important to highlight that the building location and soil characteristics are crucial in tuning the friction mass damper design.

A parametric study is performed around the reference model to characterize the sensitivity of the response to several input parameters and to optimize the settings for the friction TMD units. Friction (2 levels), mass (2 levels), and height (1 levels) of the TMD were parameters analyzed. The levels considered were: low friction (f_{slow} = 0.01, f_{fast} = 0.02) and high friction (f_{slow} = 0.08, f_{fast} = 0.12) for friction coefficients variation; increase mass (+20%) and decrease mass (-20%) of the TMD for mass variation; and finally decrease the height of the TMD by half for height distribution variation. The main results were observed from this parametric study. First, with respect to the friction, doubling the friction coefficients of friction isolator provide the best results and further decreased the base shears due to some of the shallow crustal motions by approximately 13% when compared to the reference model. The change in friction does not give rise to notable changes for overturning moment and floor displacement, or floor absolute accelerations for responses obtained when the structure is subjected to crustal motions. However, increasing the friction provides for significant improvements in floor absolute acceleration (10.5%) for the responses

induced by the subduction zone motions. Second, increasing the mass tends to reduce the base reactions, while reducing the mass reduces the effectiveness of the TMD for all the observed responses. Yet, following the same trend as before, increasing the mass reduces the floor absolute acceleration mainly for the subduction zone motions by about 7.6% with respect to the one obtained in the reference model. Lastly, although reducing the height of the mass damper only reduces the improvements observed, these reductions are small and also considerably reduces the constructability of the TMD unit considerably due to difficulties in condensing 4.67% of tall building mass in two floors only.

Adding the second mass damper that is tuned to reduce the participation of the second mode of the main structure (by placing it at the level at which the second mode produces largest displacement at the mid-height of the building) increases the seismic performance further as compared to the reference model with a single TMD unit. Additional improvement in base shear of 15% and 20% are observed for the shallow crustal and subduction zone motion respectively. The main benefit of using the double TMD is shown in the reduction of floor absolute acceleration compared to the reference model, where 9.5% improvements were achieved

In all, this thesis provides for new and interesting results towards the development of seismic design and analysis guidelines of tall diagrid steel buildings. To mitigate the seismic responses of tall structures, base isolation or distributed viscous damping is not a viable solution as they are only effective for low to mid-rise building. A new solution is proposed. Special attention was taken to make the system constructible and drawings with details were provided. A modeling and design verification approach were developed.

6.2. FUTURE STUDIES

Future studies can discuss, for example, a wide range of friction coefficients, mass, and TMD locations. Furthermore, the use of triple friction pendulum isolator

(Morgan and Mahin 2008) can also be considered as replacement of friction pendulum isolator as its multi-stage sliding behavior can be beneficial to make a TMD system that can mitigate a wide range of earthquake records (frequency contents). Other considerations, such as use of multiple TMDs should also be further explored, following initial works done in this thesis. There are many parameters that need to be adjusted and tuned in the optimal design of the TMDs for seismic response improvements of tall building structures, and the design can be challenging, providing for an opportunity for development of simple formulations that can be used in hand calculations and preliminary designs, including simplified stick models. On the opposite spectra of complexity, detailed nonlinear finite element models need to be developed to assess the seismic safety factors, for example, following the FEMA P-695 methodology, to provide seismic performance factors (R, Ω_0, C_d) to complement initial works by Baker et al. (2010).

REFERENCES

A. C. I. Committee. 2011. “Building Code Requirements for Structural Concrete (318-11) and Commentary-(318R-11).” *Detroit, Michigan: American Concrete Institute*.

Ali, Mir M., and Kyoung Sun Moon. 2007. “Structural Developments in Tall Buildings: Current Trends and Future Prospects.” *Architectural Science Review* 50 (3): 205–223.

American Society of Civil Engineers. 2010. *Minimum Design Loads for Buildings and Other Structures*. Virginia: ASCE.

ANSI, B. 2005. “AISC 360-05-Specification for Structural Steel Buildings.” *Chicago∼ AISC*.

Arup. 2009. “Sony City, Tokyo: A Diagrid Combined with Base Isolation.” *The Arup Journal* 2: 49–51.

Baker, Jack W. 2007. “Quantitative Classification of near-Fault Ground Motions Using Wavelet Analysis.” *Bulletin of the Seismological Society of America* 97 (5): 1486–1501.

Baker, William, Charles Besjak, Mark Sarkisian, Peter Lee, and Chung-Soo Doo. 2010. “Proposed Methodology to Determine Seismic Performance Factors for Steel Diagrid Framed Systems.” In *13th U.S. Japan Workshop*.

Barbosa, André R. 2011. “Simplified Vector-Valued Probabilistic Seismic Hazard Analysis and Probabilistic Seismic Demand Analysis: Application to the 13-Story NEHRP Reinforced Concrete Frame-Wall Building Design Example”. PHD Thesis, La Jolla, California: University of California, San Diego. http://escholarship.org/uc/item/4ww7g21j.

Chen, Genda, and Jingning Wu. 2001. “Optimal Placement of Multiple Tune Mass Dampers for Seismic Structures.” *Journal of Structural Engineering* 127 (9): 1054–1062.

Chopra, Anil K. 2001. *Dynamics of Structures: Theory and Applications to Earthquake Engineering*. 2nd ed. Saddle River: Prentice Hall.

Computer and Structures. 2011. *SAP2000 v15.1.0*. Berkeley: Computer and Structures.

Constantinou, Michalakis C., and Itadj G. Tadjbakhsh. 1985. “Optimum Characteristics of Isolated Structures.” *Journal of Structural Engineering* 111 (12): 2733–2750.

CSI. 2011. “Analysis Reference Manual for SAP2000, ETABS, and SAFE.” *Computers and Structures, Inc., California, USA*.

Glotman Simpson. 2001. “Project Showcase - One Wall Centre.” *Glotman Simpson Consulting Engineers*. http://www.glotmansimpson.com/Commercial/One-Wall-Centre.

Hadi, Muhammad NS, and Yoyong Arfiadi. 1998. “Optimum Design of Absorber for MDOF Structures.” *Journal of Structural Engineering* 124 (11): 1272–1280.

Inaudi, Jose Antonio, and James M. Kelly. 1992. “A Friction Mass Damper for Vibration Control”. UCB/EERC-92/15. Berkeley, California: Earthquake Engineering Research Center, University of California.

Lago, A., T. J. Sullivan, and G. M. Calvi. 2010. “A Novel Seismic Design Strategy for Structures with Complex Geometry.” *Journal of Earthquake Engineering* 14 (S1): 69–105.

Lucchini, A., R. Greco, G. C. Marano, and G. Monti. 2013. “Robust Design of Tuned Mass Damper Systems for Seismic Protection of Multistory Buildings.” *Journal of Structural Engineering*. http://ascelibrary.org/doi/abs/10.1061/(ASCE)ST.1943-541X.0000918.

McCain, Ian. “Diagrid: Structural Efficiency & Increasing Popularity.”

Moon, Kyoung Sun. 2008. “Optimal Grid Geometry of Diagrid Structures for Tall Buildings.” *Architectural Science Review* 51 (3): 239–251.

Morgan, Troy A., and Stephen A. Mahin. 2008. “The Optimization of Multi-Stage Friction Pendulum Isolators for Loss Mitigation Considering a Range of Seismic Hazard.” In *Proceedings of the 14th World Conference on Earthquake Engineering*. Beijing, China.

National Research Institute for Earth Science and Disaster Prevention. 2013. “Strong-Motion Seismograph Networks.” Accessed February 3. http://www.k-net.bosai.go.jp.

Park, Y. J., Y. K. Wen, and A. Ang. 1986. “Random Vibration of Hysteretic Systems under Bi-Directional Ground Motions.” *Earthquake Engineering & Structural Dynamics* 14 (4): 543–557.

PEER. 2011. “2011 PEER Ground Motion Database – Beta Version.” *PEER Ground Motion Database*. http://peer.berkeley.edu/peer_ground_motion_database/spectras/new.

Ramsdale, Rob. 2013. “Reference Tables - Coefficient of Friction.” *Engineer’s Handbook*. Accessed October 20. http://www.engineershandbook.com/Tables/frictioncoefficients.htm.

Romney, Kyle. 2013. “Soil-Bridge Interaction during Long-Duration Earthquake Motions”. Master’s Thesis, Corvallis, Oregon: Oregon State University.

Sadek, Fahim, Bijan Mohraz, Andrew W. Taylor, and Riley M. Chung. 1997. “A Method of Estimating the Parameters of Tuned Mass Dampers for Seismic Applications.” *Earthquake Engineering and Structural Dynamics* 26 (6): 617–636.

Scheller, Joern, and Michael C. Constantinou. 1999. “Response History Analysis of Structures with Seismic Isolation and Energy Dissipation Systems: Verification Examples for Program SAP2000.” *Technical Report MCEER* (99-0002).

U.S. Geological Survey. 2013. “U.S. Seismic Design Maps.” *Geologic Hazards Science Center*. http://geohazards.usgs.gov/designmaps/us/application.php.

Wada, A., and N. Mori. 2013. “Seismic Design for the Sustainable City: A Report on Japanese Practice.” In *Structures Congress 2008*, 1–8. American Society of Civil Engineers. Accessed November 27. http://ascelibrary.org/doi/abs/10.1061/41016%28314%29123.

Wen, Yi-Kwei. 1976. “Method for Random Vibration of Hysteretic Systems.” *Journal of the Engineering Mechanics Division* 102 (2): 249–263.

Wirsching, Paul H., and Gary W. Campbell. 1973. “Minimal Structural Response under Random Excitation Using the Vibration Absorber.” *Earthquake Engineering & Structural Dynamics* 2 (4): 303–312.

Xu, Kangming, and Takeru Igusa. 1992. “Dynamic Characteristics of Multiple Substructures with Closely Spaced Frequencies.” *Earthquake Engineering & Structural Dynamics* 21 (12): 1059–1070.

APPENDIX

A. CRUSTAL EARTHQUAKES TIME SERIES RECORDS

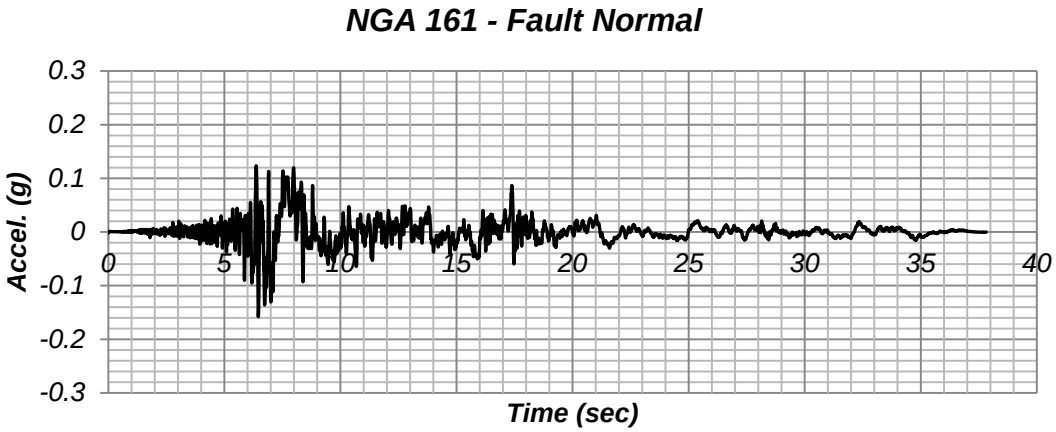

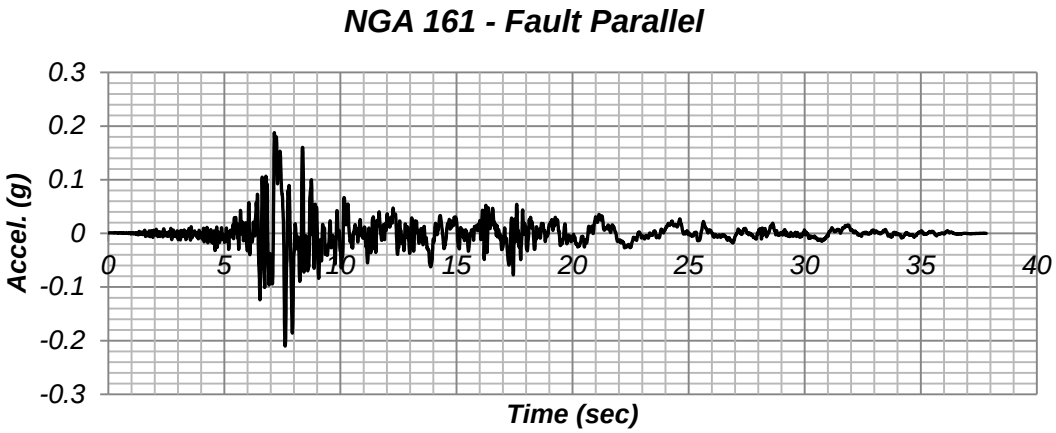

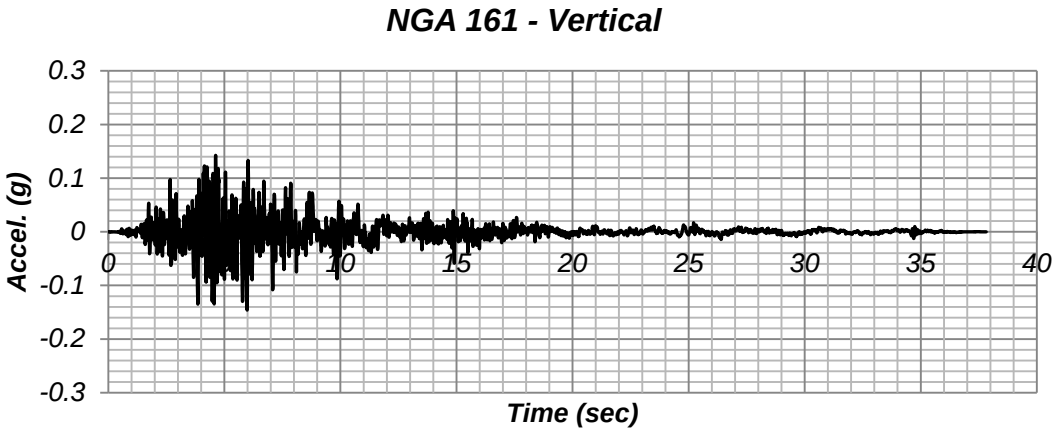

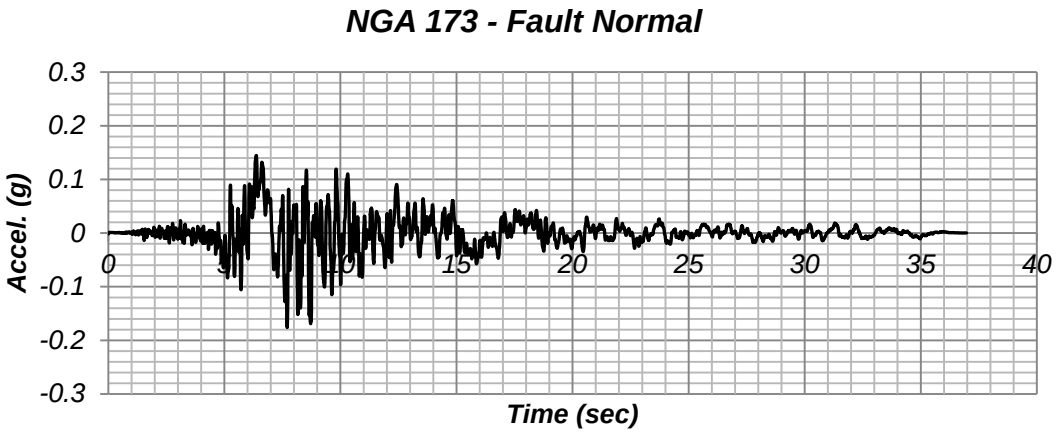
NGA 173 - Fault Normal
Accel. (g)
0.3
0.2
0.1
0
-0.1
-0.2
-0.3
0
5
10
15
20
25
30
35
40
Time (sec)

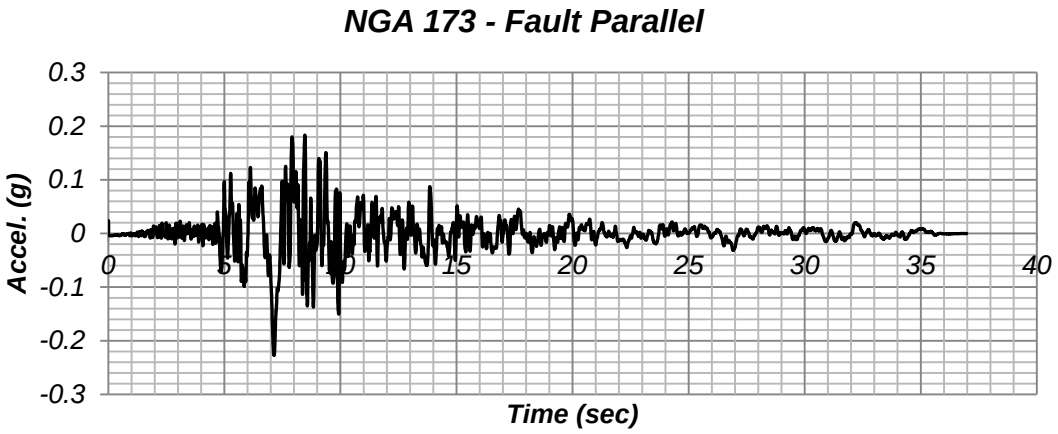
NGA 173 - Fault Parallel
Accel. (g)
0.3
0.2
0.1
0
-0.1
-0.2
-0.3
0
5
10
15
20
25
30
35
40
Time (sec)

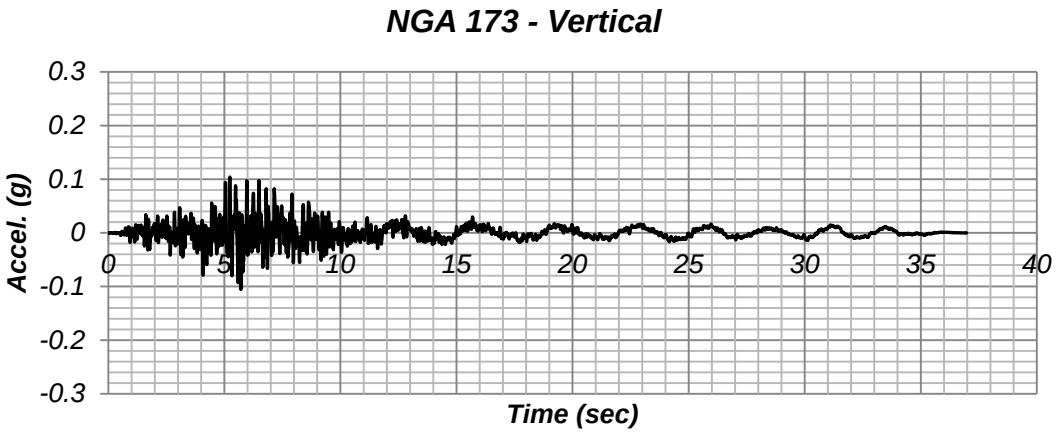
NGA 173 - Vertical
Accel. (g)
0.3
0.2
0.1
0
-0.1
-0.2
-0.3
0
5
10
15
20
25
30
35
40
Time (sec)

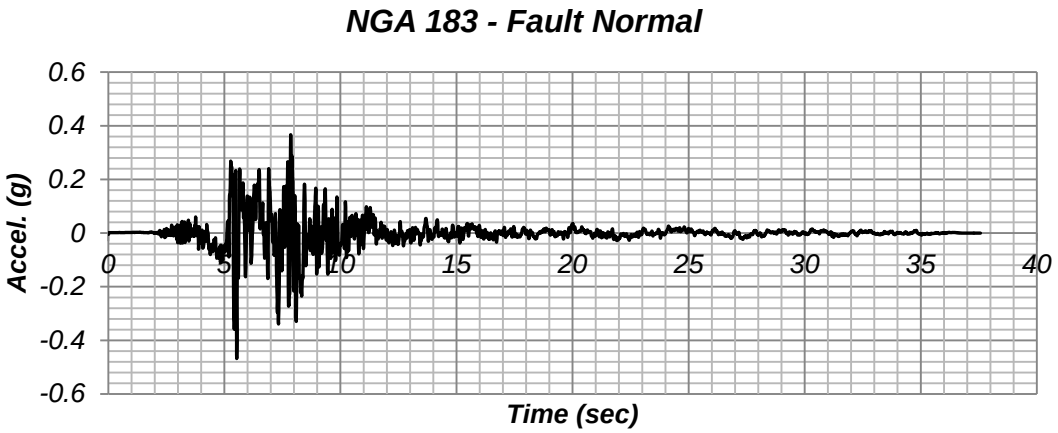
NGA 183 - Fault Normal
Accel. (g)
0.6
0.4
0.2
0
-0.2
-0.4
-0.6
0
5
10
15
20
25
30
35
40
Time (sec)

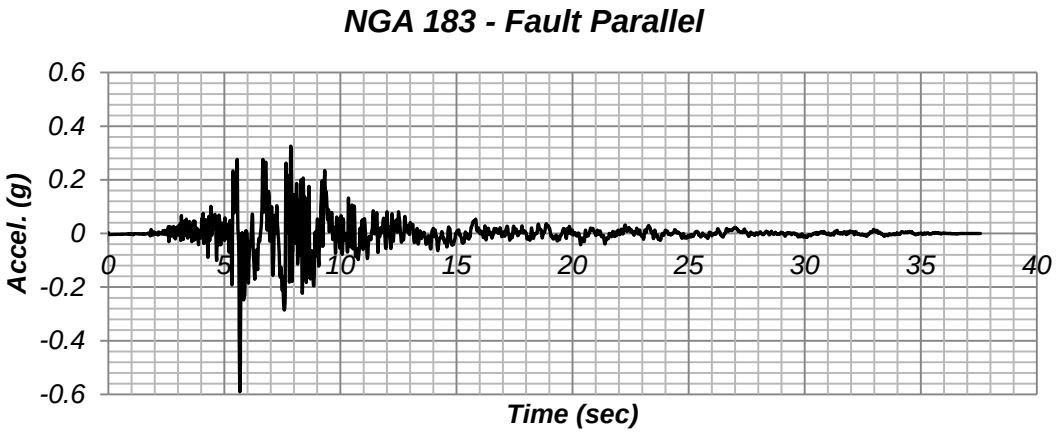
NGA 183 - Fault Parallel
Accel. (g)
0.6
0.4
0.2
0
-0.2
-0.4
-0.6
0
5
10
15
20
25
30
35
40
Time (sec)

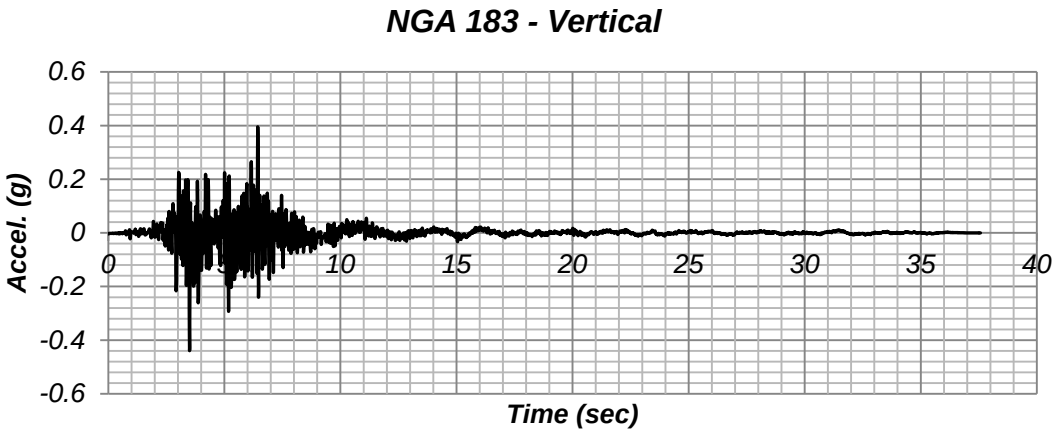
NGA 183 - Vertical
Accel. (g)
0.6
0.4
0.2
0
-0.2
-0.4
-0.6
0
10
15
20
25
30
35
40
Time (sec)

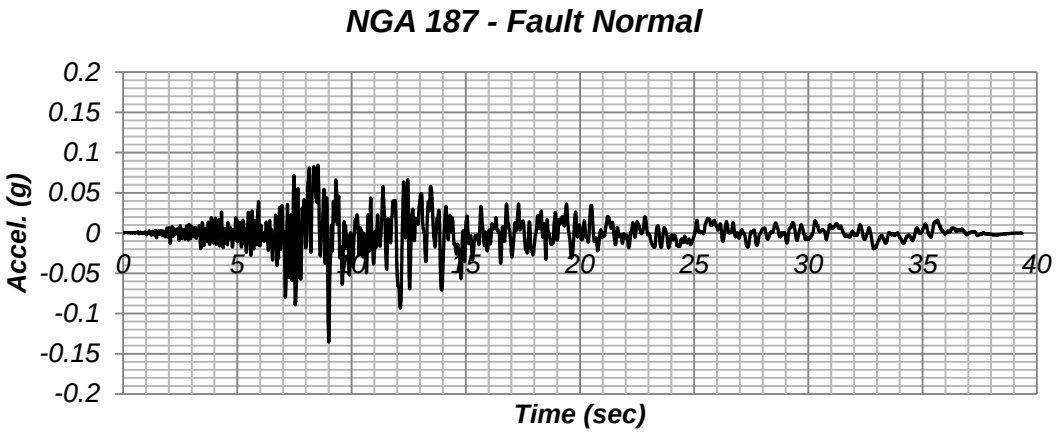
NGA 187 - Fault Normal
Accel. (g)
0.2
0.15
0.1
0.05
0
-0.05
-0.1
-0.15
-0.2
0
5
10
15
20
25
30
35
40
Time (sec)

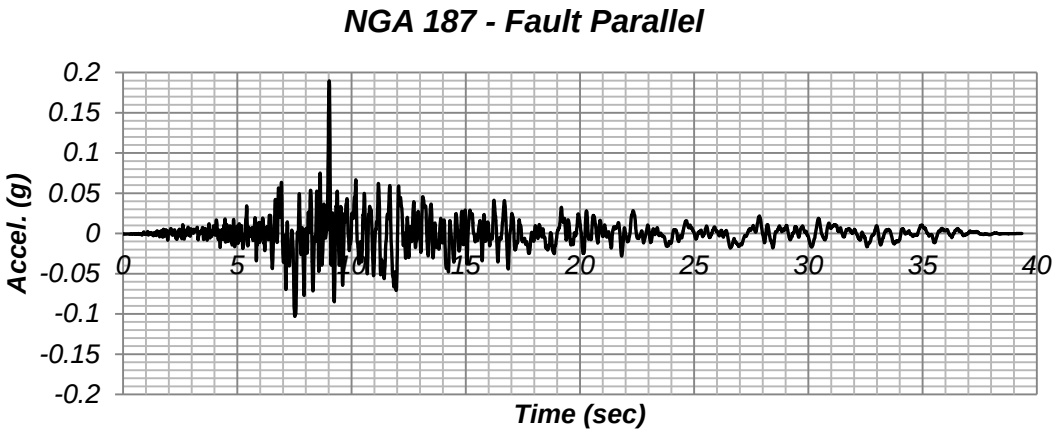
NGA 187 - Fault Parallel
Accel. (g)
0.2
0.15
0.1
0.05
0
-0.05
-0.1
-0.15
-0.2
0
5
10
15
20
25
30
35
40
Time (sec)

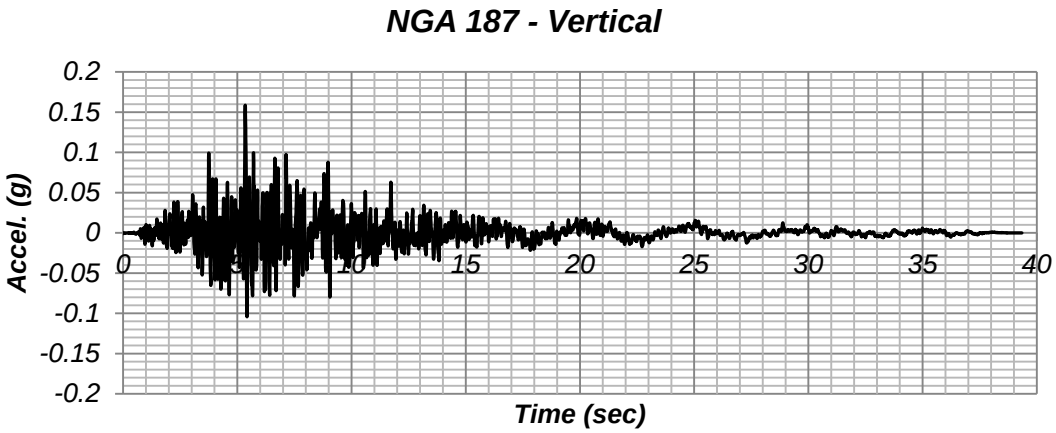
NGA 187 - Vertical
Accel. (g)
0.2
0.15
0.1
0.05
0
-0.05
-0.1
-0.15
-0.2
0
5
10
15
20
25
30
35
40
Time (sec)

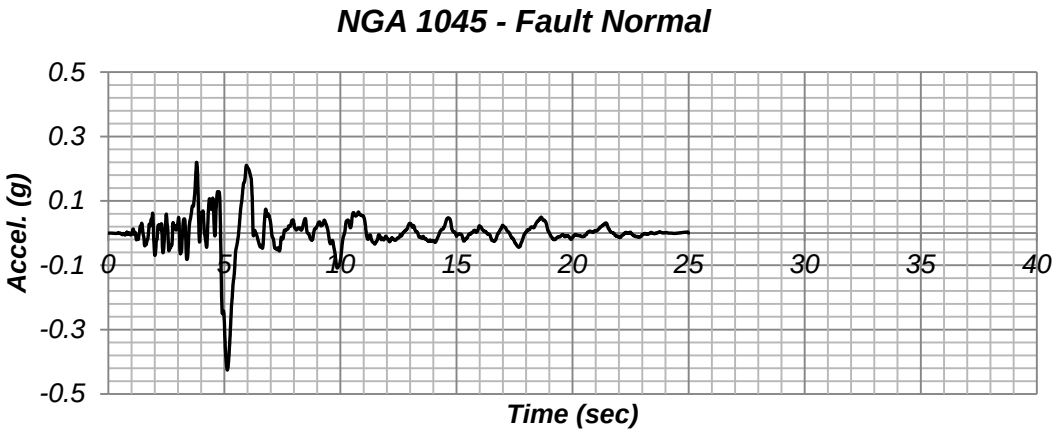
NGA 1045 - Fault Normal
Accel. (g)
0.5
0.3
0.1
-0.1
-0.3
-0.5
0
5
10
15
20
25
30
35
40
Time (sec)

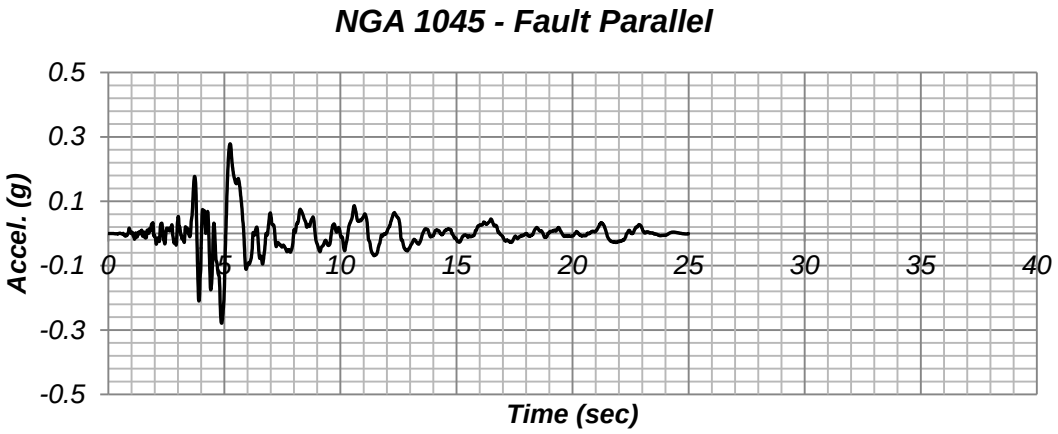
NGA 1045 - Fault Parallel
Accel. (g)
0.5
0.3
0.1
-0.1
-0.3
-0.5
0
5
10
15
20
25
30
35
40
Time (sec)

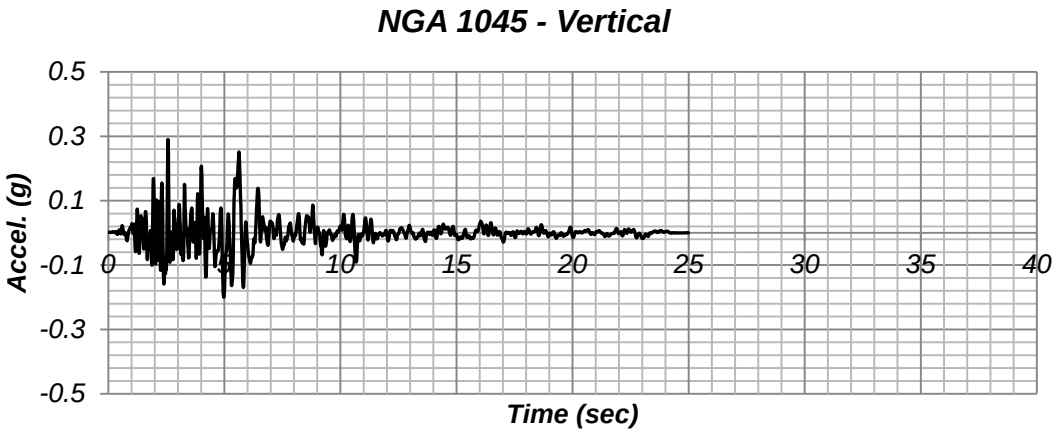
NGA 1045 - Vertical
Accel. (g)
0.5
0.3
0.1
-0.1
-0.3
-0.5
0
5
10
15
20
25
30
35
40
Time (sec)

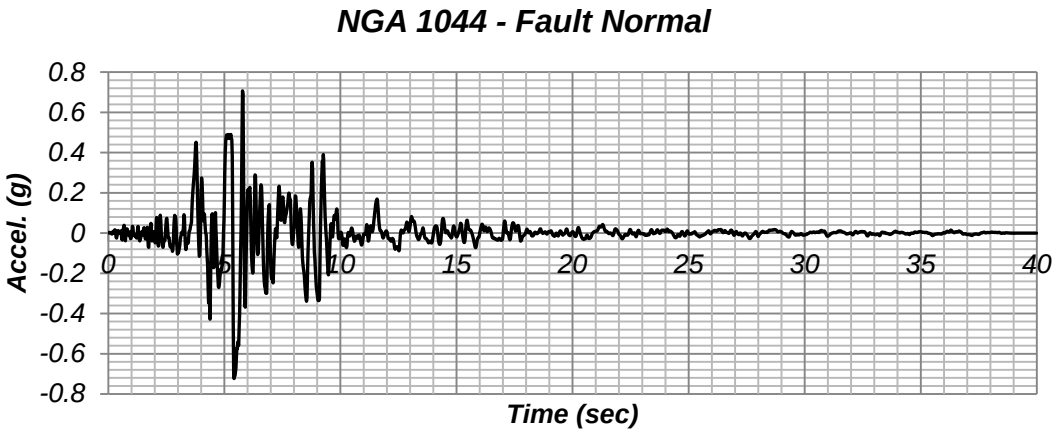
NGA 1044 - Fault Normal
Accel. (g)
0.8
0.6
0.4
0.2
0
-0.2
-0.4
-0.6
-0.8
0
5
10
15
20
25
30
35
40
Time (sec)

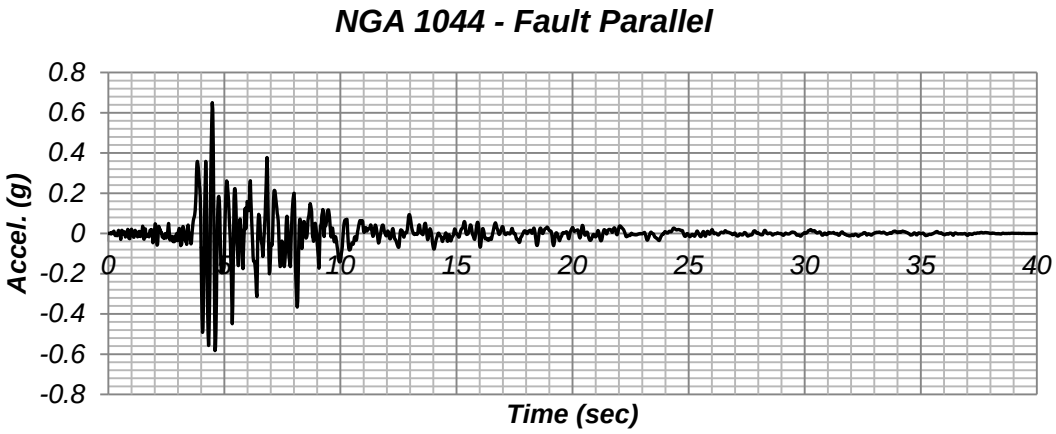
NGA 1044 - Fault Parallel
Accel. (g)
0.8
0.6
0.4
0.2
0
-0.2
-0.4
-0.6
-0.8
0
5
10
15
20
25
30
35
40
Time (sec)

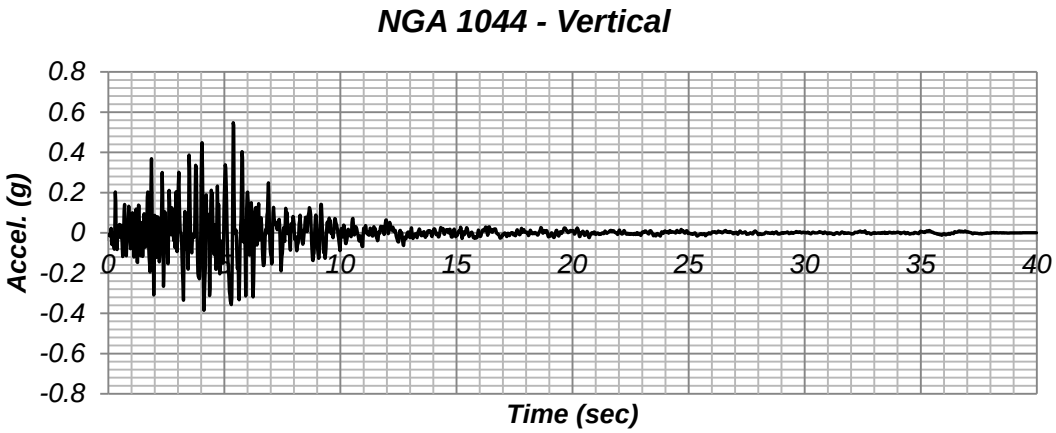
NGA 1044 - Vertical
Accel. (g)
0.8
0.6
0.4
0.2
0
-0.2
-0.4
-0.6
-0.8
0
5
10
15
20
25
30
35
40
Time (sec)

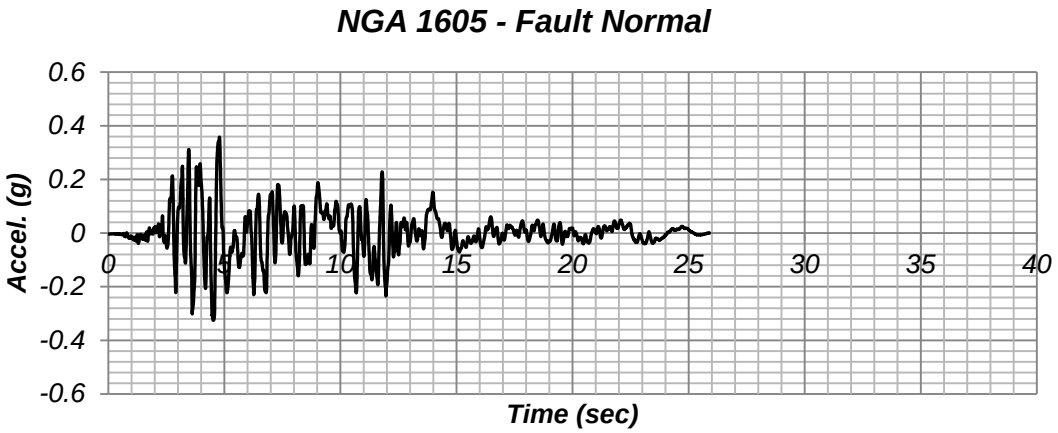
NGA 1605 - Fault Normal
Accel. (g)
0.6
0.4
0.2
0
-0.2
-0.4
-0.6
0
5
10
15
20
25
30
35
40
Time (sec)

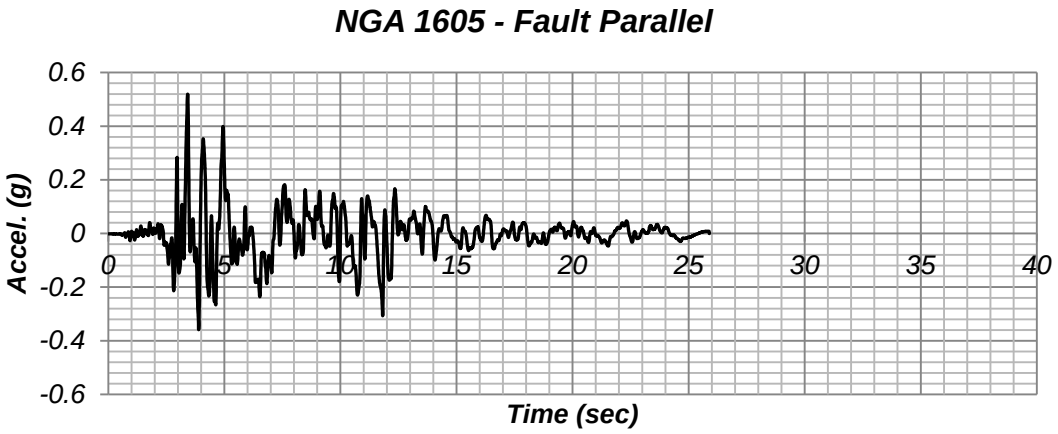
NGA 1605 - Fault Parallel
Accel. (g)
0.6
0.4
0.2
0
-0.2
-0.4
-0.6
0
5
10
15
20
25
30
35
40
Time (sec)

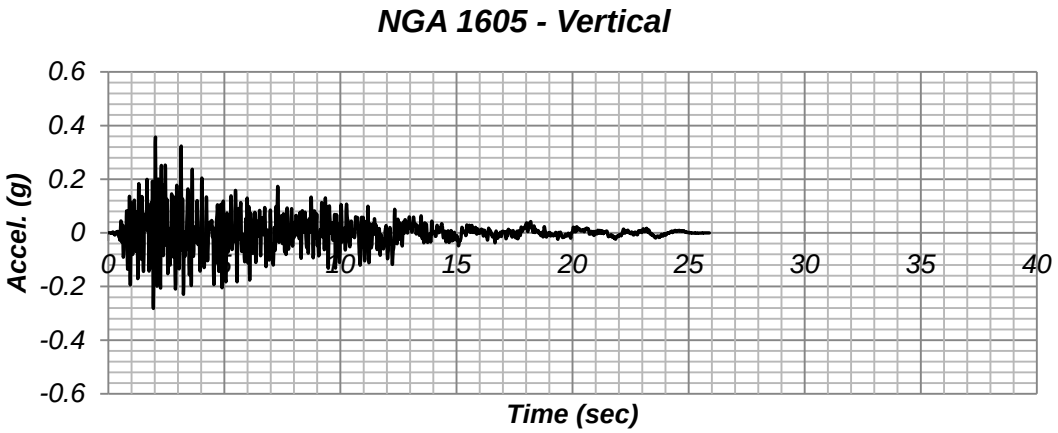
NGA 1605 - Vertical
Accel. (g)
0.6
0.4
0.2
0
-0.2
-0.4
-0.6
0
10
15
20
25
30
35
40
Time (sec)

B. SUBDUCTION-ZONE EARTHQUAKES TIME SERIES RECORDS

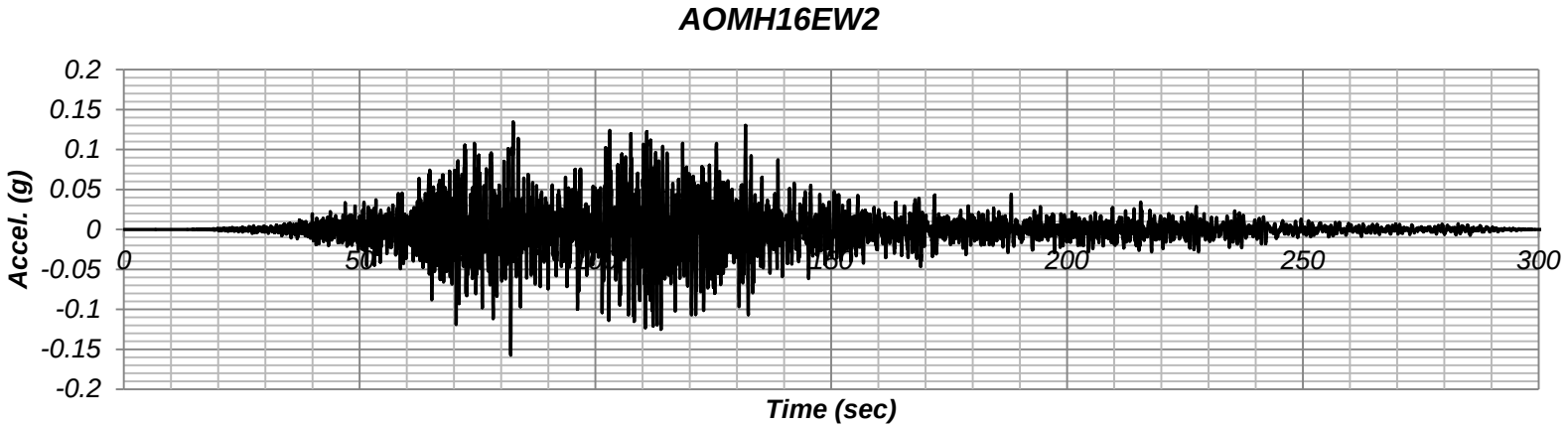

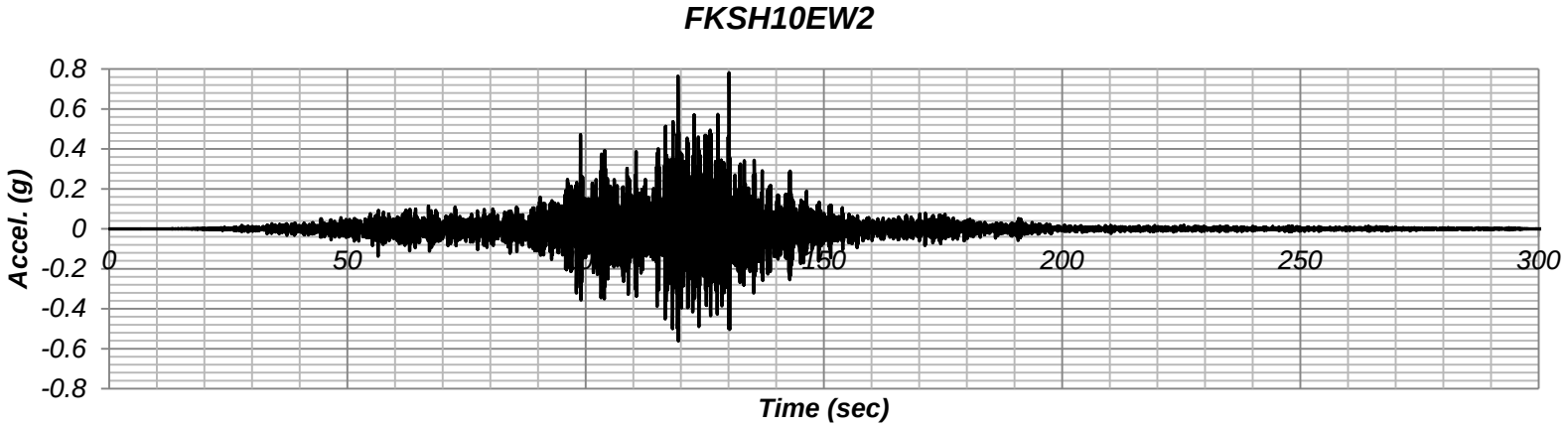

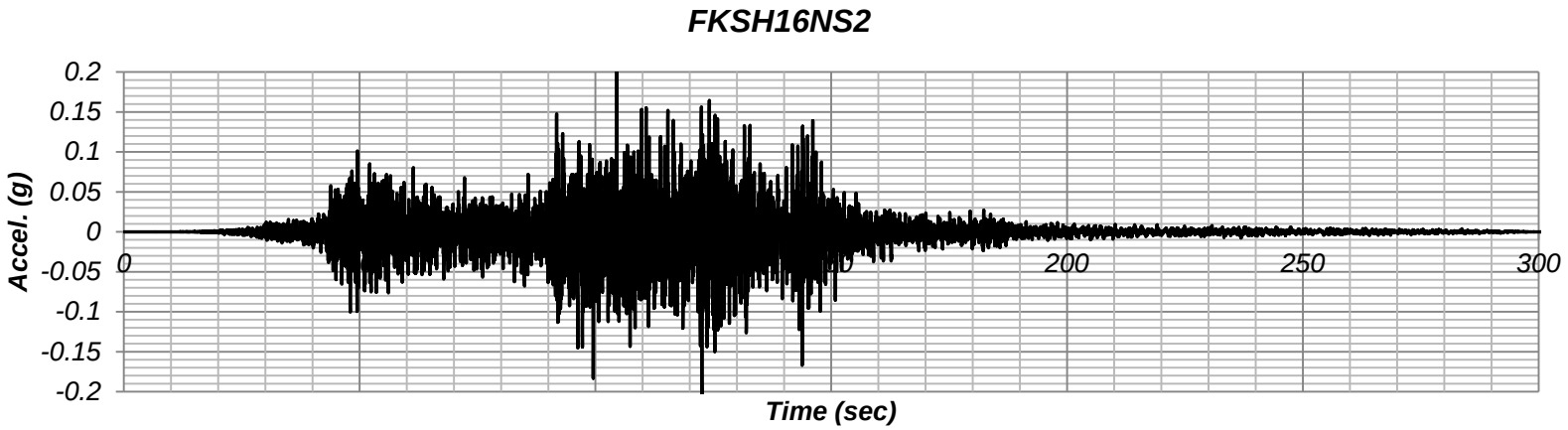
FKSH16NS2
0.2
0.15
0.1
0.05
0
-0.05
-0.1
-0.15
-0.2
Accel. (g)
0
200
250
300
Time (sec)

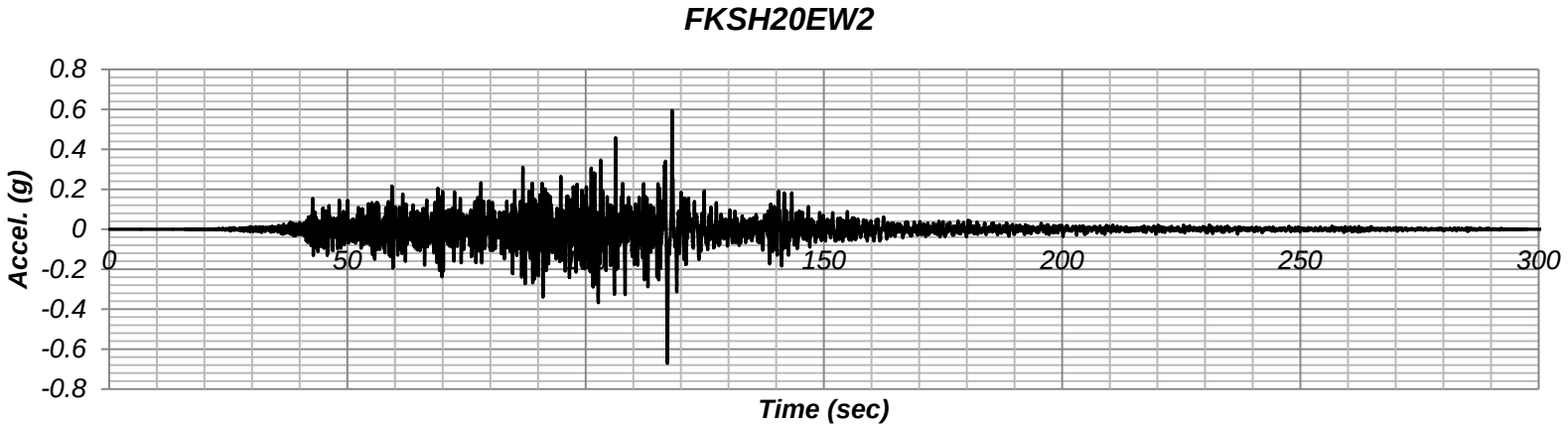
FKSH20EW2
0.8
0.6
0.4
0.2
0
-0.2
-0.4
-0.6
-0.8
Accel. (g)
0
50
150
200
250
300
Time (sec)

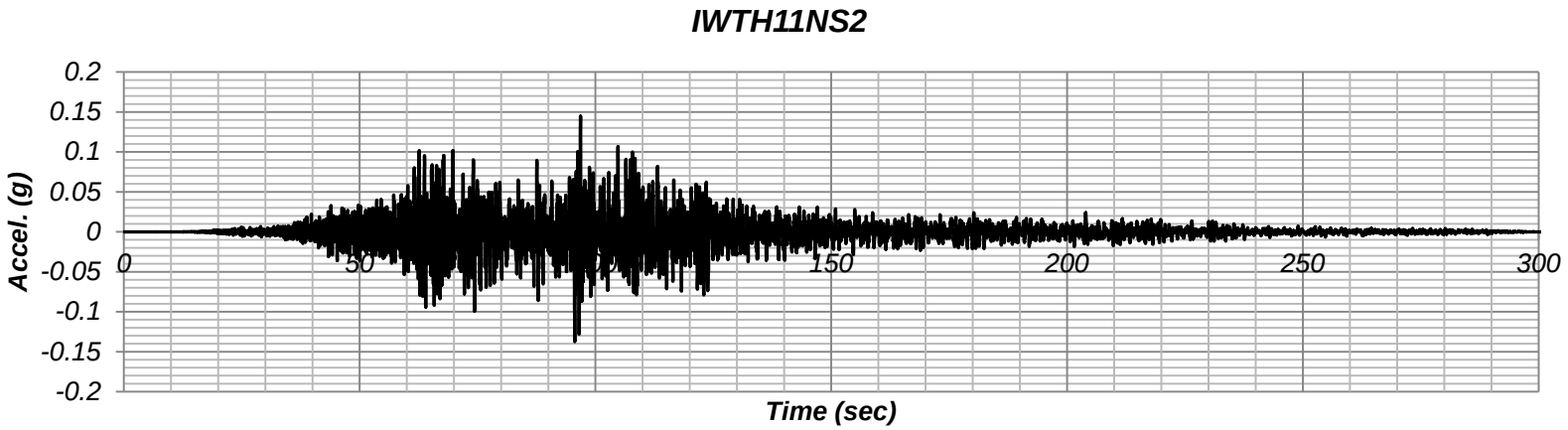
IWTH11NS2
0.2
0.15
0.1
0.05
0
-0.05
-0.1
-0.15
-0.2
Accel. (g)
0
50
150
200
250
300
Time (sec)

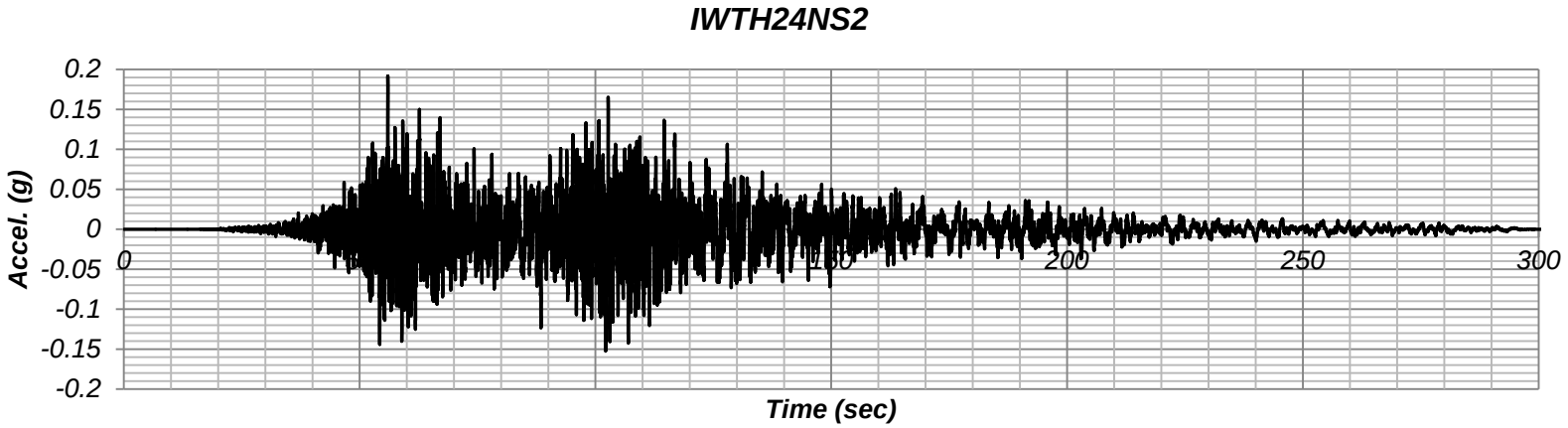
IWTH24NS2
0.2
0.15
0.1
0.05
0
-0.05
-0.1
-0.15
-0.2
Accel. (g)
0
150
200
250
300
Time (sec)

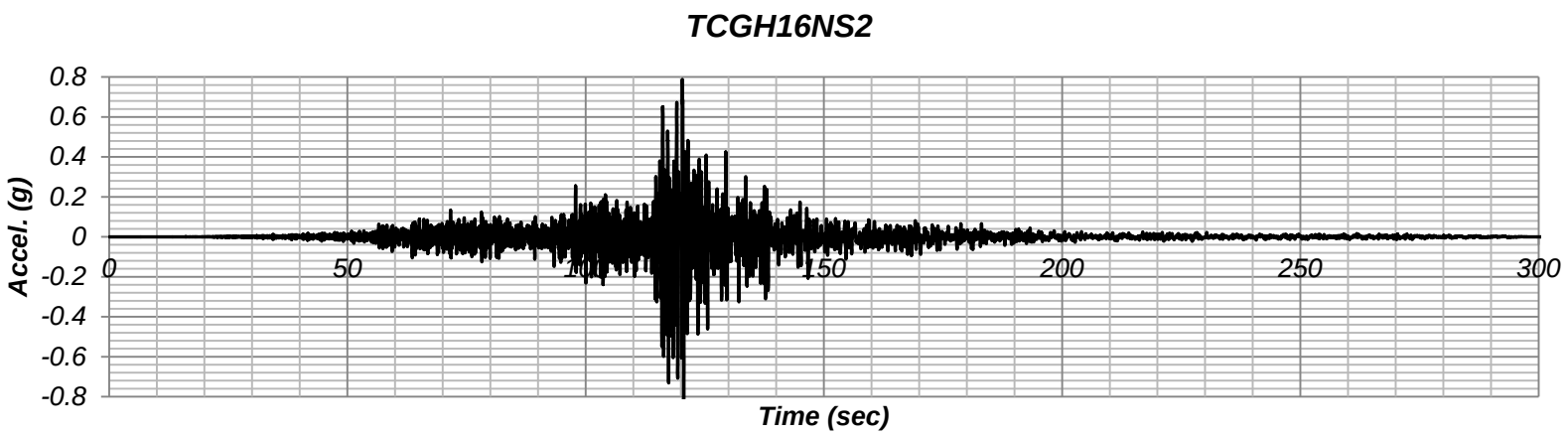
TCGH16NS2
0.8
0.6
0.4
0.2
0
-0.2
-0.4
-0.6
-0.8
Accel. (g)
0
50
150
200
250
300
Time (sec)